A SURFACE PLASMON RESONANCE ASSAY TO DETERMINE THE EFFECT OF INFLUENZA NEURAMINIDASE MUTATIONS ON ITS AFFINITY WITH ANTIVIRAL DRUGS

A thesis submitted in partial fulfilment of the requirements

for the degree of

Doctor of Philosophy in Chemical and Process Engineering

University of Canterbury

by

BALAJI SOMASUNDARAM

Biomolecular Interactions Centre and the

Department of Chemical and Process Engineering,

University of Canterbury,

Christchurch, New Zealand

2013

Abstract

The outbreak of pandemic influenza and its ability to spread rapidly makes it a severe threat to public health. Antiviral drugs such as oseltamivir and zanamivir are neuraminidase (NA) inhibitors (NI), which bind more tightly to NA than its natural substrate, sialic acid. However, the virus can acquire resistance to antiviral drugs by developing single point mutations (such as H274Y) in the target protein. Thus in some cases the drugs may not be as effective as expected. The high level of inconsistency exhibited by fluorometric assays and the short half-life of the chemiluminescent assay for monitoring drug resistance lead to the need for a simple, label-free, reliable assay. To address this problem, this work focused on three main objectives: 1) to determine the binding affinities of two common anti-viral drugs (oseltamivir and zanamivir) against the influenza NA wild type and drug resistant mutants using bioinformatics software Schrodinger Suite™ 2010. 2) To develop a reliable label-free, real-time, surface plasmon resonance (SPR) assay to measure the binding affinity between influenza viral coat protein neuraminidase (wild type and mutant) and anti-viral drugs. 3) To develop an SPR inhibition assay to quantitatively compare the interactions of sialic acid, zanamivir and oseltamivir with the viral coat protein neuraminidase (wild type and mutant).

The entire docking process was carried out using Schrödinger Suite™ 2010. The 2009 pandemic H1N1 neuraminidase (PDB: 3NSS) was used throughout the docking studies as the wild type structure. Five mutants (H274Y, N294S, H274N, A346N and I222V) and three ligands (sialic acid, oseltamivir and zanamivir) were built using the maestro module. The grid-based ligand docking with energetics (GLIDE) module and induced fit docking (IFD) module were used for docking studies. The binding affinities, Gibbs free energy change (ΔG) and molecular mechanics-generalized born energy/ solvent accessible area (MM-GB/SA) values for wild-type NA interactions show that both the antiviral drugs studied interact strongly with the wild-type protein. The ΔG values for all antiviral interactions with mutant NA forms were reduced in magnitude, thereby indicating that they are less favourable than interactions with the wild-type protein. A similar trend was observed with MM-GB/SA results. Amongst all of the computed values, MM-GB/SA was the closest to the experimental data. In several cases, the interactions between the anti-viral drugs and NA mutants were markedly less favourable than those between sialic acid and the same mutants, indicating that these mutations could confer anti-viral resistance.

Influenza NA wild-type and H274Y mutant were expressed in baculovirus expression system (BVES) in insect cells. The expressed proteins were partially purified using the standard purification techniques of anion exchange and size exclusion chromatography (SEC). A fluorometric activity assay was performed on the recombinant proteins. Both the wild type and the mutant showed similar level of activities. In addition, the recombinant NAs were used in an inhibition assay. Oseltamivir was found to be sensitive to wild type protein (IC_{50} = 0.59 nM) and resistant to the H274Y mutant protein (IC_{50} = 349.43 nM). On the other hand, zanamivir was sensitive to both wild type (IC_{50} = 0.26 nM) and the H274Y mutant (IC_{50} = 0.44 nM). This indicated that zanamivir was a more potent inhibitor than oseltamivir. These findings were in good agreement with the literature.

An SPR assay for accurate monitoring of influenza antiviral drug resistance was developed. A spacer molecule (1, 6- hexanediamine) was site-specifically tethered to the inert 7-hydroxyl group of zanamivir. The tethered zanamivir was immobilized onto an SPR GLC chip to obtain a final immobilization response of 431 response units (RU). The reference subtracted binding responses obtained for NA wild-type and H274Y mutant were analysed using the ProteOn Manager™ Software tools. The SPR curves were fitted to a simple Langmuir 1:1 model with drift to obtain association rate constant (k_a) and dissociation rate constants (k_d). The relative binding values obtained from literature and the current SPR assay (1.9 and 1.7 respectively) suggested that the current SPR assay yielded similar results to the existing labelled enzymatic assay. In addition, an SPR inhibition assay was developed. The calculated $IC_{50\text{-}spr}$ values were compared and it was observed that oseltamivir was sensitive to wild type protein ($IC_{50\text{-}spr}$ = 7.7 nM) and resistant to the H274Y mutant protein ($IC_{50\text{-}spr}$ = 256 nM). On the other hand, zanamivir was sensitive to both wild type ($IC_{50\text{-}spr}$ = 2.16 nM) and the H274Y mutant ($IC_{50\text{-}spr}$ = 2.4 nM). Sialic acid was also found to be sensitive to both wild type ($IC_{50\text{-}spr}$ = 5.5 nM) and H274Y mutant ($IC_{50\text{-}spr}$ = 3.25 nM). In the cases studied, the viral proteins remained sensitive to sialic acid, consistent with retention of virulence of these mutant strains. It was concluded that zanamivir is a more potent inhibitor than oseltamivir for treating the H274Y mutant. Comparison of the SPR inhibition results with the docking results revealed a similar trend. The wild-type NA and H27Y mutant retained binding affinity for sialic acid and zanamivir. Oseltamivir showed a significant decrease in binding affinity for the H274Y mutant compared with the wild-type. This was because of the disruption of the salt bridge formation within NA that was vital for oseltamivir activity.

To my knowledge, this is the first SPR biosensor assay developed to monitor influenza antiviral drug resistance. There is a tremendous scope to extend this study to more mutants and new antiviral drugs. This could pave the way for a reliable SPR biosensor assay to replace low consistency labelled enzymatic assays.

Acknowledgements

At the foremost, I would like to express my sincere gratitude to my supervisor Professor Conan J Fee, for giving me an opportunity to work in his lab. His constant encouragement and guidance has helped me to grow as an independent researcher. I am extremely thankful to for his massive support, particularly during the Christchurch earthquake. I am really happy to have been associated with a researcher like Conan, at a very early stage of my career.

I sincerely acknowledge the support and encouragement from my lab manager MS Rayleen Fredericks.

I also thank my co-supervisors Associate professor Emily Parker (Department of Chemistry, UC) and Dr Richard Hall (Environmental Science & Research , NZ) for their support. I would also like to thank Dr Richard Hall for conducting neuraminidase activity assays. I would like to acknowledge Professor Antony J Fairbanks and Dr Andrew Watson (Department of Chemistry, UC) for their valuable contributions in synthetic chemistry.

I would like to thank Professor Anton Middleburg for giving me an opportunity to work in the Australian Institute of Bioengineering and Nanotechnology (AIBN), University of Queensland. I would also like to express my sincere thanks to Dr Linda Lua and Ms Cindy Chang (Protein Expression Facility, AIBN, UQ) for training me in insect cell culture technique and gifting insect cell samples.

I also appreciate the financial support from Biomolecular Interaction Centre, EBOS group of company and the department of Chemical and Process Engineering (CAPE), University of Canterbury.

I am very grateful to have received samples of zanamivir and oseltamivir from GlaxoSmithKline (Stevenage, UK) and Hoffman La Roche Ltd (Switzerland), respectively

I wish to thank CAPE technical staffs, post-graduate students and administrators for their support and cooperation.

I would like to express my sincere gratitude to Dr Swaminathan Detchanamurthy for motivating me to do a PhD. I would also like to thank him for his guidance and support throughout my PhD.

I wish to acknowledge Mr Kannan Subramanian, Mr Kishorekumar Gopalakrishnan, Mr Nivaskumar Ramasamy, Mr Prasanna Ponnumallayan, Mr Suzal Samuel Shukla, Mr Navin Chandrasekaran. Ms Ashwini Raj, Mr Naveen Gabriel, Mr Suseendaran Babu, Mr Venugopalan Thamotharan, Mr Suresh Ponraj and Mr Surya Kumar for making me feel home away from home.

My special thanks to Mr Subramanian Sabapathy for helping me start my PhD journey in NZ. I would like to convey my sincere gratitude to Mrs Meenakshi Panchanathan, Mrs Saroja Sabapathy, Mrs Lalitha Kannan, Mrs Radha Annamalai, Mrs Saradha Lakshmanan, Mr Meyappan Kannan, Mr Annamalai Muthiah, Mr Lakshmanan Kannappan, Mrs Vidhya Subramanian, Mr Sriram Kannan, Mrs Sharanyaa Sabapathy, Ms Thaiyalnayaki Annamalai, Mr Venkatesh Lakshmanan and Ms Anu Subramanian for having a positive influence on my life.

I would like to express my deepest thanks and gratitude to my father Mr Somasundaram Panchanathan and loving brother Mr Siddarth Meyappan for their love and support.

Finally, I would like to dedicate this thesis to my beloved mother and best friend, Mrs Meenakshi Somasundaram. Her unconditional love and blessings have been my greatest strengths.

Preface

List of the outcomes arising from this thesis are:

Somasundaram B, Fee CJ, Watson A, Fairbanks AJ and Hall R (2013). A surface plasmon resonance assay to determine the effect of influenza neuraminidase mutation on its affinity with anti-viral drugs. Chemeca-2013, Brisbane, Australia (Oral presentation).

Somasundaram B and Fee CJ (2012). Development of a surface plasmon resonance assay to determine the effect of influenza neuraminidase mutation on its affinity with anti-viral drugs. Annual Biology Conference (ABC), School of Biological Sciences, University of Canterbury, Christchurch New Zealand (Oral presentation).

Somasundaram B (2012). Influenza War. Thesis in three competitions, University of Canterbury, Christchurch New Zealand (Third place).

Somasundaram B and Fee CJ (2011). In-Silico identification of potential drug resistant influenza neuraminidase mutations. 2nd Annual Queenstown Research Week, Queenstown New Zealand (Poster presentation).

Table of contents

List of Figures

List of Tables

Abbreviations

AcMNPV	Autographa californica multiple nuclear polyhedrosis virus
ALV	Avian leucosis virus
BAC	Bacterial artificial chromosome
BmNPV	Bombyx mori (silkworm) nuclear polyhedrosis virus
BSA	Bovine serum albumin
BVES	Baculovirus expression systems
BV	Budded virus
CMV	Cowpea mosaic virus
CNS	Central nervous system
CV	Column volumes
dpi	Days post infection
EDAC	1-ethyl-3-(3-dimethylaminopropyl) carbodiimide-HCl
ESR	Environmental Science & Research
EtOAc	Ethyl acetate
GE	Glide energy
GLIDE	Grid-based ligand docking with energetic
GOI	Gene of interest
HA	Hemagglutinin
HBV	Hepatitis B virus
HIV-1	Human immunodeficiency virus type 1
hpi	Hours post infection
HRMS-ESI/TOF	High resolution mass spectra electrospray ionization/time-of-flight
ICU	Intensive care units
IEX	Ion exchange chromatography
IFD	Induced fit docking
IC_{50}	Concentration of the inhibitor required to inhibit 50% of the enzyme reaction
$IC_{50\text{-}spr}$	Concentration of the inhibitor required to drop SPR responses by 50%
k_a	Association rate constant
K_D	Dissociation constant

k_d	Dissociation rate constant
K_i	Inhibition constant
LAK	Lock and key
LB	Luria broth
MM-GB/SA	Molecular mechanics-generalized born energy/solvent accessible area
MUNANA	2′-(4-methylumbelliferyl) -α-d-N-acetylneuraminic
NA	Neuraminidase
NANA	N-acetylneuraminic acid
NCBID	National Centre for Biosecurity & Infectious Disease
NHS	N-hydroxysuccinimide
NI	Neuraminidase inhibitor
ODV	Occlusion-derived virus
OPLS	Optimized potentials for liquid simulation
ORF	Open reading frame
PBS	Phosphate buffer saline
PBST	Phosphate buffer saline-tween
PCR	Polymerase-chain reaction
PRA	Plaque reduction assay
RB	Running buffer
RDE	Receptor-destroying enzyme
RFU	Relative fluorescence units
RI	Refractive index
RIU	Refractive index units
R_{max}	Maximum response units
RU	Response units
S.D.	Standard deviation
SDM	Site directed mutagenesis
SDS-PAGE	Sodium dodecyl sulfate polyacrylamide gel electrophoresis
SEC	Size exclusion chromatography
SFM	Serum free media
Sf9	*Spodoptera frugiperda*
SP	Standard precision
SPR	Surface plasmon resonance

TFA	Trifluoroacetic acid
TMV	Tobacco mosaic virus
UV	Ultra violet
χ^2	Average of the squared differences between the measured data point and the fit

1. Introduction

1.1 Background

The spread of influenza virus as a pandemic results in the deaths of millions of people annually (Yuen 2005 ; Maines et al. 2005). In the early 20th century new strains of the influenza virus emerged, killing up to ten million people. In April 2009, a new flu strain called the swine flu emerged that combined genes from human, pig and bird flu. On June 11, 2009, the World Health Organisation declared the outbreak of swine flu to be a pandemic. This outbreak of pandemic influenza and its ability to spread rapidly made it a severe threat to public health (http://www.cdc.gov/H1N1flu/qa.htm , 30th October, 2010). The current antiviral drugs such as oseltamivir and zanamivir inhibit the viral coat protein neuraminidase (NA), and bind more tightly to NA than its natural substrate, sialic acid. However, the virus can acquire resistance to antiviral drugs by developing single point mutations (such as H274Y) in the target protein NA. The ability of the virus to develop resistance against antiviral drugs, specifically neuraminidase inhibitors (NIs) could vary with the type of mutation it can carry. Hence, there is a need to rapidly monitor the efficacy of these drugs with new mutant strains of the influenza virus, such as during the recent swine flu pandemic. This thesis work aimed to develop a reliable label-free, real-time, surface plasmon resonance (SPR) assay to measure the binding affinity between NA and anti-viral drugs.

1.2 Influenza virus

Influenza is an infectious disease caused by the influenza viruses that belong to the family orthomyxoviridae (Amano and Cheng 2005; Shtyrya et al. 2009). Influenza viruses are classified as influenza A, B and C (von Itzstein 2007; Wagner et al. 2002). Influenza A is the most commonly occurring of these and is further classified based on its surface glycoproteins hemagglutinin (HA) and NA e.g. H1N1, H5N1, which refers to viral strains that contain identical NA (N1) but a different HA (H1 and H5) on their surface (Oxford et al. 2002). There are 16 subtypes of HA and 9 subtypes of NA (Colman 2009; Liu et al. 1995; von Itzstein 2007). The severity of each strain of the virus depends on the type of HA and NA it carries (Fouchier et al. 2004). These subtypes are classified by their interaction with antibodies. All of the variants within a

given subtype will be neutralized by a similar set of antibodies (Boonsoongnern et al. 2005). These surface glycoproteins are carbohydrate-recognizing proteins that are known in humans to recognize sialic acid (N-acetylneuraminic acid or NANA) (von Itzstein 2007). Both proteins play a significant role in viral infection.

Influenza virus particles are usually approximately spherical and 80 to 120 nm in diameter. A lipid bi-layer encapsulates the viral RNA. The six segments of viral RNA code for eight different proteins (Skehel and Wiley 2000). Table 1-1 describes the function of eight virus-encoded proteins of influenza virus A. Continuous random mutation of the viral RNA results in a process known as antigenic drift. Antigenic drift occurs when a host is infected with two or more different strains of influenza and the genetic information of these strains is recombined to form a new strain (Figure 1-2). When a new strain is produced through antigenic drift, it is highly unlikely that the human immune system has already developed immunity to this new strain of the virus (Eckert and Kim 2001) and this is thought to result in pandemic strains. This makes the new strain a real concern for health authorities and hence requires continuous monitoring of circulation of new strains of influenza viruses (Carrat and Flahault 2007; McDonald et al. 2007).

1.3 Influenza pandemic

The first laboratory diagnosis of influenza was first performed in 1932, although influenza was first reported in the year 1173 (Smith 1995). An outbreak in 1580 originated in Asia and started to spread to Africa, Europe and America. Hence, it was classified as a pandemic. An outbreak in the 17th century was considered an epidemic because the spread of the infection was confined to only America and Europe (Potter 2001; Laver and Garman 2002). The 18th century saw two influenza pandemic outbreaks, in 1729 and 1781. There were two pandemics in the 19th century (1830, 1898-1900) and four in the 20th century. The 1918 pandemic was the most severe attack and mortality increased steeply (Potter 2001). The infection could have started in America and then spread to Africa, India, China, New Zealand, the Philippines and the whole of Europe. It is estimated that up to 40% of the world's population were infected, and more than 50 million people died in the pandemic (Potter 2001).

Table 1-1: Influenza virus proteins and their functions

S.no	Protein	Function	Reference
1	PA	Viral RNA polymerase subunit A- plays important role in transcription and replication	(Perez and Donis 2001)
2	PB 1	Viral RNA polymerase subunit B1- plays an important role in transcription and replication	
3	PB 2	Viral RNA polymerase subunit B2- plays an important role in transcription and replication	
4	HA	Hemagglutinin -Adheres the virus to the target host cell	(von Itzstein 2007)
5	NA	Neuraminidase -Release of virus from the host cell and the mobility of the virus through the upper respiratory tract.	(Chong et al. 1992)
6	NP	Nucleoprotein- Changes RNA synthesis to replication mode from transcription mode	(Biswas et al. 1998)
7	M1	Matrix protein - Form a coat inside the virus envelope and plays a crucial role in budding mature viruses.	(Wakefield and Brownlee 1989)
	M2	Membrane protein -Transportation of protons into the virus	(Schnell and Chou 2008)
8	NS1	Nonstructural protein-1- Inhibits antiviral interferon production	(Salahuddin and Khan 2010)
	NS2	Nonstructural protein-2- Transport of viral ribonucleoprotein from nucleus to the cytoplasm	

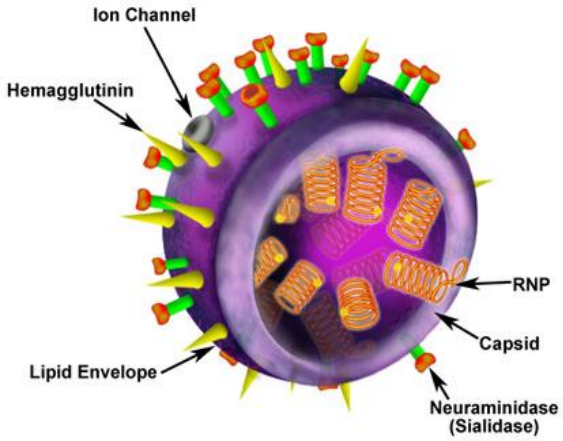

Figure 1-1: Structure of influenza virus with surface glycoproteins hemagglutinin and neuraminidase. (http://reference.medscape.com/features/slideshow/h1n1-influenza , 14th January, 2013)

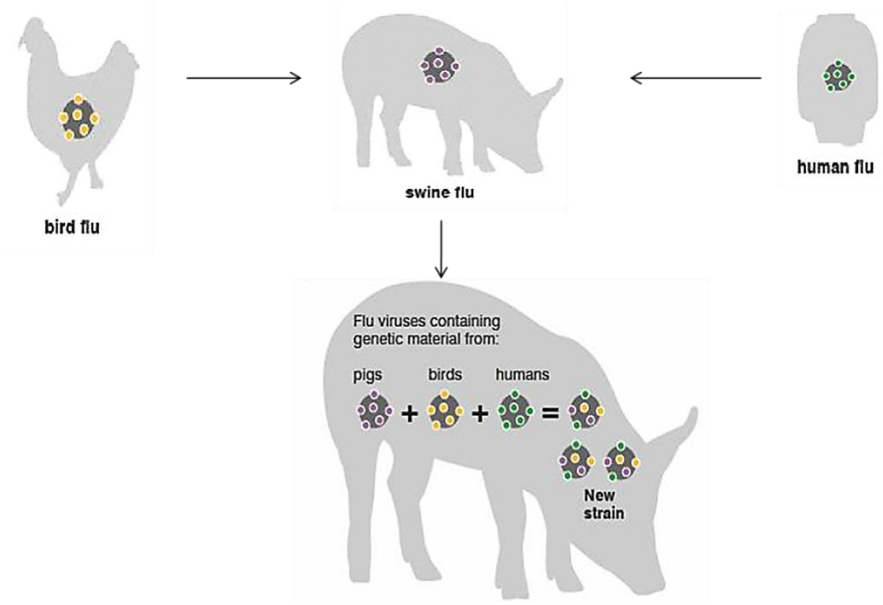

Figure 1-2: Antigenic drift occurring in a pig infected with different strains of influenza. This allows sharing of genetic information between the strain, leading to the development of an entirely new strain (http://www.bbc.co.uk/news/health-12128090 , 14th January, 2013)

The severity was at its peak in Spain, hence, this pandemic is also called the Spanish flu. In 1957, the H2N2 (combination of human and duck) virus spread throughout Asia, known as the Asian flu, killing at least two million people.The H3N2 virus outbreak in Hong Kong in the year 1968 killed up to one million people globally (Laver and

Garman 2002). In April 2009, there was an outbreak of H1N1 virus. This was a second H1N1 outbreak (the first outbreak being in 1918). This virus was characterized as a novel strain of H1N1 possessing genetic information of bird, swine and human flu viruses (Trifonov et al. 2009). The swine flu outbreak in the year 2009 affected 18% of the New Zealand population. 1122 people were hospitalized, among them 102 people carried severe infection and were treated in intensive care units (ICU). Up to 49 New Zealanders died in this pandemic (Wilson 2012).

In 1976 the outbreak of swine flu in New Jersey resulted in a mass influenza vaccination program. Low antibody titers and vaccine side-effects lead to a major failure of this program. This shifted the world's attention to antiviral drugs against influenza, which are the first line of defence available to date (Laver and Garman 2002). Based on the virus infection mechanism (described in detail in Chapter 2), influenza HA and NA became the most preferred antiviral drug targets. HA and NA interact with NANA present on the host cell surface. Several NANA analogues have been developed as antiviral drugs, namely NA inhibitors.

Table 1-2: Spread of influenza as a pandemic

Pandemic	**Year**	**Number of deaths**	**Virus sub type**	**Reference**
Spanish flu	1918	20 to 100 million	H1N1	(Laver and Garman 2002; Mills et al. 2004)
Asian flu	1968	1 to 1.5 million	H2N2	(Laver and Garman 2002)
Hong Kong flu	1957	1 million	H3N2	(Laver and Garman 2002)
2009 swine flu	2009	18,000	H1N1	(Trifonov et al. 2009)

1.4 Objectives

The major objective of this thesis was to develop an SPR assay to determine the binding affinities of two common anti-viral drugs (oseltamivir and zanamivir) against the influenza NA wild type and drug-resistant mutant H274Y. To achieve this, the following sub-objectives were addressed:

1. Docking studies of influenza antiviral drugs against the influenza protein NA (wild type and mutant) were carried out using the bioinformatics software Schrodinger Suite™ 2010.

2. Recombinant influenza NA (wild type and mutant) were expressed using baculovirus expression systems (BVES) in High-Five^{TM} insect cells and purified using standard purification techniques such as anion exchange and size exclusion chromatography .

3. A spacer molecule was tethered to the 7 hydroxyl group of zanamivir and this zanamivir spacer conjugate was immobilized on to an SPR GLC sensor chip.

4. An SPR assay was developed to measure the kinetics of interactions between influenza NA and immobilized zanamivir.

5. The immobilized zanamivir was treated as a bio-specific ligand to NA isoforms and an SPR inhibition assay was developed to quantitatively compare the interactions of sialic acid, zanamivir and oseltamivir.

1.5 Thesis organization

Chapter 2 comprises a review of the literature. The literature review is divided into four parts: a) Influenza virus and antiviral drugs, b) Molecular docking, c) BVES for recombinant protein production in insect cells and d) Application of SPR to virus detection. In the first part of this chapter, a detailed description of influenza virus structure, mechanism of infection and assays used for measuring of antiviral drugs sensitivity are described. In the second part, a brief outline of molecular docking simulations are described. In the third part, an overview of replication and assembly and the development of baculovirus and different strategies used in BVES are described. The final part of this chapter describes the principles of SPR and its application in virus detection.

In Chapter 3, the main focus is on calculating viral resistance using molecular docking simulations. Calculation of Gibbs free energy change (ΔG) and MM-GB/SA (mechanics-generalized born energy/solvent accessible area) values for the antiviral drugs and sialic acid interactions with wild type NA and different NA mutants (H274Y, N294S, H274N, I222V & A346N) are described in detail. The entire docking process

was carried out using Schrodinger Suite™ 2010. The grid-based ligand docking with energetics (GLIDE) module and induced fit docking (IFD) module in Schrödinger were used for docking studies. The optimized potentials for liquid simulation (OPLS) force field were used for all simulations. The docked results were analyzed using the GLIDE pose viewer module. The computed energy values were used to calculate binding affinities, which were compared with the binding affinities reported in the literature.

Chapter 4 describes the use of *flash*BAC™ BEVS technology for expression of NA. BEVS has been widely used for expressing foreign genes (Smith et al. 1983) in insect cells. Furthermore, growth and maintenance of two commonly used insect cell lines, Sf9 (*Spodoptera frugiperda*) and High-Five™ (*Trichoplusia ni*) are described in this chapter. In addition, cloning and site directed mutation, transfection technique and protein expression analysis used in this project are discussed in detail.

Chapter 4 also describes the purification of NA using standard purification techniques, such as anion exchange and size exclusion chromatography. The recombinantly generated NAs were sent for external testing to the Institute of Environmental Science & Research (ESR) at the National Centre for Biosecurity & Infectious Disease (NCBID). The samples were tested for NA activity using a fluorometric assay that uses fluorogenic 2′-(4-methylumbelliferyl) -α-d-N-acetylneuraminic (MUNANA) as a substrate. The results of the assays, performed in the presence and in the absence of antiviral drugs, to measure the sensitivities of the drugs to different NA isoforms are discussed in detail in this chapter. The IC_{50} values were used to compare the sensitivities of the antivirals to a particular NA isoform.

Chapter 5 describes the development of a simple, label-free, real-time surface plasmon resonance assay to measure the kinetics of zanamivir and NA (wild type and H274Y mutant) interactions. Synthesis of zanamivir-spacer conjugate, immobilization of the conjugate to the sensor chip and SPR interaction analysis are discussed in detail in this chapter. Moreover, this chapter describes the development of inhibition assays to monitor NIs drug resistance. The proposed SPR assay results were compared with results obtained from the fluorescent labelled NA activity assay (Chapter 4), molecular docking results (Chapter 3) and kinetics data reported in the literature.

An overall set of conclusions and recommendations for further work are presented in Chapter 6.

2. Literature Review

2.1 Introduction

This chapter reviews the structure of influenza surface protein NA, effect of glycosylation on NA's activity, recombinant NA expression and purification and the methods used for detecting NA's activity. This is followed by an overview of baculovirus expression systems. Finally the principle and applications of SPR for virus detection are reviewed.

2.2 Neuraminidase structure

The influenza neuraminidase (NA) was first described as receptor-destroying enzyme (RDE) by George Hirst in 1941. Hirst mixed red blood cells with allantoic fluid infected with influenza virus at 0°C and observed that cells started to agglutinate. When these cells were heated to 37°C, the virus eluted from the cells and the already infected red blood cells were not able to re-agglutinate when mixed with fresh allantoic fluid, while the eluted virus could agglutinate fresh red blood cells. Hirst concluded that the virus possessed an enzyme which might have disrupted the receptors recognized by the virus when the mixture of red blood cells and virus were warmed to 37°C (Hirst 1941). It was later discovered that the RDE was disrupting sialic acid or N-acetyl neuraminic acid (NANA) from the cell surface. Because the enzyme cleaved sialic acid, it became known as sialidase (Gottschalk 1957). As it was discovered that NA interacted with NANA, until late 1940s it was believed that NA was responsible for red blood cell agglutination at lower temperatures and destroyed NANA at 37°C. In 1949 Stone, discovered that NA was not involved in agglutination and another enzyme responsible for agglutination was later identified as hemagglutinin (HA) (Stone 1949). The first electron microscope image of influenza virus showed spiked projections of HA and NA from the virus surface coating the virus particles. After this discovery, HA and NA were called viral coat proteins.

The influenza NA is made up of 470 amino acid residues and consists of several domains such as the cytoplasmic, transmembrane, head, and stem domains. The stem connects the head to the transmembrane domain (Shtyrya 2009). Often NA's structure is described as resembling the shape of a mushroom. NA is a homotetramer with four

identical subunits (Figure 2-1). Due to variable glycosylation the molecular mass of NA is considered to be approximately 240 kDa (each monomer is approximately 60 kDa) (Colman 1994; Colman and Ward 1985). One viral particle may contain up to 50 tetramers, that can form clusters on the viral surface (Harris et al. 2006). The enzyme's head domain is formed by six identical antiparallel β-sheets that consists of the active site and calcium binding site. The β-sheets form of a propeller-like structure. Loops connecting these β-sheets in the head domain are of extreme importance for the enzyme because they are the most variable parts of the structure that correspond to a particular subtype of NA. There are eight disulfide bonds in the NA structure that helps in the stability of the structure. The calcium binding site is known to stabilize the structure of the enzyme even at low pH (Takahashi et al. 2003). Amino acid residues that form the active site of the enzyme are constant for influenza A and also for influenza B NA (Shtyrya 2009).

2.3 Effect of glycosylation on neuraminidase activity

Glycosylation is critical for the enzyme's activity and proper folding. Asparagine residues, which form the glycosylation sites are Asn83, Asn144, Asn146, Asn234 and Asn389. It has been shown that the deletion of the glycosylation site at Asn146 causes a 20-fold decrease in activity, at Asn 144 leads to changes in substrate specificity, at Asn 83 and Asn 398 causes incorrect protein folding (Li et al. 1993; Saito and Kawano 1997).

Wu et al. (2009) investigated the effect of glycosylation on the activity of the protein. As seen by Deroo et al. (1996), these researchers also found that the recombinant protein existed in monomeric, dimeric, and tetrameric forms, but only the tetrameric form of the protein exhibited activity. This suggests that there could be some unique properties associated with the tetrameric form that are absent in other inactive forms of NA. Their results demonstrate that proper glycosylation is absolutely necessary for the formation of correctly folded NA that can further form a highly active tetramer. N-glycosylation on the tetramer could also contribute to the virulence of the virus. Influenza viruses use glycans to hide their peptide epitopes to resist the host immune system. The 1918 pandemic flu virus NA contained seven N-glycosylation sites, with five of them present in the stalk region. The presence of these glycosylation sites may have protected NA from host proteolytic attack (Deroo et al. 1996). Moreover, 1918

pandemic flu virus NA also lacked a tryptic site and had no structural difference when compared to the already known NA protein backbone, with the only difference being with its unique glycosylation sites. This also suggests that the N-glycosylation not only plays a vital role in activity of the protein but is also important for the virulence of the virus.

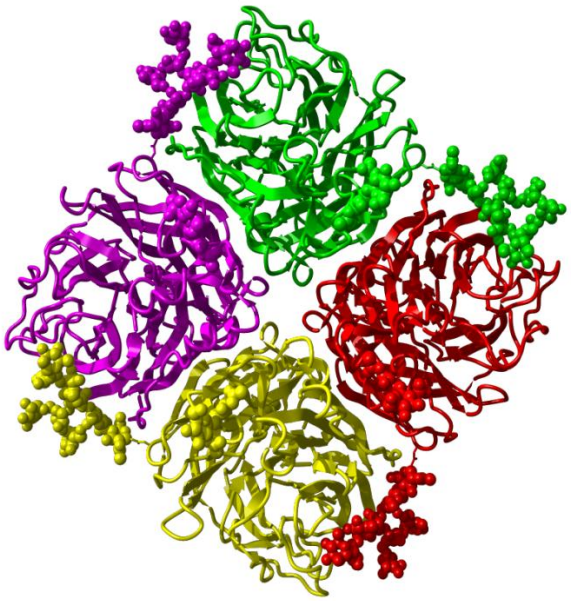

Figure 2-1: Tetramer structure of influenza H1N9 (PDBid 3R8H) (Smith et al. 2006), coloured by monomer. Protein chains are displayed in ribbon representation and carbohydrate atoms in ball representation.

2.4 Influenza infection mechanism

The presence of two proteins whose functions are exactly opposite to each other, namely: HA, which binds the receptor (glycoconjugates that display terminal α‑linked N‑acetylneuraminic acid); and NA, which cleaves the receptor is an interesting feature of the influenza virus (Shtyrya 2009). The influenza virus attaches itself to the host cell by using its surface glycoprotein HA. HA recognize the NANA present on the host cell surface. The virus then enters the host cell through a process called endocytosis (Suzuki et al. 2000; Nelson et al. 1993). Once the virus enters the host cell, it then takes control of the host cell protein expression machinery (Matrosovich and Klenk 2003). Subsequently, the host cell starts to synthesize viral proteins and viral particles. The virion progeny starts to develop when these critical viral components come together in

the host cell. The virus starts to prepare for the budding process, through which it exits the host cell (Sauter et al. 1992; Watowich et al. 1994). The enzyme NA cleaves the terminal NANA residues from virion progeny. The action of NA enables the virion progeny to detach itself from the infected cell and seek new host cells to spread the infection. The enzyme's function in the infection process is termed as the "release mechanism" (von Itzstein 2007; Oakley et al. 2010; Palese et al. 1974; Liu et al. 1995). This process starts with the formation of a sialosyl cation intermediate that represents a half-chair conformation. The tyrosine residue in the binding pocket shares an electron pair with this intermediate and retains the intermediate trapped in NA's binding pocket. This results in the formation of a negatively charged environment within the enzyme's active site and stabilizes the active site (Lentz et al. 1987; Chong et al. 1992). A water molecule stereoselectively reacts with the sialosyl cation intermediate to release α-Neu5Ac as the first product, followed by the release of a thermodynamically more favourable β-Neu5Ac (Figure 2-2) (Taylor and Vonitzstein 1994). The formation of intermediate is common for both influenza A and B viruses (von Itzstein 2007). After a clear understanding of the viral infection mechanism, scientists proposed both HA and NA as potential anti-influenza drug discovery targets (von Itzstein 2007; Colman 2009, 2002). However, the concept of developing antivirals to inhibit the function of influenza NA was first proposed by Anderson et al. (1948). The two most commonly used antivirals, zanamivir and oseltamivir are neuraminidase inhibitors (NI) that block the action of NA and inhibit the release of the virus from the host cell (Kim et al. 1997).

2.5 Antiviral drugs and drug resistance

The M2 ion channel protein inhibitors (rimantidine and amantadine) were first antiviral drugs available to treat influenza (Douglas 1990; Pinto et al. 1992; Wintermeyer and Nahata 1995) . Among all influenza strains, the M2 ion channel proteins are present only in influenza A viruses. Hence, these drugs were successfully used to treat influenza A infection (Pinto et al. 1992; Wintermeyer and Nahata 1995). However, the drug usage had serious drawbacks, such as, central nervous system (CNS) side effects and rapid emergence of drug-resistant viral strains (Pinto et al. 1992; Wintermeyer and Nahata 1995). This led to the search for new antiviral drugs. Structural studies with NANA docked into NA crystals revealed that the negatively charged region of the neuraminidase active site aligned well with the C-4-position of NANA. It was believed

that accommodating a positively charged group, in the C-4-position of NANA should enhance its binding to the active site (vonItzstein et al. 1996). After a few synthetic chemistry challenges, zanamivir was developed by replacing the C-4 hydroxyl group in NANA with a functional and positively charged guanidine group. This 4-guanidino-deoxy dehydro N-acetyl neuraminic acid analog of NANA was called zanamivir (Figure 2-3) (Vonitzstein et al. 1993). Zanamivir was found to be highly potent inhibitor of influenza A and B virus strains (Woods et al. 1993; Vonitzstein et al. 1993). However, the important drawback of this drug is that the presence of the guanidine group affects the oral bioavailablility of the drug and hence it is given as a powder which is puffed into the lungs (Colman et al. 1983; Colman 2009; von Itzstein 2007). A second generation zanamivir is being developed. This is a dimer in which two molecules of zanamivir are linked via their 7-hydroxyl groups by an appropriate spacer molecule. The reason for selecting the 7-hydroxyl group is because X-ray crystallography showed that 7-hydroxyl group had no interactions with any of the amino acids in the neuraminidase catalytic site. This dimer potentially has two advantages. The dimer could increase NA binding by 100-fold over zanamivir. Moreover, this could also increase the bioavailability of the drug, allowing the drug to be retained in the body for up to a week. Zanamivir is being administered as 2 doses/day for a period of 5 days. This could be replaced by one dose of the dimer every 5 days (Tucker et al. 2002).

In order to produce an NI that is orally bioavailable for the patients, Kim et al. (1997) synthesized a carbocyclic compound. NA has a large hydrophobic pocket in the active site that interacts with the glycerol side chain of NANA. They replaced the glycerol side chains with more hydrophobic pentyl side chain. Since the C7 hydroxyl groups of the glycerol side chain had no interactions with any of the amino acids binding pocket, this group was replaced by an oxygen atom. They retained the carboxylate and acetamido groups of NANA on this carboxylic compound. Like zanamivir, this compound has a positively charged group at the C4 position. To overcome the disadvantage caused by the guanidine group in zanamivir, an amine group rather than a guanidine group was chosen in this case. However, initial trials with this compound failed to show an increase in bioavailability. The carboxylate group was converted to the ethyl ester. The ethyl ester derivative is the pro-drug (Figure 2-3), which is

hydrolyzed in the liver to release the active carboxylate form of the drug (von Itzstein 2007; Babu et al. 2000).

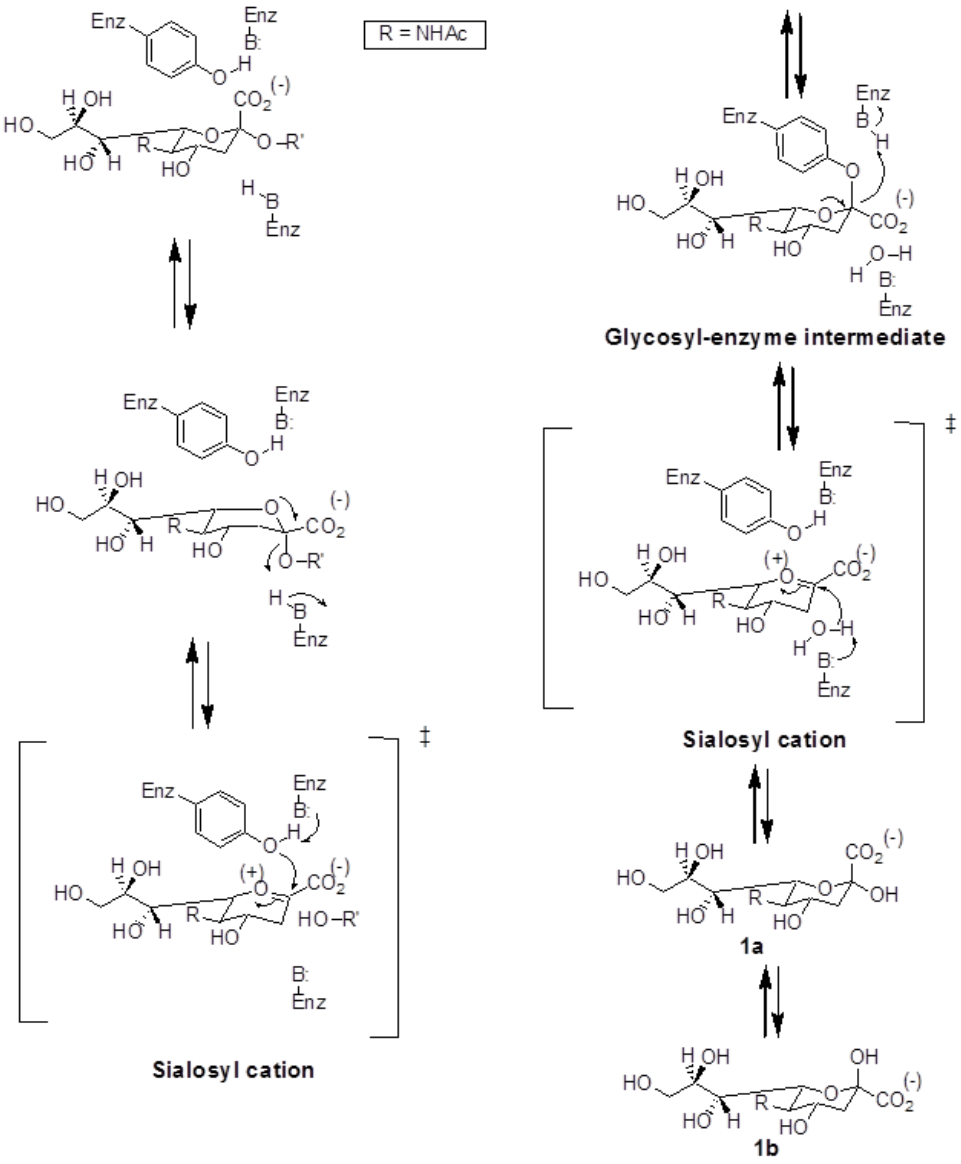

Figure 2-2 : The enzyme's release mechanism (von Itzstein 2007) (Image redrawn using ChemDraw ultra-6).

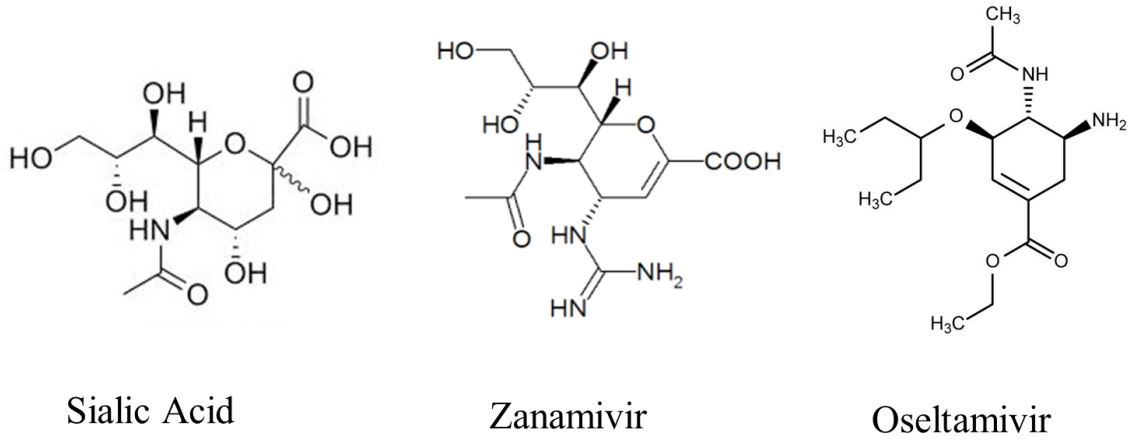

Figure 2-3: The structure of NANA and current antiviral drugs oseltamivir and zanamivir.

Extensive use of these antiviral drugs have led to the virus developing mutations to escape from NI (Russell et al. 2008). Influenza viruses resistant to the NI have been classified as HA mutants (mutants had amino acid sequence changes in the HA and none in the NA) and NA mutants (mutants that had changes in the NA but not in the HA) (Roberts 2001). The HA mutant virus was no longer dependent on NA to release the virus from the host cells, thereby enabling the virus to escape NI. However, animal model experiments suggested that the NA in these mutant strains were susceptible to NI and the NI successfully controlled the spread of infection. This indicated that NA does not only play a vital role in disrupting the receptor to release the virus, but also plays a crucial role in the mobility of the virus through the respiratory tract. Even though HA mutant strains could cleave the virus from the host cell, they were unable to spread the infection across the respiratory tract due to lack of support from NA which were inhibited by NI (Roberts 2001).

Compared with the HA mutant strain, NA mutant strains have proved to be more dangerous. The NI could be rendered ineffective by a single point mutation in their target protein NA. The ability of the virus to cause drug resistance varies with the type of mutation it can carry in NA. For example: H274Y. The recent emergence of influenza A (H1N1) carrying a mutation H274Y in neuraminidase has resulted in antiviral drug resistance (Collins et al. 2009; Trifonov et al. 2009; Wilson 2012; Orozovic et al. 2011; Ives et al. 2002; Le et al. 2005). Oseltamivir has a large

hydrophobic side chain in place of the glycerol side chain of zanamivir and sialic acid. Zanamivir and sialic acid form h-bond with Glu276 through their glycerol groups. When oseltamivir binds, the larger hydrophobic group induces a conformational movement of Glu276 to accommodate the large ligand side chain and produces a binding pocket. This allows Glu276 to rotate and form a salt bridge with Arg224. The presence of His at 274 (found adjacent to Glu276) is very critical for Glu276 to rotate and form the new binding pocket (and form the salt bridge) during oseltamivir binding. However, when the His at 274 has been mutated to Tyr, the Tyr pushes Glu 276 further into the binding pocket, thereby disrupting this conformational change. This in-turn resulted in the failure of oseltamivir (Figure 2-4) (Ferraris and Lina 2008; Smith et al. 2002; Collins et al. 2009). R292K or E119V and R152K in influenza A NA and D198N in influenza B NA are other mutations that has been characterized to potentially decrease the sensitivity of oseltamivir binding (Orozovic et al. 2011; Herlocher et al. 2004).

Alternative drug against other essential influenza viral proteins, such as the RNA polymerase (Tsai et al. 2006), the haemagglutinin protein (De Clereq and Neyts 2007) or the M2 ion channel protein (Ilyushina et al. 2006), are currently under investigation. Investigations on combination therapy are also under progress. This therapy may not only provide new classes of anti-influenza drugs but also reduce the potential of resistance development (Ilyushina et al. 2006). There is also a significant progress in influenza vaccine development (Hasegawa et al. 2007; Carrat and Flahault 2007).

BEFORE MUTATION

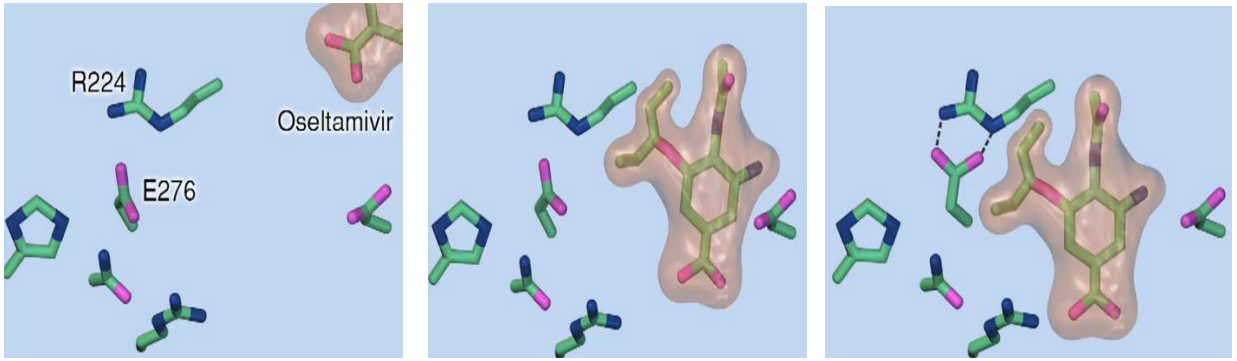

AFTER MUTATION

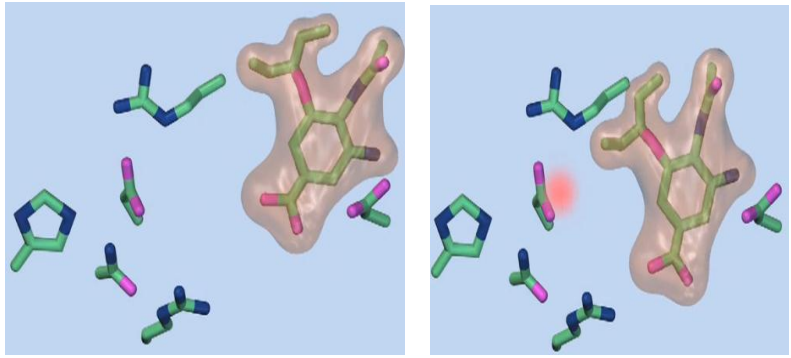

Figure2-4: Influenza-A (H1N1) carrying a mutation H274Y in neuraminidase resulting in antiviral drug resistance. (http://www.youtube.com/watch?v=auEOKWJLSSA 14th January, 2013)

2.6 Recombinant expression and purification of neuraminidase

The impact of influenza pandemic has made it a high public health priority (Collins et al. 2008). The emergence of new antiviral resistant virus strains have resulted in researchers developing extensive interest in studying NA-drug interactions. For this purpose production of large amounts of highly purified tetrametric NA is required. Traditional methods of amplifying influenza virus in eggs and cell culture systems has been problematic because this technique depends on the viability of the virus. Drop in viability results in a significant drop in levels of purity and active NA being obtained (Schmidt et al. 2011). Hence, there is a need to develop an efficient method for recombinant expression and purification of NA (Collins et al. 2008; Dalakouras et al. 2006).

It has also been noted that glycosylation is important for obtaining an active form of NA. For this reason a eukaryotic expression system is required for expressing active NA. Few research groups (Martinet et al. 1997; Yongkiettrakul et al. 2009) have used yeast expression system to express NA. Few other research groups have used insect cells for NA expression (Mather et al. 1992; Deroo et al. 1996; Oakley et al. 2010; Dalakouras et al. 2006). The vital point to note here is Deroo et al. (1996) have obtained soluble NA (secreted in to the cell culture media), while Dalakouras et al. (2006) have had to lyse the cells using detergent to obtain soluble NA, although they have used the same expression system. However, both groups managed to obtain the active form of NA. Deroo et al. (1996) have demonstrated its application as a potential vaccine in a mouse-model system. They have also managed to develop a purification technique to obtain biologically and immunologically active NA. The first step in NA purification was ammonium-sulphate fractationation followed by ion exchange chromatography, size exclusion chromatography and finally affinity chromatography with N-(p-aminophenyl) oxamic acid-agarose. The purified NA existed as tetramers, dimers, and small amounts of monomers. Among which only the tetramers were enzymatically active. Sodium dodecyl sulfate polyacrylamide gel electrophoresis (SDS-PAGE) analysis in the presence of β-mercaptoethanol resulted in a 55 kDa band. This could be due to complete denaturation of NA to a monomeric form. In the absence of a reducing agent NA migrated to 110 kDa band on SDS-PAGE. This indicated that the protein is internally linked by disulfide bridges that form dimer, which further

associates by non-covalent interactions to form a tetrameric active form of the protein (Deroo et al. 1996). Similar SDS-PAGE results showing a molecular mass around 55 kDa under reducing conditions and masses around 110 kDa under non-reducing conditions were reported by Wu et al. (2009), suggesting that the dimer contained two monomers linked by a disulphide bond, while the tetramer was a dimer of dimer.

Dalakouras et al. (2006) have expressed NA in expresSF+ insect cells using a baculovirus expression system. The expressed NA was found in the cell pellets in this case. The pellets were lysed to purify NA. They have developed a 'lock and key' (LAK) affinity resin which consists of phenylalanine and isoleucine bound to a trichlorotriazine ring for a single step affinity purification. The purity was reported to have increased by a factor of 343 with a recovery of 391% based on activity.

NA has also been purified using affinity tags. It has been reported that that modifications of the NA stalk with tags could affect the activity of the enzyme (Yano et al. 2008). Researchers (Schmidt et al. 2011; Castrucci et al. 1992) have found a negative impact on the enzyme activity due to the stalk modification. Schmidt et al. (2011) have demonstrated that the presence of FLAG in close proximity to the NA head disturbs the assembly of functional tetramers. This could be due to the electrostatic repulsion caused be the accumulation of 20 (4 FLAG tags) negatively charged aspartic acids resulting in the formation of catalytically inactive monomeric and dimeric NA. Although affinity tags interfere with the tetramerization of the protein, placing the affinity tag at the N-terminus of the recombinant NA could avoid interference with the formation of functional tetrameric NA (Xu et al. 2008).

Although both yeast and insect cell expression systems have been used to express active NA, yet the major drawback has been the low yield of active NA. However, insect cells have been used more often than yeast for expressing NA. Hence, insect cell expression system was used in this thesis. Moreover, usage of affinity tags does seem to have an effect on the activity of NA. Hence, affinity tags were not used in this thesis work.

2.7 Activity assay

NI drugs have become an important approach in the fight against influenza, particularly during early-stage. Hence, it is important to monitor the sensitivity NIs to the currently circulating strains. For initial screening studies, plaque reduction assay (PRA) is performed to detect a broad range of resistant influenza phenotypes. However, PRA has not been used successfully to determine the sensitivity of NI. The NI prevents the release of virus from infected cells, this leads to the formation of smaller plaques in a PRA. This reduction in plaque size can be used to evaluate drug sensitivity. However, the main limitation of this assay is that many clinical isolates do not form plaques well. Hence, this assay was considered unreliable to determine whether the NIs are resistant or sensitive to a particular influenza strain (Tisdale 2000; Wetherall et al. 2003). This unreliability exhibited by the cell-based assays for susceptibility monitoring of viruses from clinical isolates led to the development of a biochemical inhibition assay (Gubareva et al. 2000; Gubareva et al. 1998). A biochemical assay performed in a 96-well microtiter plate has been used successfully to detect enzyme activity. This assay has also been extended to determine sensitivity of NI drugs. The most commonly used substrate for detecting enzyme activity and inhibition is the fluorogenic 2′-(4-methylumbelliferyl)-α-d-N-acetylneuraminic acid known as MUNANA (Figure 2-5) (Wetherall et al. 2003). The use of this substrate was initially described by Potier et al. (1979). Cleavage of MUNANA by neuraminidase in the test sample releases a fluorescent substance called methylumbelliferone (Figure 2-6). The amount of fluorescence detected is directly propotional to the amount of enzyme activity. Currently, there are several fluorometric enzyme assays used in practise that work by the same principle, with varying MUNANA concentration and assay buffers (Wetherall et al. 2003). In enzyme kinetics the two constants, V_m and K_m, are important to understand enzyme activity and the effects of different types of enzyme inhibitors.The maximal velocity, or V_m, reflects how fast the enzyme can catalyze the reaction, while describes the substrate concentration at which half the enzyme's active sites are occupied by substrate. A high Km means a lot of substrate must be present to saturate the enzyme, meaning the enzyme has low affinity for the substrate. On the other hand, a low Km means only a small amount of substrate is needed to saturate the enzyme, indicating a high affinity for substrate. In most experiments, IC_{50} values of the NI

drugs are determined. This value corresponds to the concentration of the inhibitor required to inhibit 50% of the enzyme reaction. In general, the lower the IC_{50} value, the stronger is the inhibitory effect. Time dependant enzyme assays were also performed to determine the inhibition constant (k_i). The k_i, values were used to evaluate the effectiveness of the inhibitor. Similar to IC_{50} , the lower the magnitude of k_i, the more effective is the inhibitor. Collins et al. (2008) have used the time dependent fluorometric enzyme assay for measuring the kinetics of NI drugs and NA interaction. Kinetic data obtained from fluorometric enzyme assay were used to determine which of the two commonly used NI drugs could serve as potential inhibitor to treat a particular mutant strain. Based on their kinetic data (Table 2-1) they have concluded that zanamivir is a more potent inhibitor than oseltamivir for the mutant stains they studied.

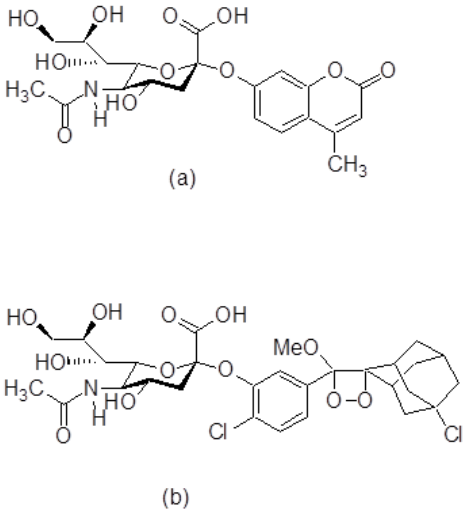

Figure 2-5: Structures of commonly used substrates in NA activity assay and susceptibility monitoring a) MUNANA b) 1,2-dioxetane derivative of sialic acid (Image redrawn using ChemDraw ultra-6.

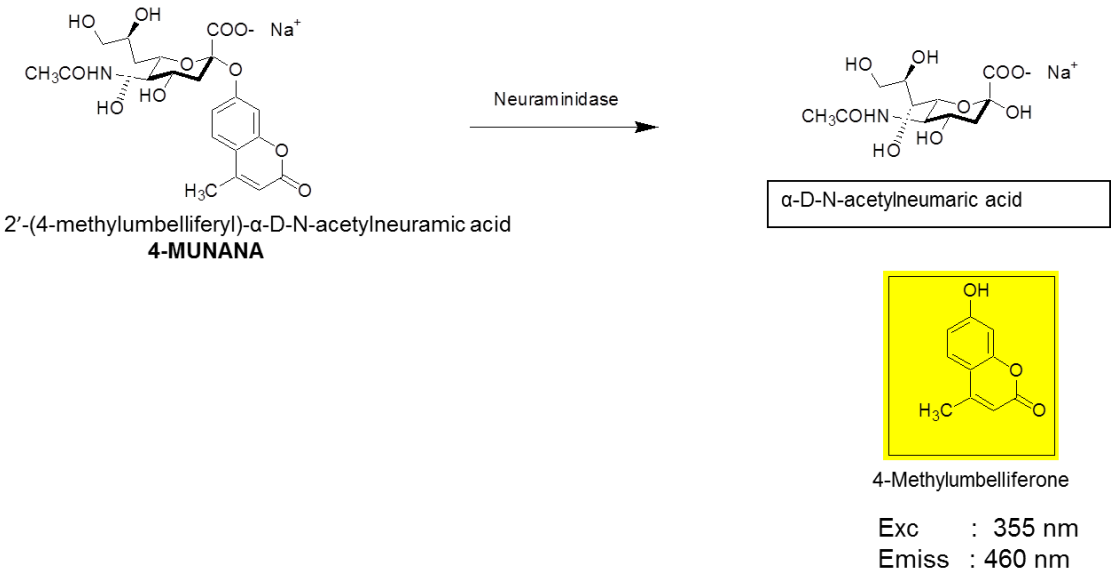

Figure 2-6: Schematic diagram for MUNANA activity assay described by Potier et al. (1979). (Image redrawn using ChemDraw ultra-6).

Table 2-1: Kinetic parameters for N1 neuraminidase adapted from Collins et al. (2008)

NA type	**V_m Relative to wild type**	**K_m (µM)**	**Oseltamivir relative K_I***	**Zanamivir relative K_I +**	**k_{on} ($\mu M^{-1} s^{-1}$) Oseltamivir**	**k_{off} (s^{-1}) Oseltamivir (x 10^4)**	**k_{on} ($\mu M^{-1} s^{-1}$) Zanamivir**	**k_{off} (s^{-1}) Zanamivir (x 10^4)**
Wild-type	1.0	6.3	1.0	1.0	2.52 (0.21)	8.1 (1.2)	0.95 (0.08)	0.95 (0.13)
His274Tyr	0.8	27.0	256	1.9	0.24(0.06)	180(30)	0.35(0.02)	0.67(0.08)
Asn294Ser	1.15	53.0	81	7.2	1.1(0.18)	235(40)	0.52(0.04)	3.7(0.6)
Tyr252His	0.94	7.5	0.1	1.2	3.9(0.15)	1.25(0.13)	1.38(0.15)	1.66(0.33)

k_{on} and k_{off} are the association and dissociation rate constants, respectively.

* Oseltamivir relative K_I is K_I (mutant)/ K_I (wild type), where wild type = 0.32 nM.

+Zanamivir relative K_I is K_I (mutant)/ K_I (wild-type), where wild type = 0.1 nM.

Gubareva et al. (2002) tested the performance of four commonly used modifications for the MUNANA assay, to investigate whether the inhibition assay sensitivity would change with the change of buffer system and concentration of MUNANA. Table 2-2 describes the buffer systems and MUNANA concentrations of the four assay systems tested by Gubareva et al.

Table 2-2: Modified NA inhibition assays tested by Gubareva et al. (2002)

Assay	**Buffer system**	**Ca2+ mM**	**MUNANA substrate µM**	**Reference**
I	0.1 M sodium phosphate, pH 5.9	6.8	1000	(Gubareva et al. 1998; Gubareva et al. 2000; Mitnaul et al. 1996; Goto et al. 1997)
II	0.033 M MES, pH 6.5	4	100	(Relenza ™ : Laboratory manual, 2000)
III	0.033 M MES, pH 6.5	4	75	(Bantia et al. 2000)
IV	0.1 M sodium acetate	10	100	(Blick et al. 1995; McKimm-Breschkin et al. 1998)

Table 2-3: Assessment of zanamivir susceptibility of influenza viruses adapted from Gubareva et al. (2002)

Virus type and NA subtype	**Amino Acid**	**AssayI**		**Assay II**		**Assay III**		**Assay IV**	
		IC_{50}	**Fold**	**IC_{50}**	**Fold**	**IC_{50}**	**Fold**	**IC_{50}**	**Fold**
	Glu 119 Arg 292 (wt)	3	1	2	1	2.5	1	3	1
	Gly 119 Arg 292	1000	333	400	200	100	40	210	70
	Ala 119 Arg 292	1250	417	200	100	50	20	150	50
	Asp 119 Arg 292	10,000	3333	700	350	150	60	350	117
A/N2	Glu 119 Lys 292	35	12	18	9	20	8	24	8
	His 274 (wt)	2	1	0.9	1	1.5	1	1.5	1
A/N1	Tyr 274	2.5	1.3	1	1.1	1.8	1.2	2	1.3
	Arg 152 (wt)	3.2	1	3.2	1	3.3	1	3	1
B	Lys 152	10,000	3125	220	69	100	30	100	33

Table 2-4: Assessment of oseltamivir susceptibility of influenza viruses adapted from Gubareva et al. (2002)

Virus type and NA subtype	**Amino Acid**	**Assay I**		**Assay II**		**Assay III**		**Assay IV**	
		IC_{50}	**Fold**	**IC_{50}**	**Fold**	**IC_{50}**	**Fold**	**IC_{50}**	**Fold**
A/N2	Glu 119 Arg 292 (wt)	0.9	1	0.2	1	0.4	1	0.3	1
	Gly 119 Arg 292	1	1.1	0.6	3	0.5	1.3	0.3	1
	Ala 119 Arg 292	24	27	3	15	1.1	2.8	1	3.3
	Asp 119 Arg 292	3	3.3	1.3	6.5	0.5	1.3	2.7	9
	Glu 119 Lys 292	>1000[e]	>1000	3000	15,000	3750	9375	5000	16,666
A/N1	His 274 (wt)	2	1	0.9	1	2	1	0.9	1
	Tyr 274	>1000	>500	800	890	450	225	350	390
B	Arg 152 (wt)	40	1	28	1	4.3	1	8	1
	Lys 152	>1000	>25	1500	54	750	174	600	75

The results were analysed based on the IC_{50} values that were determined from the assays. It was interpreted that a mutant virus has developed resistance to a particular NI drug, if the IC_{50} is consistently higher than for the wild type virus. They have also compared the assays with a parameter called "fold", which is the ration between the IC50 values of a mutant viruses to that of the corresponding wild type virus (mutant IC_{50} / wild type IC_{50}) (Gubareva et al. 2002). The inhibition assay results are presented in Table 2-3 & Table 2-4. For zanamivir inhibition, the results from all four assay systems showed no substantial difference in zanamivir sensitivity to the wild-type A (N1 and N2) and B viruses. This consistency was also observed in the oseltamivir-resistant virus with an NA containing a His274Tyr mutation. However, with the zanamivir resistant viruses, the assay results were not so comparable. The results show that assay I was more sensitive, while assay III was the least sensitive among the four. The sensitivity of the assays II and IV for zanamivir resistant viruses were found to be in between the IC_{50} determined from assays I and III. For the oseltamivir inhibition assay, all four assays consistently demonstrated resistance to oseltamivir with the oseltamivir-resistant mutant (His274Tyr). However, significant differences in the IC_{50} values were observed. These values varied from 350 nM to more than 1000 nM. Also in each assay, the wild-type virus (N1) was found to be sensitive to the drug (range, 0.9–2 nM). In addition to this, the sensitivity of the wild-type B virus to oseltamivir was highly inconsistent. The IC_{50} values were much lower in assays III (4.3 nM) and IV (8.0 nM) than assays I (40 nM) and II (28 nM). This also indicated that the sensitivity of antivirals varied, depending on assay conditions (Gubareva et al. 2002).

Monitoring resistance relies mainly on the enzymatic assay. There is a high level of inconsistency exhibited by the MUNANA assays currently in practice. This lead to the development of a more sensitive chemiluminescent (1, 2-dioxetane derivative of sialic acid, NA-STAR) substrate (Figure 2-5). The chemiluminescence enzyme assay showed up to 67-fold higher sensitivity for NA detection than the fluorometric enzyme assays. However, the chemiluminescent substrate is a flash emitter with a half-life of 5 min and the signal intensity must therefore be measured immediately (Wetherall et al. 2003). This calls for a high level of technical competence to perform the assay, which otherwise might give false positive or false negative results. This limitation has been the major reason for not using this substrate to monitor drug resistance. Hence, the need for a simple and a reliable assay to monitor drug resistance has still not been satisfied.

The ultimate aim of this thesis is to develop a simple, label free, real time reliable surface plasmon resonance assay that could be used to monitor NI drug resistance.

2.8 Molecular docking

Molecular docking simulation is a useful theoretical tool for analyzing the binding of a ligand to a protein (Liu et al. 2010) and is mainly aimed at finding the lowest possible energy for the ligand-receptor complex (Sengupta et al. 2007; Chen and Shoichet 2009). In molecular docking simulation, a coulombic van der Waals interaction-energy score is computed based on the charge-charge, charge-dipole and dipole-dipole interactions between the ligand and protein (Shukla et al. 1995; Gadakar et al. 2007; Zhong et al. 2009). This score is used in the comparison of the binding of different ligands with a given protein. However, in order to identify favourable interactions, the Gibbs free energy change (ΔG) must be determined. ΔG can be determined by the following scheme (Equations 2-1 - 2- 4) (Sengupta et al. 2007; Chen and Shoichet 2009; Kuhn and Kollman 2000).

$$\Delta \boldsymbol{G} = \Delta \boldsymbol{H} - \boldsymbol{T}\Delta \boldsymbol{S} \qquad \textit{(2-1)}$$

The change in enthalpy (ΔH) can be determined from the non-bonded and bonded interaction energy values (Equation 2-2). Here, E_{ele} and E_{vdw} are the coulomb and van der waals energies, respectively (Liu et al. 2010; Chong et al. 2009), which represent the non-bonded interaction energy values. The bonded interaction (hydrophobic interaction and hydrogen bonding) energies are represented by $E_{hydrophobic}$ and $E_{hydrogen\ bond}$. The total ΔH is defined as

$$\Delta \boldsymbol{H} = \boldsymbol{E}_{\boldsymbol{ele}} + \boldsymbol{E}_{\boldsymbol{vdw}} + \boldsymbol{E}_{\boldsymbol{hydrophobic}} + \boldsymbol{E}_{\boldsymbol{hydrogen\ bond}} \qquad \textit{(2-2)}$$

On binding, the system becomes more ordered because of reduced rotation, torsion, and side chain flexibility of the receptor (Shukla et al. 1995; Santos-Filho and Cherkasov 2008), resulting in a change in the entropy of the system. This can be calculated from the rotational and torsional energy values (Equations 2-3 and 2-4).

$$-\boldsymbol{T}\Delta \boldsymbol{S} = \boldsymbol{E}_{\boldsymbol{rotational}} + \boldsymbol{E}_{\boldsymbol{torsion}} \qquad \textit{(2-3)}$$

$$\boldsymbol{E}_{\boldsymbol{torsion}} = \boldsymbol{E}_{\boldsymbol{bond\ length}} + \boldsymbol{E}_{\boldsymbol{bond\ angle}} \qquad \textit{(2-4)}$$

Among the several docking programs available for studying protein-ligand interactions, the most commonly used programs are AutoDock, Discovery Studio and Schrödinger. The docking programs follow the lock and key model for predicting the the best conformation a protein can take to accommodate a ligand. However, it is important to note that protein-ligand interactions cannot be completely described by a rigid lock and key model. The docking programs should have the ability to account for flexible side chain movements during protein-ligand interaction. The grid-based ligand docking with energetics (GLIDE) module and the induced fit docking (IFD) module of Schrodinger program allows the user to study rigid and flexible docking respectively. It is for this reason Schrodinger Suite™ 2010 docking program was used in this thesis.

2.9 Overview of baculoviruses

Baculoviruses are viruses known to infect the insect cells. These viruses posses double-stranded, circular, supercoiled DNA molecules enclosed in a rod-shaped capsid. Among the 500 baculovirus that have been identified, autographa californica multiple nuclear polyhedrosis virus (AcMNPV) and bombyx mori (silkworm) nuclear polyhedrosis virus (BmNPV) are the most commonly used viruses for foreign gene expression (Hitchman et al. 2009; Smith et al. 1983; Volkman and Summers 1977; Volkman et al. 1976). The expression of foreign genes by infecting insect cells with the baculoviruses is popularly called as baculovirus expression vector system (BEVS). Currently BEVS are extensively used for expressing recombinant proteins (Smith et al. 1985; Pennock et al. 1984). The BEVS is a eukaryotic expression system. Hence, it possesses several advantages over the traditional bacterial expression systems, such as, the BEVS enables many protein processing and modification present in higher eukaryotic cells. Unlike the bacterial system, majority of proteins remains soluble in BEVS (Hitchman et al. 2009; Volkman and Summers 1977; Volkman et al. 1976).

The virus enters the insect cells by a process called endocytosis. The virus sheds its genetic material in the host cell nucleus for replication and viral assembly. Two types of viral progeny are generated, namely, budded virus (BV) and occlusion- derived virus (ODV) (Figure 2-7). The BVs have a rod shaped nucleocapsid [(35–40) x (200–400) mm in dimensions] surrounded by a lipid envelope. The 134 kb circular double stranded DNA is surrounded by the core protein p39 and major envelope protein gp64 (Ayres et al. 1994). Both *in-vivo* and *in-vitro*, the BV is responsible for the spread of

infection through cell-to-cell transmission of the virus. The ODVs are produced in the later stages of the infection and are covered by polyhedral protein, which protects the virus particles from proteolytic inactivation (Miller et al. 1983; Rohrmann et al. 1982). Among the two commonly used viruses (AcMNPV and BmNPV), the AcMNPV baculovirus is extensively used for recombinant protein expression by infecting commercial insect cell lines.

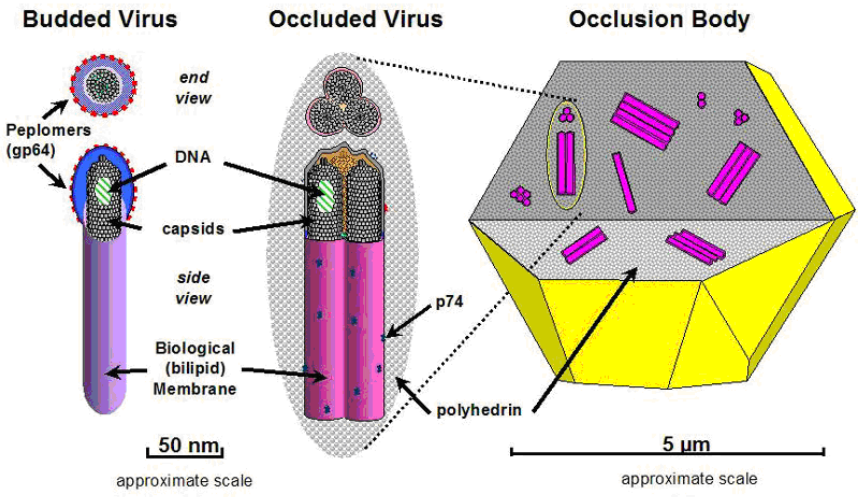

Figure 2-7: Types of virus progeny generated during virus replication and assembly in the host cell system (drawn by Dr D. Lynn, USDA, Agricultural Research Service, US). Reproduced from Wikipedia, The Free Encyclopedia, 14th May, 2011.

2.10 Commercial insect cell lines for baculovirus expression systems

Sf21 and Sf9 insect cells are commonly used cell lines for baculovirus expression systems. Sf21 cells were originally derived from the ovarian cells of the fall army worm (Spodoptera frugiperda), while Sf9 cells are a clonal isolate of Sf21 cells. The High-five™ cell line is another predominantly used cell line derived from the ovarian cells of cabbage looper (Trichoplusia ni) (Hink 1970, 1973). Successful culture of insect cells requires a basic familiarity with insect cell morphology and general cell culture methods. Table 2-5 describes the cell morphology of three widely used cell lines.

Table 2-5: Insect cell lines commonly used in BEVS applications.

Insect Species	**Cell Line**	**Cell morphology**
Spodoptera frugiperda	Sf9	Spherical with some granular appearance—regular in size. Firm attachment to surfaces
Spodoptera frugiperda	Sf-21	Spherical with some granular appearance—different sizes. Firm attachment to surfaces
Trichoplusia ni	High-Five™	Spherical with some granular appearance—different sizes. Loose attachment to surfaces

Insect cell lines are cultured either as suspension cultures in shake flasks, or monolayer cultures in T-flasks at 28°C. The present day commercially-available serum-free media (SFM), such as Sf-900 II SFM and Express-five™ SFM have few advantages over serum supplemented media. Unlike the serum-supplemented media which possess nutritional deficiencies, SFM contains amino acids, carbohydrates, vitamins and lipids required for cell growth. Continuous supply of essential nutrients results in faster cell doubling time and promotes high cell densities. This becomes a very crucial factor during recombinant protein production resulting in higher protein yields (Invitrogen Instruction manual).

2.11 Baculovirus expression system

In nature the baculovirus expresses very high levels of polyhedron proteins. In the baculovirus expression system, recombinant baculoviruses are generated by replacing the polyhedrin gene with a foreign gene through homologous recombination. To produce a recombinant virus, firstly the gene of interest (GOI) is cloned into a transfer vector. Selecting a suitable transfer vector depends on the type of technology used for generating recombinant viruses.

1. ***flashBAC:*** This technology was developed by Oxford Expression Technologies Ltd, Oxford, UK. The baculovirus transfer vectors in this case contain the polyhedrin promoter followed by restriction enzyme recognition sites for cloning the GOI. Once the GOI is cloned into the transfer vector, the gene is flanked by viral-specific sequences at 5 ′ and 3 ′ ends. The flashBAC™ DNA

contains an AcMNPV genome that lacks an open reading frame (ORF) 1629 and contains a bacterial artificial chromosome (BAC) replacing the polyhedrin gene. The essential gene deletion prevents virus replication within insect cells. When the insect cells are co-infected with the a transfer vector containing the GOI and flashBAC™ DNA, homologous recombination takes place. This restores the function of the essential gene which is necessary for viral DNA replication and simultaneously inserts the GOI under the control of the polyhedrin gene promoter, replacing the BAC sequence (Figure 2-8). In this case the survival of the non-recombinant virus is not possible. This reduces the time and effort required for screening recombinant viruses (Invitrogen Instruction manual).

2. **Bac-to-Bac:** This method is based on site-specific transposition technology. The GOI is cloned into a donor plasmid (eg: pFastBac™) that possess a mini-Tn7 gene. This recombinant plasmid is then transformed into DH10Bac™ bacterial competent cells. The competent cells contain a baculovirus shuttle vector called the bacmid. The bacmid contains a kanamycin resistance gene, a lacZα gene and a short segment called the bacterial transposon Tn7 (mini-attTn7) which helps in site-specific transposition. The bacteria also contain a helper plasmid that encodes for transposase (gene that supports the site-specific transposition). Successful transposition results in recombinant bacmids. Recombination results in the disruption of the lacZα gene. Recombinant colonies are identified by blue and white colony selection method. DNA from selected *E. coli* clones containing the recombinant bacmid are extracted and used to transfect insect cells (Figure 2-9) (Invitrogen Instruction manual).
3. **BaculoDirect:** In this method the GOI is cloned into an entry clone containing attL sites. The BaculoDirect™ Linear DNA (detination vector) contains attR sites. Recombination of an attL site in the entry clone with an attR site in the destination vector results in the formation of attB-containing expression clone (Figure 2-10). The LR Clonase™ II enzyme is used to catalyze this reaction. The resulting recombinant baculovirus can be used to infect insect cells for protein expression (Figure 2-10) (Invitrogen Instruction manual).

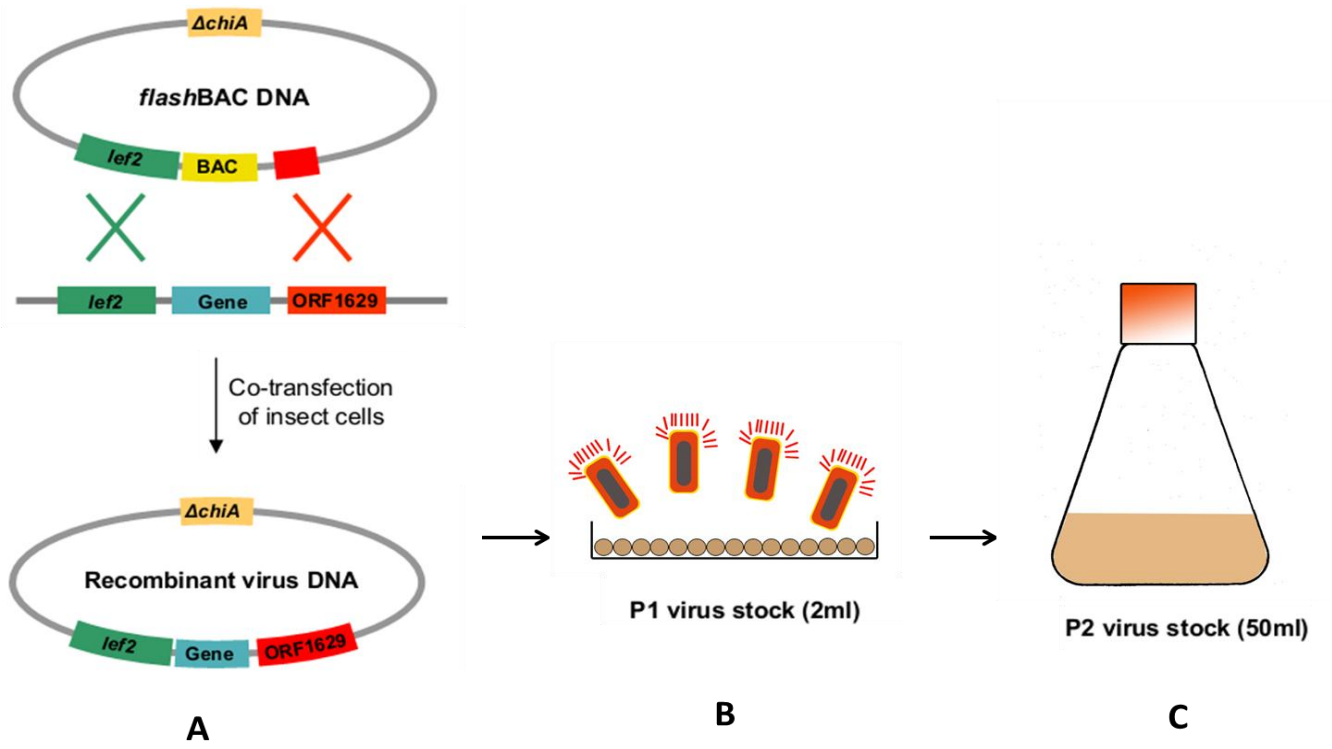

Figure 2-8: Schematic showing various stages of protein expression using of flashBAC™ system. A) Homologous recombination inside the insect cells resulting in the formation of recombinant virus. B) P1 stock containing recombinant baculovirus. C) P1 stock is then used to infect a larger volume of insect cells (50 mL) to produce P2 recombinant virus stock. This stock is then used for large scale protein expression.

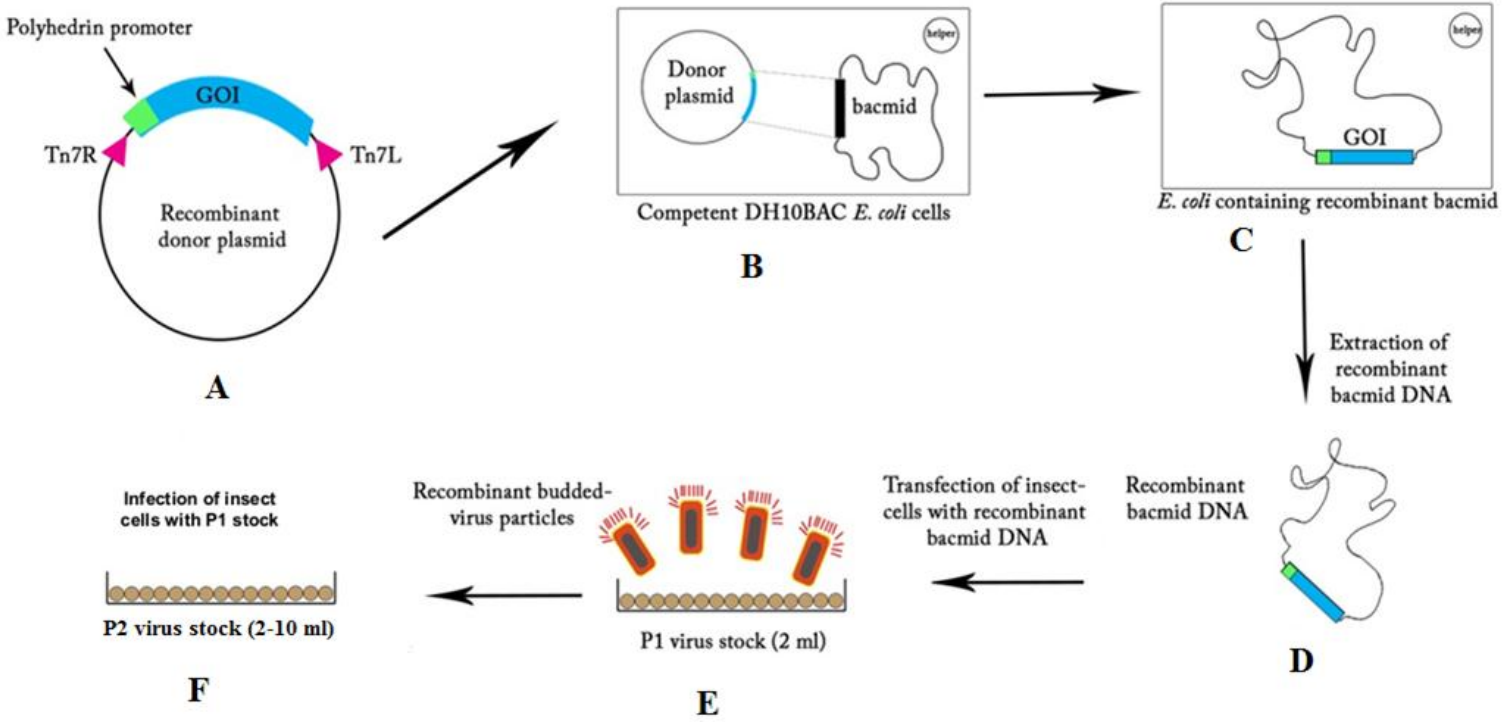

Figure 2-9: Schematic representation of stages of protein expression using Bac-to-Bac system. A) The GOI is cloned into a donor plasmid containing a promoter and mini-Tn7 gene. B) The recombinant donor plasmid is transformed into DH10Bac™ bacterial competent cells for the recombinant bacmid formation. C) The recombinant bacmid is extracted D) and used to transfect insect cells. E) P1 virus stock is generated. F) Higher volume (2 to 10 mL) of insect cells is infected with P1 stock to generate P2 stock.

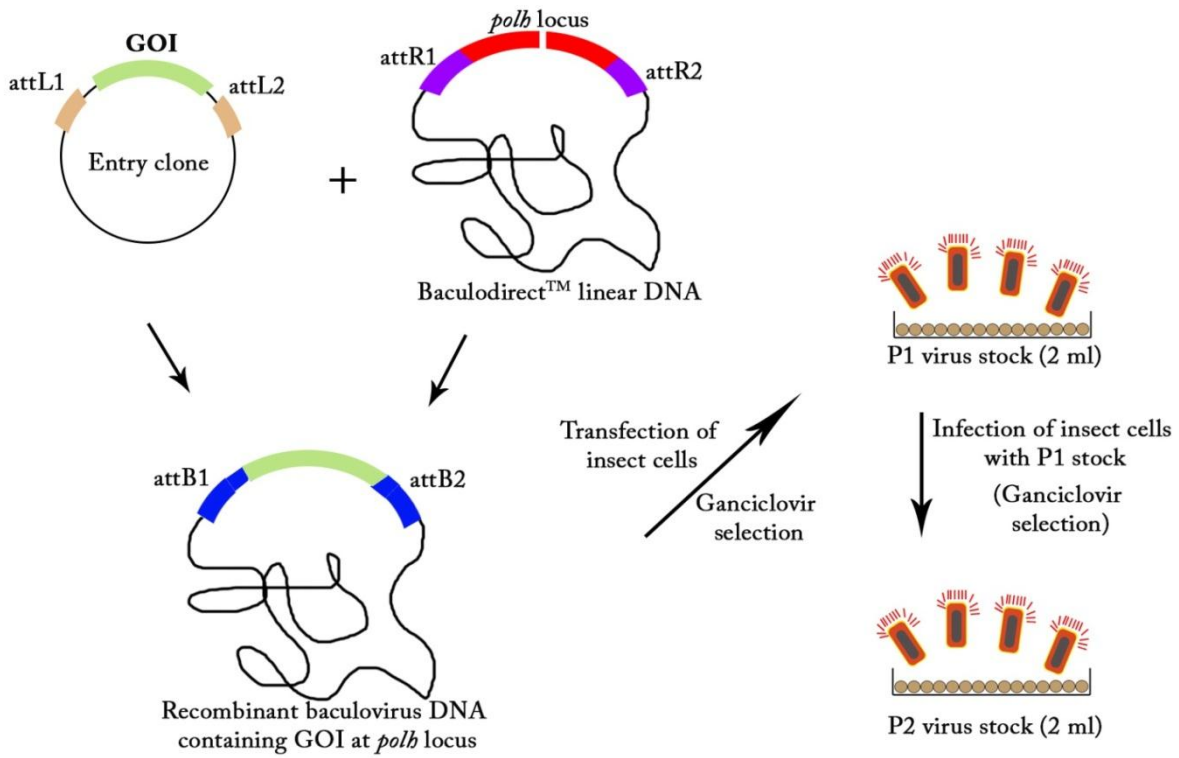

Figure 2-10: Schematic representation of stages of protein expression using BaculoDirect™ system. A) Recombinant baculovirus is generated using an LR reaction between the entry clones carrying the GOI and BaculoDirect™ Linear DNA. B) P1 virus stock is generated by transfecting the insect cells with the recombinant baculovirus and subsequent selection with ganciclovir. C) P1 stock is used to generate high.

2.12 Surface plasmon resonance

SPR is an optical biosensor technique. The initial practical work with SPR was started by Kretschmann back in 1971 (Liedberg et al. 1995). In 1983 Liedberg et al., for the very first time used the SPR as a biosensor (Liedberg et al. 1995). Today, SPR technology has grown tremendously and is being used for measuring various biomolecular interactions such as protein-protein, antigen-antibody and receptor-ligand interactions (Lee et al. 2008; Navratilova and Myszka 2006).

2.13 SPR principle

The surface of the SPR chip has a metal coating with either gold or silver. The binding events on a SPR chip are detected by angular modulation or wavelength modulation. In wavelength modulation, the photon of light incident on the metal surface comes in resonance with the wavelength of metal on the surface of the chip, when their wavelengths equal one another. Binding of macromolecules such as proteins or antibodies to the surface bound ligand, results in a change in resonance wavelength (Figure 2-11). This shift in the wavelength corresponds to the refractive index (RI) change, which is detected by the optical detection unit and quantified as SPR sensogram (Figure 2-12) (Mitchell 2010). In angular modulation, a monochromatic light strikes on the metal surface. At a specific angle a part of the light energy is converted to electron waves that travel along the chip surface. This travelling electron wave is called surface plasmon (Fee 2013). The specific angle at which this phenomenon occurs depends on the difference in RI between the glass and aqueous sides of the metal layer. Binding of macromolecules on the metal layer leads to change in refractive index. This in turn alters the angle of light energy associated with the surface plasmon wave. The optical detectors detect the angle of lowest reflected light intensity, which corresponds to the amount of macromolecule bound to the metal surface (Homola et al. 1999; Abdulhalim et al. 2008). The ProteOn XPR36 protein interaction system (Bio-Rad Laboratories, Hercules, CA, USA) used in this thesis works on the angular modulation.

While studying the interaction between two biomolecules, the relative change in the mass of the biomolecules absorbed on the surface is measured from the beginning of the SPR experiment. The change in RI is proportional to the mass of the analyte interacting with the ligand (Homola et al. 1999; Mitchell 2010; Baac et al. 2006). In a

typical SPR sensogram the change in RI, refractive index units (RIU), is represented as resonance units (RU), where 1 RU = 1 x 10^{-6} RIU (Mitchell 2010). SPR has been widely used to determine the binding kinetics of biomolecular interactions. This allows us to gain more insights into the mechanism of interaction taking place in biomolecules. Considering a 1:1 stoichiometry, the response is proportional to concentration of complex formed on the surface of the chip (Štěpánek et al. 2006). In case where the analyte has occupied all the surface bound ligand, a maximum RU (R_{max}) is reached. Once R_{max} is achieved, further increase in the analyte concentration will not change the response.

2.14 SPR biosensor experiment

A typical SPR experiment has three major steps,

A) Ligand immobilization

Ligand molecules are immobilized to an SPR sensor chip surface using several techniques, such as covalent immobilization, affinity capture to a specific capturing molecule and adsorption of lipid bilayers. The commonly used covalent immobilization techniques are, amine coupling, thiol coupling, aldehyde coupling and biotin-streptavidin coupling. Amine coupling is the most extensively used coupling technique (Homola et al. 1999; Mitchell 2010). The Bio-Rad Laboratories, Hercules, USA provides three amine coupling ProteOn™ sensor chips. These chips posses a modified (carboxylated) alginate layer coated on top of the gold surface of the sensor prism. When activated using N-hydroxysuccinimide (NHS) and N'-(3-dimethylaminopropyl) carbodiimide hydrochloride (EDC), this layer provides a net negative charge for ligand immobilization. It is absolutely critical measure the functional integrity of the immobilised ligand. This is can be tested by injecting an analyte that binds to immobilized ligand. The ability of the analyte to bind to its natural ligand is a useful evidence that the immobilised ligand is functionally active. A control surface is required to compensate the effect of non-specific binding of the analyte and background response. A control surface can be generated by immobilizing an inactive ligand (like BSA). If a control with inactive ligand is not available, a control surface can be generated by just activating and deactivating the surface.

B) Interaction analysis

The interaction between the analyte and ligand involves three steps. Firstly, the association phase, starts when the analyte is injected. When the analyte is in correct orientation, the ligand recognizes the analyte and binding occurs. Binding of analyte to the ligand involves two stages. Firstly, the analyte is transferred to the chip surface from the solution phase, this is known as mass transfer. Finally, the analyte binds to the ligand. Therefore, calculated kinetic constants under this condition represents the mass transfer rate and not the true binding kinetics. The best way to minimize mass transfer is to immobilize less ligand. When the injection of analyte continues, the binding reaches equilibrium, where the rate of association equals the rate of dissociation. When the analyte injection stops, the buffer injections begin. This allows the analyte to dissociate from ligand (Oshannessy et al. 1993; Huang et al. 2006).

C) Regeneration of the sensor surface

A good regeneration technique is important for biosensor assay reproducibility. Repeated analysis on the same ligand bound surface allows the user to reduce the cost of the assay. This requires a method to remove the analyst bound to the immobilized ligand, without disrupting the activity of the ligand. The most commonly used regeneration buffers are 10-100 mM HCl or 10 mM Glycine-HCl pH 1.5-3.0. The ligand- analyte complex is subjected to the low pH buffer for a very short time (18 s). This is sufficient to partly unfold the analyte thereby making the binding site no longer available for the ligand to recognize (Štěpánek et al. 2006; Mitchell 2010).

2.15 Application of surface plasmon resonance in virus detection

The detection of large pathogens such as bacteria using SPR can create a difficult situation because the typical size of a bacterium is approximately 1–5 μm, while the penetration depth of the SPR field is only 100 nm. This places the majority of the cell outside the SPR field (Rich and Myszka 2008). This in turn reduces the capability of the SPR to immobilize the bacterium on the chip and follow the binding of antigens to the target bacterium (Rich and Myszka 2006; Abdulhalim, Zourob et al. 2008). However, immobilizing the antigen(s) on the SPR chip and binding the bacterium should result in large SPR signals. This technique has also been extended to virus detection.

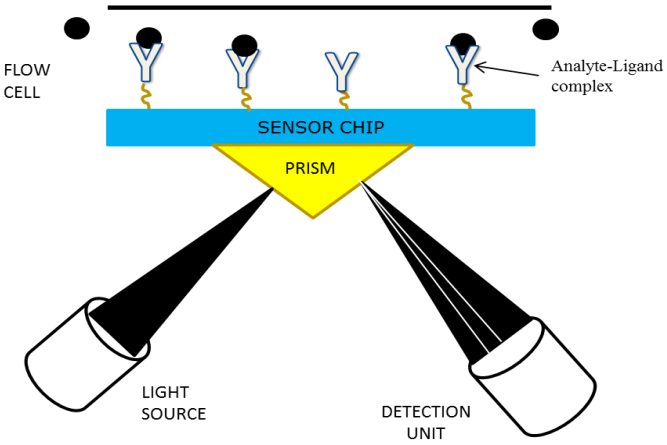

Figure 2-11: A schematic of optical configuration of SPR biosensor. Binding of analyte to surface bound ligand, results in refractive index (RI) change, which is detected by the detection unit and quantified as SPR sensogram.

In early 1997, a real-time molecular diagnosis of human immunodeficiency virus type I (HIV-I) was performed using SPR technology (Bianchi et al. 1997). A biotinylated HIV-1 oligonucleotide probe was immobilized on a sensor chip and a single stranded DNA obtained by asymmetric polymerase-chain reaction (PCR) was passed over the surface as the analyte and hybridization was detected by SPR, giving a simple, fast and reproducible diagnostic procedure for the detection of HIV-1 (Bianchi et al. 1997).

SPR biosensor has been for medical diagnosis of human hepatitis B virus (hHBV) in serum samples (Chung et al. 2005). The hepatitis B surface antigen (HB_SAg) was immobilized on the SPR chip using the standard amino coupling technique. Serum samples from patients containing hHBV antibodies were used as analytes. The detection limit of the SPR biosensor was found to be comparable to that of ELISA for the medical diagnosis of hHBV antibodies (Chung et al. 2005)

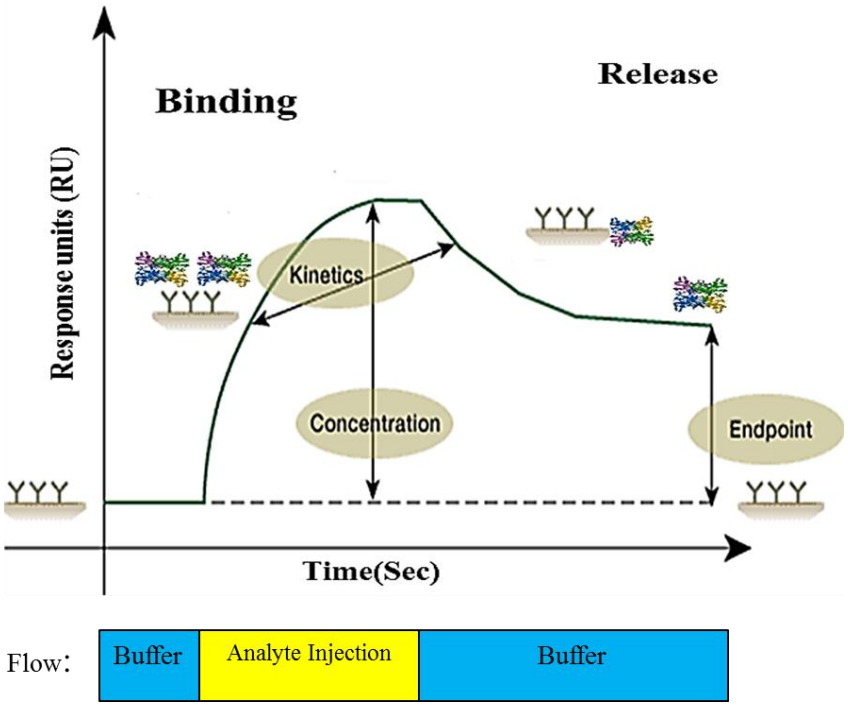

Figure 2-12: Sensogram plot of RU change with time: The figure shows when the injection of analyte begins, the ligand recognizes the analyte and binding occurs. This results in change in RU. Continuous injection of analyte leads to binding equilibrium, where the rate of binding equals the rate of release. When the analyte injection stops and buffer injections begins, analyte is relaeased from the ligand.This results in drop in RU.

In 2004, SPR experiments were designed for rapid diagnosis of intact plant viruses, particularly, tobacco mosaic virus (TMV) (Boltovets et al. 2004). IgG was immobilized to the surface and *Bracteacoccus minor* cells infected with TMV was used as analyte. Signal levels registered from the mixture of virus and that from the sample without virus were compared (Boltovets et al. 2004). However, the authors failed to present sensograms which were obtained after subtracting the reference channel responses. Although they have used controls for their experiments, a reference subtracted sensograms is obsolutely critical in a SPR scientific paper.

During the following year, a single-chain antibody (scFvCLcys) was engineered for cowpea virus detection. Three concentrations of virus and bovine serum albumin (BSA) (negative control) were injected as analytes (Torrance et al. 2006). The authors have presented the net result, after subtraction of BSA response. After subtracting the

reference, SPR sensogram shows negative response for BSA, which should have only been zero.

Using an antibody based assay, SPR experiments were developed to directly detect an intact form of insect pathogens (the baculovirus, AcMNPV). A mouse IgG monoclonal antibody raised against a surface protein of the target viral pathogen was bound to the chip. The response to the AcMNPV was then compared with the response for TMV (control). The authors claim that successive experiments with both viruses confirmed a specific response to AcMNPV only (Baac et al. 2006). The authors have not presented convincing SPR sensogram data to support their detection protocol. They only report the averages and standard deviations of multiple measurements for each step of angle shift. A typical SPR sensogram result has not been reported here. This raises the question on the quality of the experiment and the quality of the data obtained.

The binding properties of sialic acid-containing carbohydrates (Neu5Acα2-3nLc4Cer & Neu5Acα2-6nLc4Cer) that are recognized by human and/or avian influenza viruses were studied using an SPR (Hidari et al. 2007). From the kinetic analysis data it was reported that avian and human strains had different binding preferences to carbohydrates. An avian strain bound to Neu5Acα2-3nLc4Cer with a much slower dissociation rate than Neu5Acα2-6nLc4Cer. In contrast, a human strain bound equally to both carbohydrates (Hidari et al. 2007). There were few positives in terms of SPR data presentation in this paper. The authors here reported SPR sensograms. They have also managed to fit their data into simple 1:1 model. The authors have presented figures with data overlaid with the fit of the model. This assures that the SPR data are of good quality. However, there are two limitations in this experiment. Firstly, the virus contains HA and NA. If HA binds sialic acid, then NA would probably cleave the virus from sialic acid, that in turn would lead to loss in binding. But the data reported shows that the virus is interacting with the immobilized ligand. The authors have diluted the virus in running buffer supplemented with 2 μg/mL zanamivir. Zanamivir is an NI drug. Probably the use of the drug might have inhibited NA's activity. Secondly, they did not perform any experiment or cite the literature to suggest that 2 μg/mL of zanamivir was sufficient to inhibit all the NA present on the virus surface. This aspect of the experiment was not discussed clearly by the authors.

Table 2-6: SPR assay for virus detection

Virus	**Assay**	**Instrument**	**Reference**
Epstein-Barr virus	Direct immunoassay	A custom-made wavelength division multiplexing	(Vaisocherova et al. 2007)
Avian leucosis virus (ALV)	Direct immunoassay	Wavelength modulated Waveguide SPR	(Huang et al. 2006)
Hepatitis B virus (hHBV)	Direct immunoassay	Spreeta (Texas Instruments)	(Chung et al. 2005)
Cowpea mosaic virus	Direct immunoassay	Biacore	(Torrance et al. 2006)
Human immunodeficiency virus type 1 (HIV-1)	Using specific hybridization of immobilized biotinylated HIV-1 oligonucleotide probe	Biacore	(Bianchi et al. 1997)

Although researchers have been trying to expand the application of SPR for using the whole viral pathogen as an analyte (Table 2-6), there are no sufficient supporting data to proceed with whole virus as an analyte. For influenza viruses, the presence of HA and NA (proteins with exactly the opposite function) would make it more difficult to interpret the SPR binding response. Hence, the assay development in this project will be limited to influenza NA as the analyte rather than whole virus.

2.16 Summary of literature review

The spread of influenza virus as a pandemic result in the deaths of thousands of people annually. In the early 20th century, new strains of the influenza virus emerged, killing up to ten million people. The virus is classified based on its viral proteins, HA and NA e.g. H1N1, H5N1. The severity of each strain of influenza virus depends on the particular type of "HA" and "NA" present on the surface of the virus. The appearance of new strains occurs when an existing flu virus spreads to humans from other animal species resulting in genetic reassortment. In 2009, a new flu strain called the "swine flu" emerged that combined genes from human, pig and bird flu. The World Health Organization declared the outbreak of swine flu to be a pandemic. Several analogues of NANA were developed as antiviral drugs. These drugs are NA inhibitors (NI). The two most extensively used antiviral drugs to treat influenza are oseltamivir and zanamivir. These antiviral drug could be rendered ineffective by changing a single amino acid in the target protein NA. The ability of the virus to cause drug resistance varies with the type of mutation it can carry. Hence, there is the need to continuously monitor the sensitivities of antiviral drugs to currently circulating influenza viral strains. Biochemical assays with labelled substrates are currently used for this purpose. However, these assays have serious limitations with respect to reliability and half life of labelled substrate. Hence there is a need for a more reliable, label free real time assay. The aim of this thesis was to develop an SPR assay to measure kinetics of NA-drug interactions. In addition, I also aimed to take the first step towards a label-free SPR assay for monitoring drug resistance, by developing an SPR inhibition assay.

With the recent innovation and instrumentation there has been a tremendous increase in the use of SPR for medical diagnosis. Like any other technology, SPR also has certain

limitations. The penetration depth of SPR field is only 100 nm. Hence, it has been very difficult to expand this technology to detect whole virus, which is approximately 80 to 120 nm in diameter. This will leave the majority of the analyte outside the SPR field, undetected. For this reason we limit the scope of this research project to influenza viral proteins as analytes rather than whole virus.

BEVS are widely used technique to express desired proteins in cultured insect cells using recombinant technology. With specialized media, transfection reagents, and vectors, the BEVS are advantageous, particularly for large-scale protein expression. The very important step in this process is the selection of BEVS. In this research project I have preferred to use the flashBAC^{TM} vector system over the other systems, because the flashBAC system is a direct and a faster method because it bypasses the selection process exhibited in other BEVS. The methods, results and the important findings of this thesis are presented in the subsequent chapters.

3. In-silico identification of potential antiviral drug-resistant influenza neuraminidase mutations

3.1 Introduction

In this chapter, molecular docking studies carried out to analyse viral resistance are reported.

Molecular docking studies were carried out to predict whether there were any significant differences in binding affinity, ΔG and MM-GB/SA value for wild-type and mutant NA species interacting with antiviral drugs and sialic acid.

3.2 Selection of point mutations

Site-directed mutation of the active site of influenza neuraminidase showed that out of fourteen mutant proteins examined experimentally, seven proteins completely lost their biological activity for the substrate, namely those carrying the mutations R152K, W178L, D198N, E277D and Y406F (Lentz et al. 1987). A R371K mutant had only 4% of the wild type activity, while I222V and A346N were fully active**.** Both mutations at residue H274Y and H274N retained about 75% of the wild-type activity. It is interesting to note that the recent emergence of influenza A (H1N1) carrying a mutation H274Y in neuraminidase has not only retained its biological activity, but also resulted in antiviral drug resistance (Collins et al. 2009; Trifonov et al. 2009; Wilson 2012; Orozovic et al. 2011; Ives et al. 2002; Le et al. 2005).The four mutants identified by Lentz et al. (1987) as mutants that retained significant biological activity (H274Y, H274N, I222V and A346N) were used in the current investigation. In addition, a naturally occurring and widely studied drug resistant mutant, N294S (von Itzstein 2007; Collins et al. 2008), was included in the docking studies. The N294S mutant used in the docking studies helped in comparing the results with the data reported in literature.

3.3 Methods

3.3.1 Protein and ligand preparation

The entire docking process was carried out using Schrödinger Suite™ 2010. The 2009

pandemic H1N1 neuraminidase (PDB: 3NSS) was used throughout the docking studies as the wild type structure. The protein PDB has two identical subunits, each containing a functionally complete binding site. Thus, only one subunit (subunit A) was used for docking studies. The protein model was prepared using the Schrödinger protein preparation wizard following the supplier's instructions. The five mutants, H274Y, N294S, H274N, A346N and I222V were built using the Maestro module. The impact minimization module of the software was used to minimize the wild type and mutant structures to energetically stable states. Sialic acid, oseltamivir and zanamivir molecules were built using the Maestro build module. Ligand energy minimization was then performed using the impact minimization module to bring the ligand structures to energetically stable structures.

3.3.2 Docking

The grid-based ligand docking with energetics (GLIDE) module in Schrödinger was used for docking studies. Docking was carried out in two steps. First, a receptor grid was generated. The grid represents the shape and properties of the active sites of NA wild type and mutants. This ensures that any possible binding of the ligand into the active site of the protein is not missed. The optimized potentials for liquid simulation (OPLS) force field were used for grid generation. Finally, the energetically minimized ligands were docked into the generated grid files. Standard precision (SP) docking with the OPLS force field was used throughout the docking studies. The docked results were analysed using the GLIDE pose viewer module.

3.3.3 Induced fit docking

The Induced Fit protocol (IFD) was carried out as per the supplier's instructions. The IFD protocol uses the Glide module with reduced Van der Waals radii and an increased Coulomb- Van der Waals cut-off to dock the active ligand. The Prime structure prediction module then tries to accommodate the ligand by reorienting nearby side chains. This accounts for receptor flexibility during docking. Finally, each ligand is re-docked into low energy protein structures resulting in protein-ligand complexes which are ranked according to Glide Score. Prime MM-GB/SA is the ratio of molecular mechanics-generalized Born energy (MM-GB) generated by Prime module to that of solvent accessible area (SA). This energy value is used to estimate relative binding affinity for a list of ligands.

3.4 Results and discussion

3.4.1 Docking of sialic acid and antivirals into the active site of NA and its mutants

To study the molecular basis for interaction and the binding affinities of sialic acid and antiviral drugs with NA (wild type & mutants), each molecule was docked into the active site of NA. The docking results for these ligands are given in Table 3-1. The Glide score was generated as the output for a particular protein-ligand interaction.

$$GScore = a * vdW + b * Coul + Lipo + HBond + Metal + BuryP + RotB + Site \quad (3\text{-}1)$$

where vdW is the van der Waal's energy; Coul is the Coulomb energy; Lipo is the lipophilic contact term; HBond accounts for hydrogen-bonding; Metal is the metal-binding term; BuryP represents the penalty for buried polar groups; RotB is the penalty for freezing rotatable bonds; Site represents polar interactions at the active site; and the coefficients of vdW and Coul where a = 0.065, b = 0.130 (Sengupta et al. 2007).

3.4.2 The binding affinity

The Glide energy (GE) is the combination of the coulombic and Van der Waal's energies, which are long-range forces that attract a ligand to a particular protein. For spontaneous interaction, GE must be negative and the more negative the energy required for attracting a ligand to a protein, the more favoured the resulting interaction will be. In this thesis, the term binding affinity is used to refer to the attraction between a protein and ligand that leads to binding. From (Table 3-1), it can be seen that the GE values for sialic acid and oseltamivir interacting with the wild-type protein were negative (spontaneous) and very similar (-27.54 and -25.7 kcal/mol), whereas zanamivir appears to be a strong binder, with a more strongly negative energy (-38.65 kcal/mol). When comparing the GE for the two antiviral drugs interacting with the wild-type protein and the mutants (Figure 3-1), it was observed that there was a decrease in the magnitude of the GE when the antiviral drugs interacted with the mutants. This meant the interaction of the antivirals with the mutants was less favourable than with the wild-type. On the contrary, sialic acid showed a greater negative GE for the mutants. This indicated that sialic acid interacted

more favourably with the mutants. The differences in GE were the most marked in the case of mutation H274Y. The GE magnitude for sialic acid increased from -27.54 to -35.7 kcal/mol, while that for zanamivir decreased from -38.65 to -31.17 kcal/mol and that for oseltamivir decreased from -25.70 to -21.71 kcal/mol. The marked decreases in binding affinity for the anti-viral drugs, particularly compared with the increase in binding affinity for sialic acid were consistent with the observed drug resistance of mutant H274Y (Orozovic et al. 2011; McKimm-Breschkin 2000).

3.4.3 Calculated Gibbs free energy of binding

The ΔG value includes both enthalpic and entropic contributions. The enthalpy of the protein-ligand complex was determined from both bonded and non-bonded interactions between the protein and the ligand, while the entropic term was calculated from rotational and tortional energy, which correspond to the degree of order imposed by binding. The calculated enthalpy and entropy values are given in (Table 3-2). It was observed that the rotational energies were 0.77, 1.11 and 1.17 (kcal/mol) for oseltamivir, sialic acid and zanamivir, respectively. Because these energies were calculated independently for each ligand, and remained constant for all interactions involving that particular ligand. The calculated ΔG values are shown in Table 3-3 and Figure 3-3. The ΔG values increased in magnitude for the interactions of sialic acid with all mutants, compared with the wild-type, indicated that sialic acid interactions with the mutants were more favourable.

3.4.4 Wild type interactions

The changes in free energy when oseltamivir and sialic acid interacted with the wild-type protein were very similar (-25.2 and -25.44 kcal/mol, respectively) but the change in free energy was significantly more negative for the interaction of zanamivir with the wild-type protein (-33.74 kcal/mol). The same trend was observed when the binding affinities of the ligands with the wild-type protein (Figure 3-1& Figure 3-3) were compared. This showed that the antiviral drugs were well designed for binding with the wild-type NA protein.

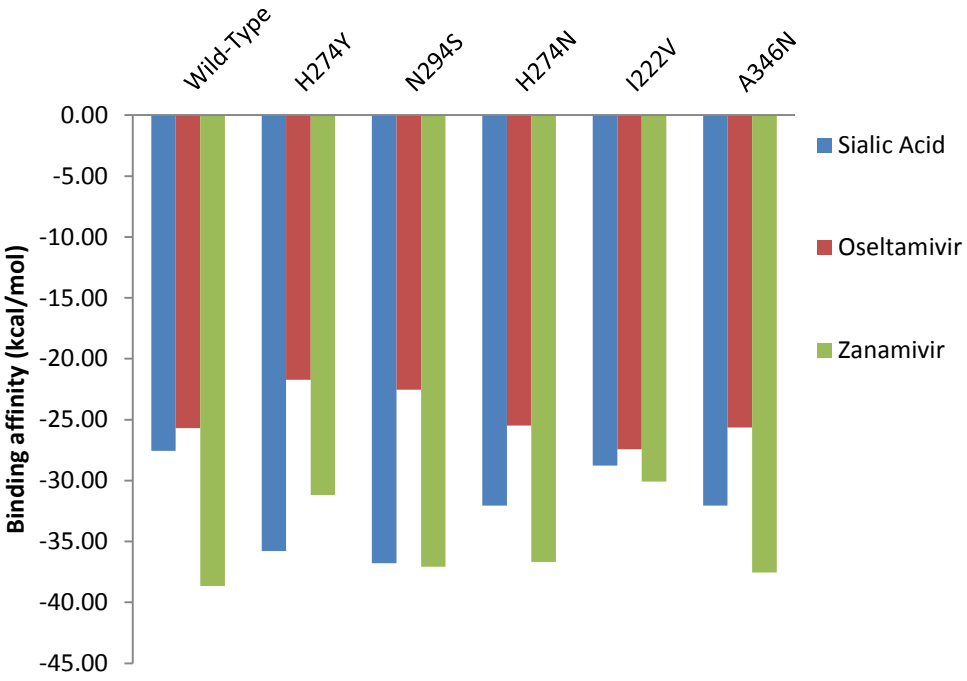

Figure 3-1: Comparison between the binding affinity (glide energy (GE)) values for interactions of sialic acid and antiviral drugs with NA (wild-type & mutants). There was a decrease in the magnitude of GE for the interactions of both antiviral drugs with the mutant proteins compared to wild-type NA.

Table 3-1: Docking results for sialic acid and antiviral drugs into NA (wild type & mutants) using GLIDE

Interaction	Glide score (kcal/mol)	E model (kcal/mol)	Glide energy (kcal/mol)
Sialic acid-WT	-5.2	-57.5	-27.5
Sialic acid-H274Y	-5.3	-58.9	-35.8
Sialic acid -N294S	-5.9	-58.4	-36.8
Sialic acid -H274N	-5.1	-58.6	-32.5
Sialic acid -I222V	-5.5	-58.5	-28.8
Sialic acid -A346N	-5.1	-58.6	-32.1
Oseltamivir-WT	-4.2	-52.4	-25.7
Oseltamivir-H274Y	-4.3	-49.1	-21.7
Oseltamivir-N294S	-4.1	-48.3	-22.5
Oseltamivir-H274N	-4.1	-52.6	-25.5
Oseltamivir-I222V	-5.4	-51.9	-27.4
Oseltamivir-A346N	-4.2	-52.8	-25.6
Zanamivir-WT	-5.8	-52.7	-38.7
Zanamivir -H274Y	-5.4	-59.1	-31.2
Zanamivir -N294S	-5.8	-64.7	-37.1
Zanamivir -H274N	-5.8	-49.6	-36.7
Zanamivir -I222V	-5.01	-48.1	-30.1
Zanamivir -A346N	-5.7	-52.1	-37.5

Table 3-2 : Calculated enthalpies and entropies for sialic acid and antiviral drugs interactions with NA (wild-type & mutants)

Interaction	Glide-Lipophilic (kcal/mol)	Glide-HBond (kcal/mol)	Glide-Vdw (kcal/mol)	Glide-Coul (kcal/mol)	ΔH (kcal/mol)	Rotational energy (kcal/mol)	Torisonal energy (kcal/mol)	-TΔS (kcal/mol)
Sialic acid-WT	-0.83	-2.30	-23.38	-4.16	-30.68	1.11	4.38	5.48
Sialic acid-H274Y	-0.84	-1.44	-26.23	-9.56	-38.07	1.11	8.10	9.21
Sialic acid -N294S	-0.81	-2.07	-29.22	-7.56	-39.65	1.11	8.82	9.93
Sialic acid -H274N	-0.88	-1.53	-26.70	-5.35	-34.45	1.11	3.27	4.37
Sialic acid -I222V	-0.87	-2.04	-20.80	-7.97	-31.68	1.11	5.01	6.11
Sialic acid -A346N	-0.88	-1.53	-26.70	-5.35	-34.45	1.11	3.27	4.37
Oseltamivir-WT	-1.63	-0.40	-28.83	3.13	-27.73	0.77	1.51	2.29
Oseltamivir-H274Y	-1.44	-1.21	-20.25	-1.46	-24.36	0.77	3.11	3.88
Oseltamivir-N294S	-1.40	-1.03	-22.49	-0.04	-24.96	0.77	1.33	2.10
Oseltamivir-H274N	-1.52	-0.44	-27.93	2.44	-27.45	0.77	2.48	3.26
Oseltamivir-I222V	-1.08	-2.03	-21.85	-5.58	-30.52	0.77	2.76	3.53
Oseltamivir-A346N	-1.65	-0.40	-28.52	2.90	-27.68	0.77	1.49	2.27
Zanamivir-WT	-1.06	-1.36	-27.76	-10.88	-41.06	1.17	6.15	7.32
Zanamivir -H274Y	-0.86	-2.82	-23.16	-8.02	-34.85	1.17	9.39	10.56
Zanamivir -N294S	-0.85	-2.88	-24.36	-12.71	-40.80	1.17	8.80	9.97
Zanamivir -H274N	-0.99	-1.64	-22.31	-14.35	-39.29	1.17	13.66	14.83
Zanamivir -I222V	-0.93	-1.63	-18.73	-11.34	-32.63	1.17	6.26	7.43
Zanamivir -A346N	-1.10	-1.49	-27.57	-9.97	-40.13	1.17	7.73	8.90

3.4.5 H274Y interactions

In the case of the H274Y mutation, the ΔG values changed markedly. There was a decrease in the magnitude of free energy change for both the antivirals, with that for zanamivir decreased from -33.74 to -24.29 kcal/mol and that for oseltamivir from -25.44 to -20.48 kcal/mol. This, in turn, reduced the strength of their interactions. On the contrary, the free energy change from the interaction between sialic acid and the mutant protein was more favourable, changed from -25.20 to -28.86 kcal/mol, such that its interaction was equally favourable with zanamivir and both (zanamivir and sialic acid) were more favourable than oseltamivir. A similar trend was observed for the binding affinity, in agreement with the reduced efficacy of oseltamivir against the H274Ymutant strain.

3.4.6 N294S interactions

The free energy change for sialic acid interaction with the N294S mutant increased to -29.72 kcal/mol. Although there was a decrease in the magnitude of the free energy change for both antivirals, the decreases were not as high as the values observed with the H274Y mutant. Zanamivir retained a slightly stronger ΔG value (-30.84 kcal/mol) than the sialic acid interaction with the mutant, hence the N294S mutant was not as problematic as H274Y. This observation was in good agreement with the inhibition kinetics results reported by Collins et al. (2008).

3.4.7 H274N interactions

While studying the interaction between sialic acid and the H274N mutant, it was observed that the ΔG value changed to -30.08 kcal/mol. Amongst the six sialic acid interactions studied, the interaction between sialic acid and H274N had the most highly negative ΔG value, making this interaction highly favoured when compared to the other proteins (the wild-type and the other four mutants). Moreover, the ΔG value for oseltamivir decreased to -24.19 kcal/mol, which is larger than the ΔG observed with H274Y. As previously reported (Collins et al. 2008), the binding of oseltamivir to wild-type NA involved a conformational change in the side chain of Glu 276, leading to the formation of a salt bridge between Glu 276 and His 274. Because the His at 274 had been replaced by Tyr, the latter group pushed Glu 276 farther into the binding pocket, thereby disrupting the salt bridge formation (Figure 3-2). In contrast, for mutant H274N, where

His had been replaced by Ser, the latter group was not as bulky as Tyr so did not push Glu 276 as far away. Hence, oseltamivir had a stronger interaction with H274N than with H274Y. On the other hand, zanamivir, having a polar glycerol group, did not depend on the formation of a salt bridge between His 274 and Glu 276. Thus, the movement of Glu 276 within the binding pocket did not affect the binding of zanamivir. This resulted in zanamivir possessing very similar ΔG values for mutations H274Y and H274N (-24.29 and -24.46 kcal/mol, respectively).

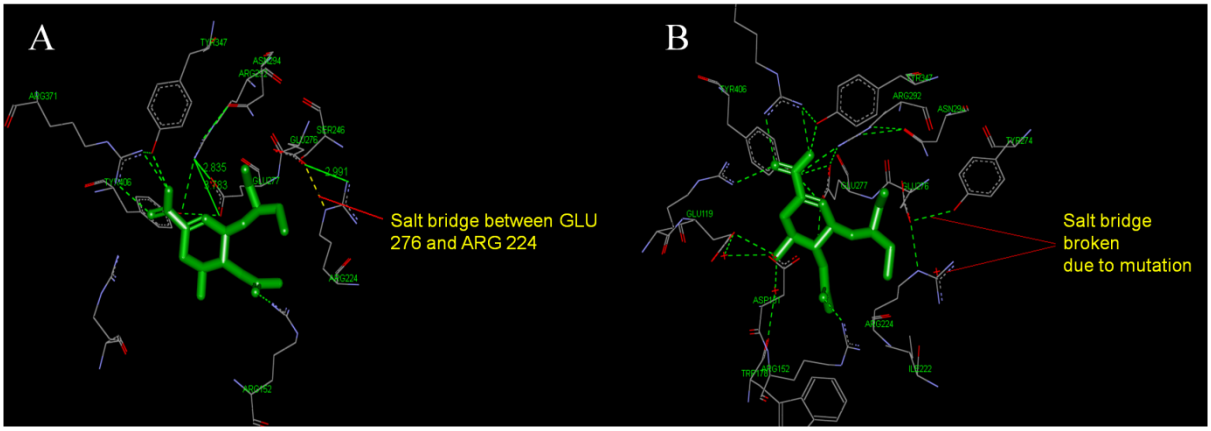

Figure 3-2: Docked images of NA (wild type and H274Y mutant) with oseltamivir. A) Binding of oseltamivir to wild-type NA involved the formation of a salt bridge between Glu 276 and His 274. B) The replacement of His at 274 by Tyr resulted in the disruption of the salt bridge.

3.4.8 I222V interactions

Oseltamivir had the greatest ΔG value, -26.99 kcal/mol, for interaction with the I222V mutant, thereby making this interaction more favourable than the others. The ΔG values for zanamivir and sialic acid interactions with I222V were very similar (-25.21 and -25.57 kcal/mol, respectively). Because the antiviral drugs had either stronger or similar interactions with I222V compared with sialic acid, this mutation may not be expected to cause increased drug resistance.

3.4.9 A346N interactions

Here, zanamivir had a similar but slightly greater ΔG value (-31.23 kcal/mol) compared with the sialic acid interaction, while oseltamivir had a smaller ΔG value (-25.41 kcal/mol), which was similar to its interaction with the wild-type protein. Thus, for mutant A346N, oseltamivir may be less effective binder than zanamivir.

Table 3-3 : Gibbs free energy change for sialic acid and antiviral drugs interaction with NA (wild type & mutants)

Protein	Sialic Acid			Oseltamivir			Zanamivir		
	ΔH (kcal/mol)	-TΔS (kcal/mol)	ΔG (kcal/mol)	ΔH (kcal/mol)	-TΔS (kcal/mol)	ΔG (kcal/mol)	ΔH (kcal/mol)	-TΔS (kcal/mol)	ΔG (kcal/mol)
Wild-type	-30.68	5.48	-25.20	-27.73	2.29	-25.44	-41.06	7.32	-33.74
H274Y	-38.07	9.21	-28.86	-24.36	3.88	-20.48	-34.85	10.56	-24.29
N294S	-39.65	9.93	-29.72	-24.96	2.10	-22.85	-40.80	9.97	-30.84
H274N	-34.45	4.37	-30.08	-27.45	3.26	-24.19	-39.29	14.83	-24.46
I222V	-31.68	6.11	-25.57	-30.52	3.53	-26.99	-32.63	7.43	-25.21
A346N	-34.45	4.37	-30.08	-27.68	2.27	-25.41	-40.13	8.90	-31.23

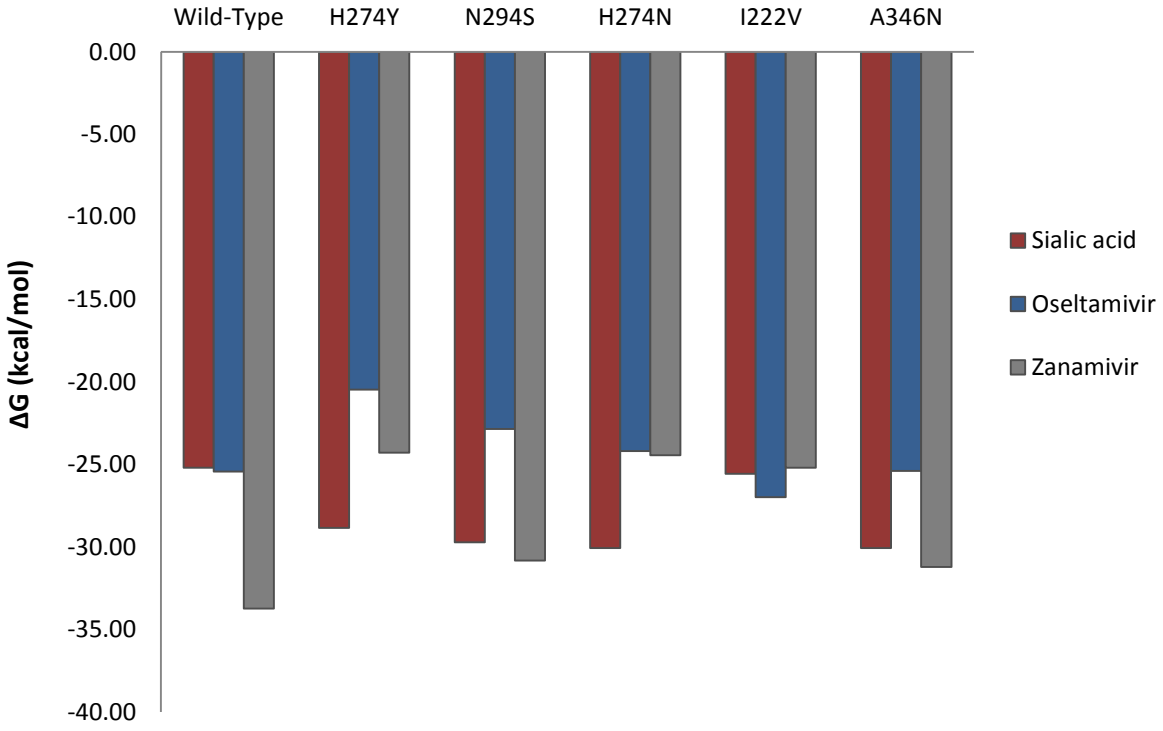

Figure 3-3 : Comparison between the ΔG values for interactions of sialic acid and antiviral drugs with NA (wild-type & mutants). This graph indicated a decrease in the magnitude of ΔG for the interactions of both antiviral drugs with the mutant proteins compared to wild-type NA, similar to the GE values.

Table 3-4 : Comparison between experimental and predicted ΔG values

Protein	Oseltamivir				Zanamivir			
	ΔG_{exp} (kcal/mol)	ΔG_{pre} (kcal/mol)	$\Delta\Delta G_{exp}$ (kcal/mol)	$\Delta\Delta G_{pre}$ (kcal/mol)	ΔG_{exp} (kcal/mol)	ΔG_{pre} (kcal/mol)	$\Delta \Delta G_{exp}$ (kcal/mol)	$\Delta \Delta G_{pre}$ (kcal/mol)
Wildtype	-13.12	-25.44	-	-	-13.82	-33.74	-	-
H274Y	-9.77	-20.48	3.35	4.96	-13.43	-24.29	0.39	9.45
N294S	-11.87	-22.85	1.25	2.59	-12.63	-30.84	1.18	2.9

3.4.10 Glide docking comparison with experimental data

The docking results were compared with experimental data reported in the literature. Direct experimental comparisons are not currently available to my knowledge, so experimental ΔG values for interactions of oseltamivir and zanamivir with wild-type NA, N294S and H274Y were calculated from the inhibition kinetic data reported by Collins et al. (2008) (Table 3-4). Collins et al. (2008) reported that the experimental inhibition constant (K_i) in their work was the disassociation constant for the antiviral drugs. Hence, this value was used to calculate experimental ΔG. However, it should be noted that it is not possible to provide direct, quantitative comparisons with docking results because the experimental data were generated by competitive activity assays carried out in the presence of each inhibitor. In docking studies only one ligand was presented to the protein at a time and the interaction between each ligand and the proteins were studied, resulting in greater ΔG magnitudes. The ΔG values calculated from experimental results decreased in magnitude in all cases when going from wild-type to the mutant forms of NA, for zanamivir and oseltamivir, consistent with the predictions from the molecular docking studies. Furthermore, the experimental trends showed that zanamivir had more favourable ΔG values than oseltamivir in all cases, again as predicted. The prediction that the interaction between zanamivir and N294S should be more favourable than with H274Y was the only case not in agreement with the experimental data. The ΔΔG value in Table 3-4 was the change in ΔG between the wild type and the mutant protein interactions with the antiviral drugs and was, in all cases, positive. Therefore, an increase in the magnitude of ΔΔG indicated that interaction with the mutant protein was weakened

so the mutation had more potential to cause drug resistance. The values in Table 3-4 indicated that H274Y had greater potential to cause drug resistance than N294S, in good agreement with the ΔΔG value calculated from the experimental observations. The predicted ΔΔG values were very similar in magnitude to the experimental ΔΔG values, except for zanamivir-H274Y interaction. The experimental ΔΔG value for zanamivir-H274Y interaction was 0.39 kcal/mol. This suggested that there was only a slight difference between zanamivir's interaction with the wild type protein and the mutant protein. On the contrary, the predicted ΔΔG value for the same interaction was much larger, at 9.45 kcal/mol. This large predicted change was influenced mainly by a change in the enthalpic contribution to ΔG through reduced electrostatic interactions. Replacing His with Tyr at 274 has been suggested to push the Glu at 276 deep into the binding pocket (Collins et al. 2008), reducing the access of the hydroxyl groups in the glycerol side chain of zanamivir to the carboxylate oxygens of Glu276. Experimentally, this movement of Glu276 into the binding pocket may not have been as significant as that predicted, therefore having less effect than predicted on weakening the interaction between NA H274Y mutant and zanamivir. Moreover, the glide docking did not account for receptor flexibility. Hence, induced fit docking (IFD), also known as flexible docking was used for further analysis.

3.4.11 Induced fit docking

When using IFD, MM-GB/SA was used to estimate relative binding affinity for the ligands. The absolute values calculated (Figure 3-4 and Table 3-5) may not be quantitatively in agreement with experimental binding affinities, however, the ranking of the ligands based on the calculated MM-GB/SA was reasonably in agreement with ranking based on experimental binding affinity. The IFD results were closer to the experimental values (Figure 3-5). This could be because the IFD takes receptor flexibility into consideration, unlike GLIDE docking where the receptor binding pocket was converted to a mathematical grid. Based on this ranking it can be observed that in H274Y and H274N mutants, the interactions with the anti-viral drugs were less favourable than with sialic acid and the same mutants, indicating that these mutations could confer anti-viral resistance.

Table 3-5: Calculated MM-GB/SA values for sialic acid and antiviral drugs interaction with NA (wild type & mutants)

Interaction	MM- GB (kcal/mol)	Surface area (SA)	MM-GB/SA (kcal/mol)
Sialic acid-WT	-926.87	35.25	-26.29
Sialic acid-H274Y	-934.76	37.91	-24.66
Sialic acid -N294S	-1004.03	38.96	-25.77
Sialic acid -H274N	-957.46	29.50	-32.46
Sialic acid -I222V	-927.98	39.91	-23.25
Sialic acid -A346N	-936.13	34.50	-27.13
Oseltamivir-WT	-858.62	37.28	-23.03
Oseltamivir-H274Y	-886.14	45.64	-19.41
Oseltamivir-N294S	-916.15	41.53	-22.06
Oseltamivir-H274N	-900.48	38.18	-23.58
Oseltamivir-I222V	-884.51	38.35	-23.07
Oseltamivir-A346N	-897.21	40.19	-22.33
Zanamivir-WT	-908.77	39.38	-23.07
Zanamivir -H274Y	-963.68	42.20	-22.84
Zanamivir -N294S	-1003.30	45.46	-22.07
Zanamivir -H274N	-953.61	40.37	-23.62
Zanamivir -I222V	-945.82	39.75	-23.80
Zanamivir -A346N	-957.46	35.10	-27.28

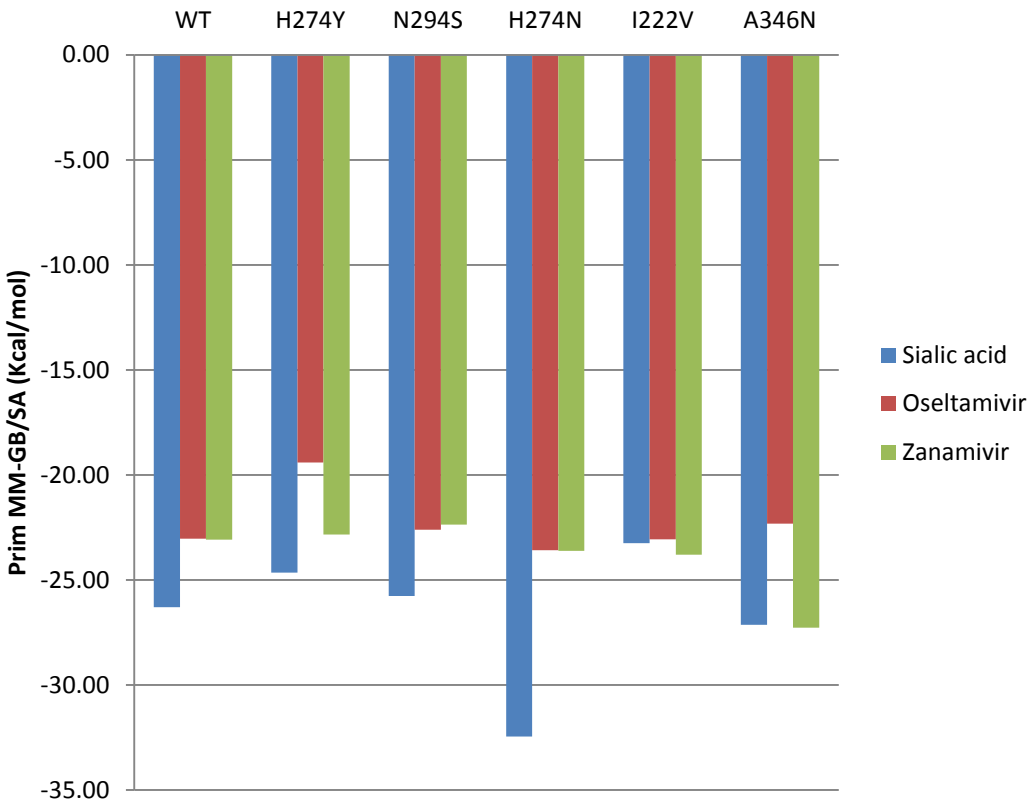

Figure 3-4: Comparison between the MM-GB/SA values for interactions of sialic acid and antiviral drugs with NA (wild-type & mutants).

3.4.12 IFD comparison with experimental data

The ΔΔG values for experimental results were calculated as described in 3.4.10. These values were compared with ΔMM- GB/SA, which was the difference in MM- GB/SA values computed for wild type and the mutant protein interactions with the antiviral drugs. The computed ΔMM- GB/SA values were very similar in magnitude to the experimental ΔΔG values and were, in all cases, positive. Therefore, an increase in the magnitude of ΔMM- GB/SA indicated that interaction with the mutant protein was weakened so the mutation had more potential to cause drug resistance. The values in Table 3-6 indicated that ΔMM- GB/SA values were similar for N294S interaction with both antivirals, while H274Y had greater potential to develop oseltamivir resistance and remained sensitive to the zanamivir. This was in good agreement with the ΔΔG value calculated from the experimental observations. This suggested that zanamivir could be a more potent inhibitor than oseltamivir.

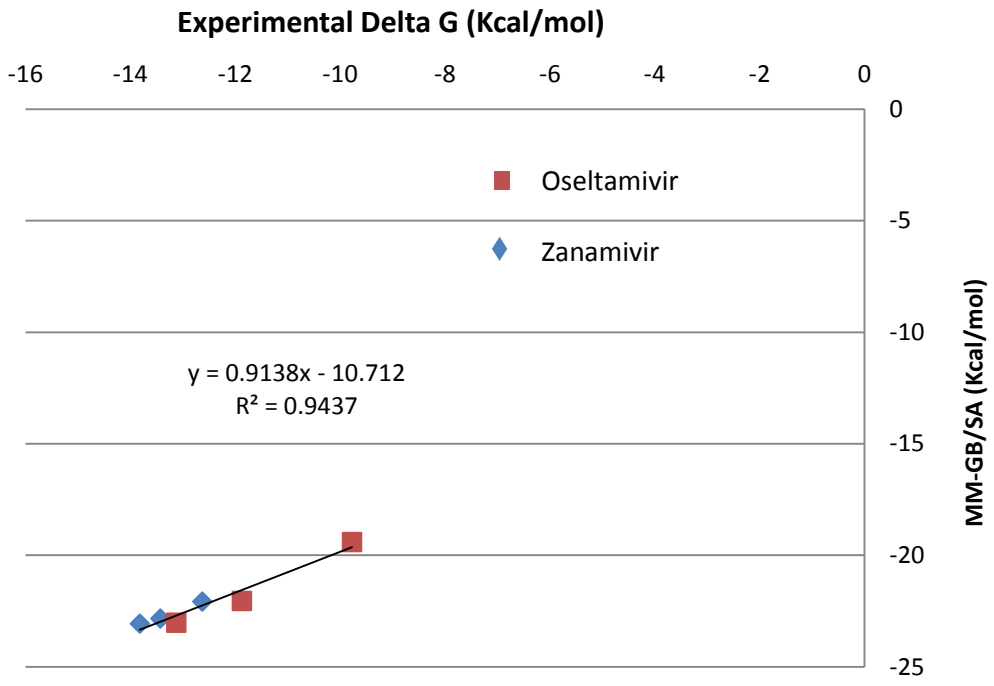

Figure 3-5: Comparison between experimental ΔG and MM-GB/SA. The R^2 correlation coefficient between experimental ΔG and MM-GB/SA is 0.94. This indicated that the IFD method was comparable to the experimental data reported in the literature.

Table 3-6: Comparison between experimental and MM-GB/SA values

Protein	Oseltamivir				Zanamivir			
	ΔG_{exp} (kcal/mol)	MM-GB/SA (kcal/mol)	$\Delta\Delta G_{exp}$ (kcal/mol)	ΔMM-GB/SA (kcal/mol)	ΔG_{exp} (kcal/mol)	ΔMM-GB/SA (kcal/mol)	$\Delta \Delta G_{exp}$ (kcal/mol)	ΔMM-GB/SA (kcal/mol)
Wildtype	-13.12	-23.03	-	-	-13.82	-23.07	-	-
H274Y	-9.77	-19.41	3.35	3.62	-13.43	-22.84	0.39	0.23
N294S	-11.87	-22.06	1.25	0.97	-12.63	-22.07	1.19	1

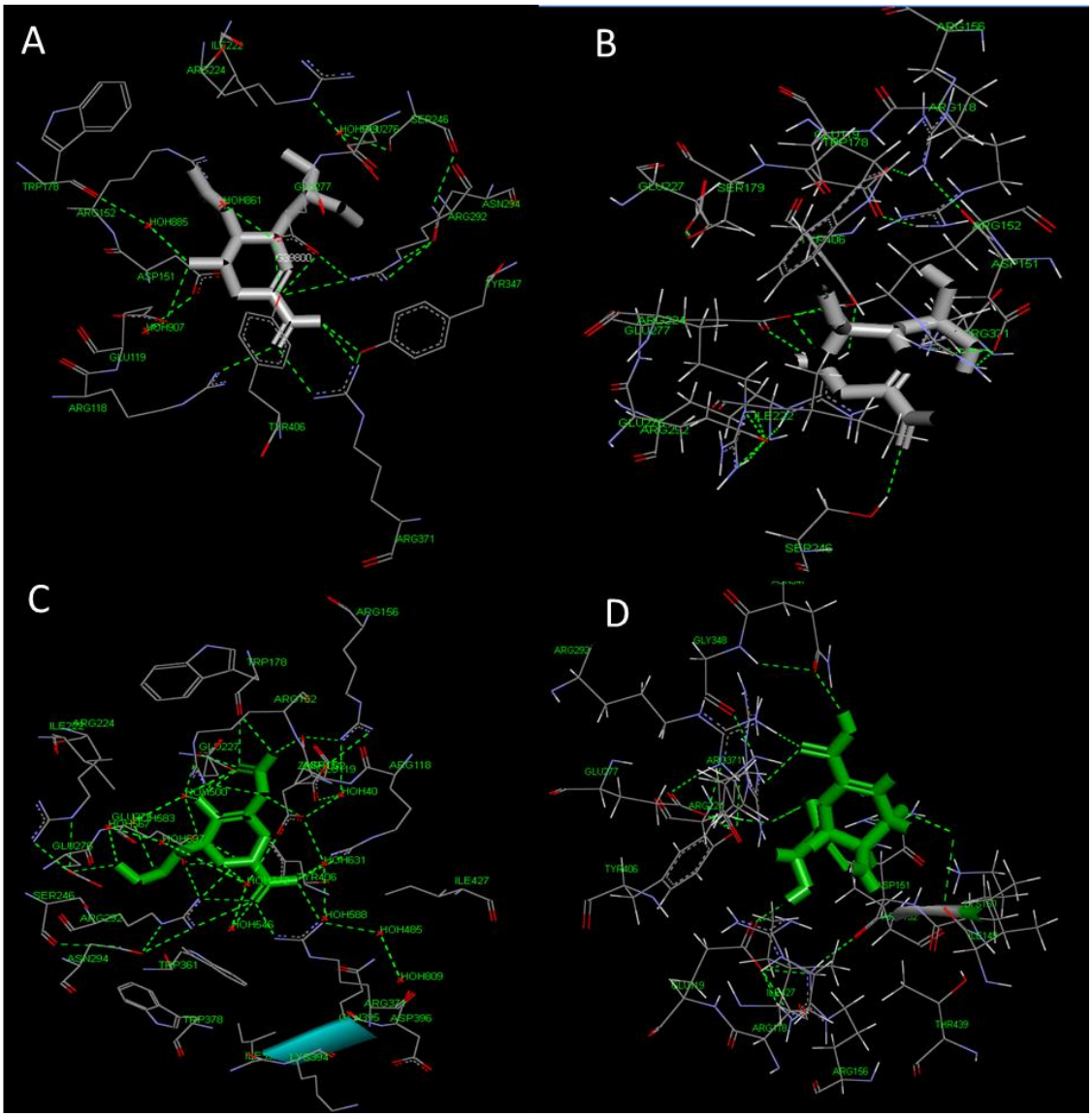

Figure 3-6: Comparison of docked poses for H274Y mutant with oseltamivir (B) and zanamivir (D) with respective PDB crystal structures 3CLO (A) and 3TI5 (C). Significant differences observed in the protein-ligand hydrogen bonding between the crystal structures and docked structures

3.5 Comparison with crystal structure

Molecular docking simulation is a useful tool for analysing the binding of a ligand to a protein (Liu et al. 2010) and is mainly aimed at finding the lowest possible energy for the ligand-receptor complex (Sengupta et al. 2007; Chen and Shoichet 2009). However, docking simulation is only a theoretical tool. Therefore, it requires validation with experimental data. The docking results were compared with experimental ΔG values in Sections 3.4.10 and 3.4.12 of this chapter. However, the most important step in any

docking study is to validate the docking program by comparing the binding mode of the docked structure with the known crystal structure. For this purpose the docked poses for H274Y mutant with oseltamivir and zanamivir were compared with PDB crystal structures 3CLO and 3TI5, respectively (Figure 3-6). The docked and crystal structures are usually superimposed to observe the subtle differences in interactions. However, in this case the interactions observed in the docked structures were significantly different from the crystal structures and a superimposed figure will not be useful to follow these differences in interactions. Therefore, the docked structures and the crystal structures are presented separately, in a best possible orientation that will be useful to compare the differences in interactions between the docked and crystal structures. For both oseltamivir and zanamivir the docked structures did not give the same binding mode as observed in the crystal structure. In the docked structure it can be observed that there are more hydrogen bonds within the protein binding site and not between the protein and the ligand. The reason for this could be that the docking program aims to find a stable conformation for the protein during ligand binding. Hydrogen bonding is a key parameter for computing ΔG values, glide energy and glide score. The significant differences observed in the protein-ligand hydrogen bonding (Appendix E) between the crystal structures and docked structures suggest that the comparisons made in Sections 3.4.10 and 3.4.12 may just be coincidentally similar with the experimental data. Due to the differences observed in hydrogen bonding, the computed energy values cannot be used to confirm the efficacy of the anti-viral drugs to treat a particular mutant.

3.6 Conclusions

The binding affinities, ΔG and MM-GB/SA values for wild-type NA interactions showed that both the antiviral drugs studied interact strongly with the wild-type protein. The marked changes observed in predicted binding affinities, ΔG and MM-GB/SA values for the H274Y and N294S interactions may explain reduced antiviral efficacies. The ΔG values for all antiviral interactions with mutant NA forms reduced in magnitude. This indicated that they were less favourable than interactions with the wild-type protein. Similar trend was also observed with MM-GB/SA results. Moreover, replacing the His at 274 prevented the formation of a salt bridge with Glu 276, which appeared to be a conformational feature that was critical for oseltamivir interactions. Among all the computed values, MM-GB/SA was closer to the experimental data. In several cases, the interactions between the anti-viral drugs and NA mutants were markedly less favourable

than those between sialic acid and the same mutants, indicating that these mutations could confer anti-viral resistance. However, when the docked structures were compared with PDB crystal structures, it was observed that the modelling program did not produce docked structures similar to crystal structures. Hence, the computed ΔG values may just be coincidentally similar to the experimental ΔG values. It is a widely-accepted fact that docking programs describes the best conformation a protein can take to accommodate a ligand. However, they lack the ability to simulate the relevant macromolecular movement (such as protein side chain and backbone movement and key catalytic residue movements) that help the protein to maintain this confirmation for accommodating a ligand. This calls for a more reliable experimental validation. Hence, a SPR assay to measure the binding affinity between influenza viral coat protein NA (wild type and mutant) and anti-viral drugs was developed. The SPR measurements (Chapter 5) were used to compare the docking results reported in this chapter.

4. Cloning, expression and purification of influenza neuraminidase

4. 1 Introduction

Protein expression is a process that uses recombinant DNA technology to convert genetic information (DNA) into a functional protein. The commonly used expression systems are the bacterial, baculovirus, yeast and mammalian expression systems. Influenza NA has been successfully expressed using the baculovirus expression vector system (BEVS) (Dalakouras et al. 2006; Deroo et al. 1996). This chapter describes methods used to clone and express influenza NA in the BVES. Two insect cell lines (sf9 and High-Five) were tested for expression of NA. A time course expression analysis was also performed to optimize the expression of NA. Western blot was used to confirm the expression of NA in insect cells. The expressed NA was purified using standard purification techniques.

Generally the first step in most of the bio separation processes is to lyse the cells to release the desired gene product. The cell is usually lysed by physical methods (bead mill, sonication and freeze thaw cycling) or chemical methods (addition of detergents, enzymes and solvents). Using centrifugation, the soluble fractions can be separated from insoluble fractions of the cell lysate. Influenza NA was released from the insect cells using sonication technique (Dalakouras et al. 2006). NA was solubilized by the addition of excess non-ionic detergent (triton-100) (Dalakouras et al. 2006). Ion exchange chromatography (IEX) and Size exclusion chromatography (SEC) were used to purify NA from the cell extract. Methods and results for the chromatography steps are discussed in detail in this chapter.

Influenza NA activity was measured using fluorometric assay described by Potier et al. (1979). The assay was performed in the presence and absence of NI drugs to determine the sensitivities of the inhibitors to the recombinant NA expressed in the lab. The activity assay results are also discussed in this chapter.

4. 2 Materials

4.2. 1 Cell culture

Cell lines (sf9 and High-Five) were gifted by the Protein Expression Facility (University of Queensland, Brisbane, Australia). Sf-900II serum free medium (SFM) (Gibco Cat number 10902) and 0.1% trypan blue (Gibco Cat number 15250-061) were purchased from Life Technologies Corporation (Carlsbad, California, USA).

4.2. 2 Cloning and site directed mutagenesis (SDM)

The construct (gene of interest {GOI} in pFastbac) was purchased from Epoch Life Science (Missouri City, Texas, USA). The pBac 1 vector (Novagene product number 70003-3) was purchased from Merck KGaA (Germany). PureLink™ quick plasmid miniprep kit (Invitrogen cat number K2100-10) was purchased from Life Technologies Corporation. QuikChange® multi-site-directed mutagenesis kit (Cat number 200514) was purchased from Stratagene (San Diego, California, USA).

The following primers were purchased from Gene Works (Australia):

Forward primer (5' AATAAAAAAACCTATAAATATAGGATCCATGAACCCG AACCAGAAA ATT 3')

Reverse primer (5' AGTGGTGGTGGTGGTGGTGCTCGAGTTATTTATCAAT GGTAAACGGCAGTTCCG 3')

SDM primer ("5'-G AAC GCG CCG AAC AGC TAT TAT GAA GAA TGC AG-'3")

4.2. 3 Transfection

FlashBAC DNA (product code 100201) was purchased from Oxford Expression Technologies (Oxford, UK). Cellfectin reagent (Invitrogen Cat number 10362-010), Grace's insect medium, unsupplemented (Gibco Cat number 11595), antibiotics and antimycotics, 100X (Gibco Cat number 15240-062) were purchased from Life Technologies Corporation.

4.2. 4 P4 BV Timecourse expression analysis

Influenza A H1N1 (Swine Flu 2009) NA / Neuraminidase Antibody (cat number 11058-MM07), Mouse IgG secondary antibody HP conjugate (cat number 50323-RP02) were purchased from Sino Biological (Beijing, China). GE image-quant LAS 500 gel

documentation unit (GE, Healthcare Life Sciences) was used for blot detection.

4.2. 5 Purification

Resource ^{TM} Q GL prepacked ion exchange column (cat number 17-1177-01), Superdex 200 10/300 GL prepacked gel filtration column (cat number 17-5175-01) were purchased from GE, Healthcare Life Sciences. All purification experiments were conducted using AKTA Explorer 10 chromatography system (GE, Healthcare Life Sciences).

4. 3 Buffers and media

A) Buffers

Table 4-1: List of buffers used

Buffer	**Recipe**
PBS buffer	137 mM NaCl, 2.7 mM KCl, 10 mM Na_2HPO_4, 1.8 mM KH_2PO_4 , pH 7.4
PBST buffer	137 mM NaCl, 2.7 mM KCl, 10 mM Na_2HPO_4, 1.8 mM KH_2PO_4 , 0.05% Tween 20, pH 7.4
Transfer buffer	48 mM Tris, 39 mM glycine, (20% methanol) The buffer will range from pH 9.0 to 9.4, depending on the quality of the Tris, glycineand methanol.
Blocking buffer	5% Skim milk powder in PBST
Lysis Buffer	20mM Sodium phosphate, 5.7% TritonX-100, pH 6.0
Buffer A (Ion exchange binding buffer)	20mM Sodium phosphate, 0.1% TritonX-100, pH 6.0
Buffer B (Ion exchange Elution buffer)	20mM Sodium phosphate, 0.1% TritonX-100, 1M NaCl, pH 6.0
Buffer C (Size exclusion buffer)	137 mM NaCl, 2.7 mM KCl, 10 mM Na_2HPO_4, 1.8 mM KH_2PO_4 , 0.1% TritonX-100, pH 7.4

All buffers were filtered using 0.22 µm Millipore filter before use.

B) Media

i) Luria broth (LB) medium

Bacto tryptone 10 g, bacto yeast 5 g and NaCl 10 g were dissolved in 950 mL deionized water. Volume was adjusted to 1000 mL with deionized water after the pH was set to 7.5 with NaOH. The LB medium was autoclaved for 20 min at 121˚C and was stored at 4˚C until use.

ii) LB agar plate

Bacto tryptone 10 g, bacto yeast 5 g, NaCl 10 g and 15 g of agar were dissolved in 950 mL deionized water. Volume was adjusted to 1000 mL with deionized water after the pH was set to 7.5 with NaOH. The medium was autoclaved for 20 min at 121˚C and cooled down to 50˚C. The appropriate antibiotics (ampicilin) were added and 25 mL were poured into each Petri-dish. The plates were allowed to solidify. Solid LB agar plates were wrapped with Parafilm and stored at 4˚C until use.

iii) SOC media

SOC media is similar to super optimal broth (SOB) media but the presence of glucose. Bacto tryptone 2 g, bacto yeast extract 0.5 g, 0.2 mL of 5 M NaCl, 0.25 mL of 1 M KCl, 1 mL of 1 M $MgCl_2$, 1 mL of 1 M $MgSO_4$, 2 ml of 1 M glucose were dissolved in 90 mL deionized water. Volume was adjusted to 100 mL with deionized water. The medium was autoclaved for 20 min at 121˚C and cooled down to 50˚C.

4. 4 Methods

4.4.1 General DNA methods

A) Transformation

XL1-Blue competent cells (50 µL) were thawed and transferred into a pre-chilled transformation tube. 2 µL of DNA was added to the tube. The tube was placed on ice for 30 min, followed by heating at 42˚C for 45 s and finally cooled on ice for 2 min. 950 µL of pre-warmed soc media (RT) was added and incubated at 37˚C, 200 rpm for 1 h. Agar plates with ampicilin was prepared (50 µL of ampicilin (100 mg/mL)). After 1 h incubation, 100 µL of the sample was plated on one LB agar plate. The remaining 900 µL was spun down and 800 µL of the supernatant was discarded. The pellet was resuspended in 100 µL of supernatant, which was platted on to the second LB agar plate.

The plates were incubated at 37˚C overnight. The following day the plates were removed from the incubator and colonies were found. Three random colonies were picked up and an overnight culture was grown (5mL LB medium + 50 µL of ampicillin). The following day the three overnight cultures were minipreped (extraction and purification of transformed DNA). The concentration of the 3 samples was measured on a Nanodrop and the samples were sent for sequencing. A glycerol stock was made from the colonies with positive sequencing results and stored at -80˚C

B) Glycerol stocks

An overnight culture (5 mL LB medium + 50 µL of ampicillin) was grown from a single colony. The following day 850 µL cell culture was mixed with 150 µL sterile glycerol in cryotubes. The samples were snap freezed with liquid nitrogen and stored at - 80˚C.

C) Miniprep protocol

The S.N.A.P. ™ MiniPrep Kit (Life Technologies Corporation cat no. K1900-01) was used for miniprepping (extracting and purifying DNA) transformed DNA. The overnight cultures were transferred to a 50mL falcon tube and centrifuged at 4000 rpm, 4˚C for 10 min to pellet the cells. The supernatant was discarded and the pellets were resuspended in 150 µL of resuspension buffer (provided in kit) by gently pipetting up and down. The lysis buffer provided in kit (150 µL) was added and mixed gently by inverting the tube 6 times. The tubes were incubated for 3 min at room temperature. 150 µL of ice-cold precipitation salt (provided in kit) was added and mixed well by inverting the tubes 8 times. The tubes were centrifuged at 14,000 x g for 5min. A S.N.A.P. ™ MiniPrep column (A) was placed inside the 2 mL collection tube provided. 600 µL of binding buffer (provided in kit) was added to the supernatant and mixed by inverting 6 times. This mixture was transferred to the collection tube containing the column (A). The S.N.A.P. ™ MiniPrep column/collection tube was centrifuged at room temperature at 3,000 x g for 30 s. The column flow through was discarded. The wash buffer provided in the kit (500 µL) was added and centrifuged at room temperature at 3,000 x g for 30 s. The column flow through was discarded. The 1X final wash buffer provided in the kit (900 µL) was added and centrifuged at room temperature at 3,000 x g for 30 s. The column flow through was discarded. The collection tube was again centrifuged for 1min to dry the resin. 60 µL of sterile water was added to tubes and incubated for 3 min at room temperature. The column was centrifuged for 30 s at maximum speed and the column

was discarded. The flow through containing the DNA was collected.

D) Gel purification of DNA

The desired DNA band was cut from the agarose gel and placed inside a 1.5 mL Eppendorf tube (pre weighed). The weight of the cut band was determined and solublization buffer from the Quick Gel kit was added (volume of buffer added 3 times the weight of the gel). The tubes were incubated at 50˚C for 10 min. A quick gel extraction column was placed in the quick gel wash tube. The dissolved gel containing the desired DNA was placed in the centre of the column. The tube was centrifuged at 12,000 rpm for 1 min and the flow through was discarded. 700 µL of wash buffer containing ethanol from the kit was added. The tube was centrifuged at 12,000 rpm for 1 min and the flow through was discarded. The tubes were again centrifuged at 12,000 rpm for 3 min to remove residual wash buffer. The column was placed in the quick gel recovery tube. The quick gel elution buffer (50 µL) was added and incubated at room temperature for 1 min. The recovery tube was centrifuged for 1 min at 12,000 rpm. The flow through collected in the recovery tube contained the desired DNA.

E) Agarose-gel preparation

Agarose-gel (1-2%) was prepared by dissolving 0.8 g to 1.6 g agarose was dissolved in 80 mL 0.5x TBE buffer. The agar was dissolved by heating in a microwave. Agarose solution was cooled to about 50˚C. Five µL of SYBR® safe DNA gel stain and the solution was poured into a pouring electrophoresis chamber. DNA samples were loaded on the gel (14 well set-up). The gel electrophoresis was run at 120V for 45 mins. The DNA fragments were visualized and documented using GE image-quant LAS 500 gel documentation unit

4.4.2 Cloning of NA into pBac 1 vector

Influenza NA (GOI) was obtained from a commercial source (Genescript) in pFastBac vector. The pFastBac was chosen for expressing the protein in Bac-to-Bac BEVS. Later it was decided that using FlashBac BEVS would be more advantageous than Bac-to-Bac method. Hence the GOI was cloned into pBac 1 vector through homologous cloning method.

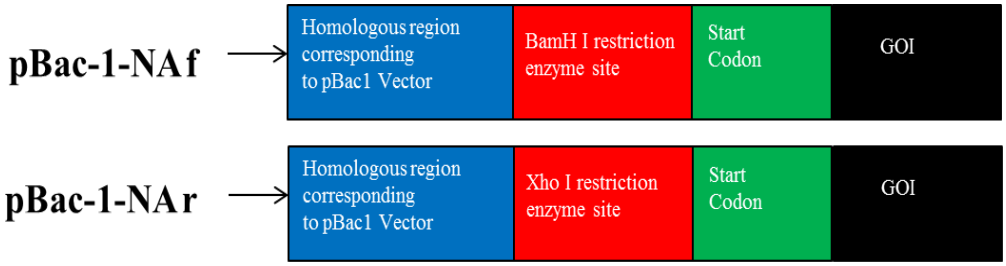

pBac-1-NA F 5' AATAAAAAAACCTATAAATATA GGATCC ATG AAC CCG AAC CAG AAA ATT 3'

pBac-1-NA R 5' AGTGGTGGTGGTGGTGGTG CTCGAG TTA TTTATCAATGGTAAACGGCAGTTCCG 3'

Figure 4-1: Primer design for obtaining NA with homologous pBac 1 overhang.

The construct obtained from the commercial source was in a filter paper. The DNA was cut out from the filter paper and transferred to a 1.5mL Eppendorf tube. 30 µL of TE buffer was added. The tubes were incubated at room temperature for 5mins and spun at maximum speed for 5mins, to obtain the construct. The construct was transformed to XL1-Blue competent cells and miniprepped to obtain the NA-pFastbac construct. In order to clone the NA into pBac 1 vector, NA with homologous regions corresponding to pBac 1 vector was obtained from PCRing the construct. The primers used were pBac1-NAf (69ºC) and pBac1-NAr (66˚C).

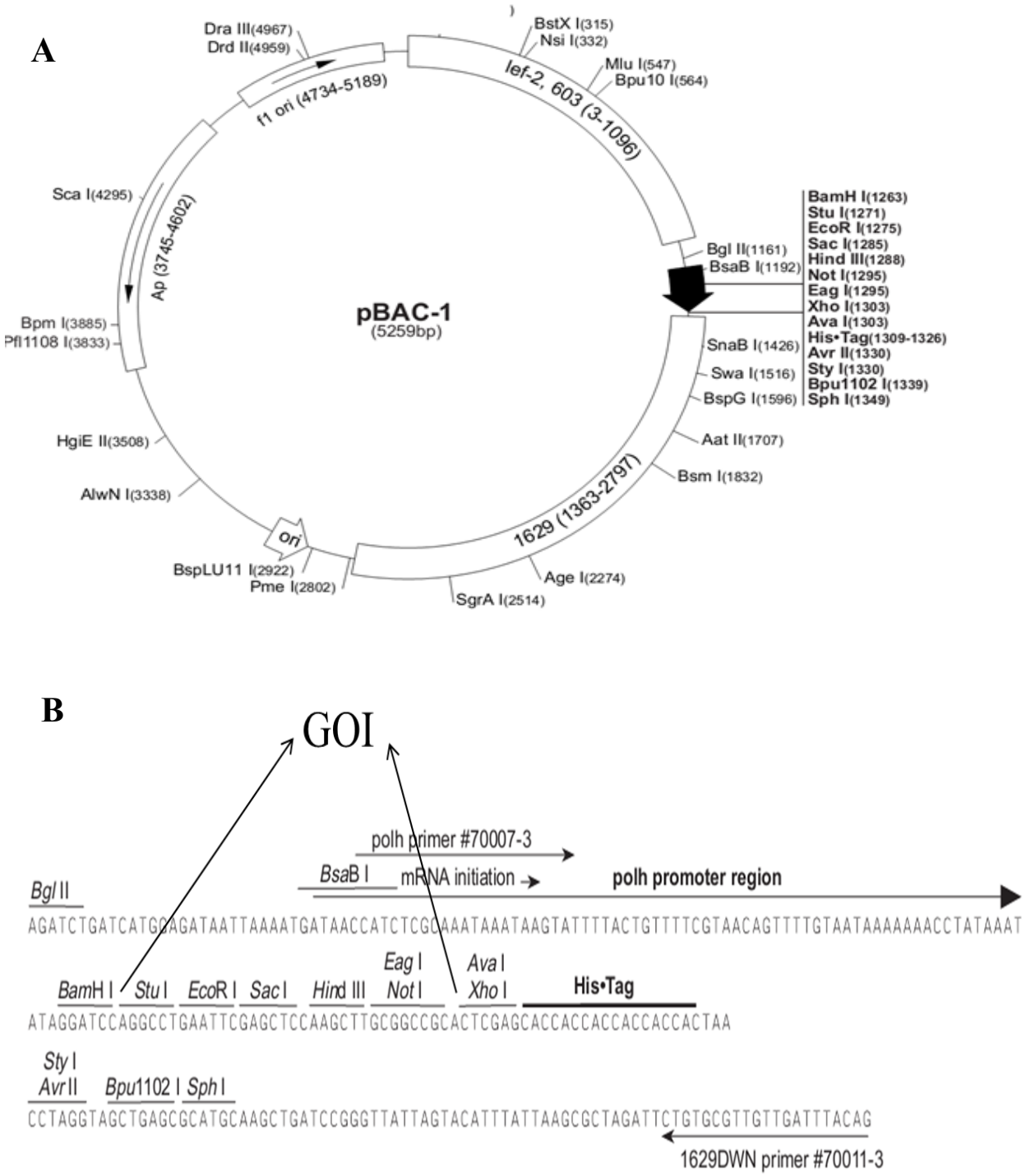

Figure 4-2: Cloning of GOI into pBac 1 vector between BamH I and Xho I restriction site. A) pBac 1 vector map. B) pBac 1 cloning region **(Novagene product sheet).**

Table 4-2 : PCR reaction mix

10 µL 10× KOD buffer
66 µl double-distilled H_20 to a final volume of 100 µL
2 µL ds-DNA template
3 µL each primer(0.3 µM)
10 µL dNTP mix
2 µL KOD enzyme
4 µL $MgSO_4$

Table 4-3: PCR parameters

Steps	**Temperature**	**Time**	**Cycle**
Initial denaturation	95˚C	2 min	X 1
Denaturation	94˚C	15 s	X 30
Annealing	60˚C	30 s	
Extension	72˚C	30 s	
Final extension	72˚C	10 min	X 1

The PCR product was run on agarose gel. The band corresponding to the correct molecular size of 1.4 kb was cut and gel-purified. The concentration of the gel-purified DNA was 54 ng/µL. This DNA was then cloned into pBac 1 vector.

Calculation for cloning:

$$\frac{[(ng\ of\ vector)X\ (kb\ of\ insert)X(\ ratio)]}{(Kb\ of\ vector)} = ng\ of\ DNA \qquad 4\text{-}1$$

Using Equation (4-1) the amount of DNA required was calculated to be 21.63 ng. This corresponds to 2.5 µL of the gel purified DNA. 25 ng of the vector and 21.63 ng of the DNA were mixed. Seven µL of this mixture was then transformed into 50 µL of the XL1-Blue cells. This was then plated on a LB agar plate with ampicillin. The following day 6 random colonies were picked and was analysed using a colony PCR.

4.4.3 Colony PCR

Six random colonies were picked and resuspended in 30 µL of sterile water. 2 µL of this

mixture was used as the template for colony PCR.

Table 4-4: Colony PCR reaction mix

2 µL 10× buffer
12.6 µL double-distilled H_20 to a final volume of 20 µL
2 µL template (colony)
1 µL each primer(0.3 µM)
0.2 µL dNTP mix
0.2 µL Taq enzyme
1 µL $MgSo_4$

Table 4-5: Colony PCR parameters

Steps	**Temperature**	**Time**	**Cycle**
Initial denaturation	95˚C	2 min	X 1
Denaturation	94˚C	30 s	X 30
Annealing	55˚C	30 s	
Extension	72˚C	1.5 min	
Final extension	72˚C	10 min	X 1

The PCR products were analysed on agarose-gel electrophoresis. An overnight culture was grown from the positive colony. The culture was minipreped. The minipreped DNA was sent for sequencing.

4.4.4 Restriction enzyme digestion

BamH I and Xho I restriction endonucleases were used to double-digest the DNA at 37˚C for 3 h according to Table 4-6. The digested fragment were analyzed by agarose-gel electrophoresis.

Table 4-6: Composition of double digestions of the NA (wild type and H274Y) with BamH I and EcoR I

Reagents	NA wild-type (µL)	NA H274Y (µL)
DNA	1	1
BamH I	1	1
Xho I	1	1
10 X React ® 2	2	2
10 X NEB ® 4	2	2
Sterile H_2O	13	13
Total	20	20

4.4.5 Site directed mutagenesis (SDM)

The desired mutation of H274Y (Histidine 274 Tyrosine) was introduced by designing specific primers. To obtain the mutant clone, a single nucleotide had to be changed from C to T. Thus based on the following conditions, SDM primer was designed.

- Primers should be between 25 and 45 bases in length, with a melting temperature (*T*m) of ≥75˚C.
- The following formula was used for estimating the *T*m of primers:

$$T_m = 81.5 + 0.41(\%GC)\ 675/N - \%\ mismatch \qquad 4\text{-}2$$

  - *N* is the primer length in bases
  - values for %GC and % mismatch are whole numbers

- The desired point mutation should be close to the middle of the primer with ~10–15 bases of template-complementary sequence on both sides.
- Optimum primers should have a minimum 40% GC content.

The primer used for SDM is "5'-G AAC GCG CCG AAC AGC TAT TAT GAA GAA TGC AG-'3" (The T will introduce the desired mutation), The GOI cloned into pBac1 vector is the template used in this reaction.

Table 4-7: SDM experimental reaction mixture

2.5 µL 10× QuikChange® Multi reaction buffer
18.9 µL double-distilled H20 to a final volume of 25 µL
0.6 µL ds-DNA template (100 ng)
1 µL mutagenic primers (100 ng)
1 µL dNTP mix
1 µL QuikChange® Multi enzyme blend

Table 4-8: SDM PCR Parameters

Steps	**Temperature**	**Time**	**Cycle**
Initial denaturation	95˚C	1 min	X 1
Denaturation	95˚C	1 min	X 30
Annealing	55˚C	1 min	
Extension	65˚C	14 min	
Final extension	65˚C	5 min	X 1

Extension: 2 min/kb of plasmid length (2x7 kb=14 min)

1 µL of *Dpn* I restriction enzyme (10 U/µL) was added directly to the PCR product. The reaction mixture was mixed gently and thoroughly by pipetting. The reaction mixture was spun down in microcentrifuge for 1 minute, then immediately incubated at 37˚C for 1 h to digest the parental (non-mutated) ds-DNA. 50 µL of XL1-Blue competent cells were thawed and transferred into a pre-chilled transformation tube. 2 µL of *Dpn* I digested DNA was transformed into XL1-Blue competent cells. A glycerol stock was made for positive clones (identified using sequencing) and stored at -80˚C.

4.4.6 Insect cell culture

A) Insect cell recovery

1 mL of liquid nitrogen stock of Sf9 cells and Highfive cells were gifted by the protein expression facility at the Australian institute for bioengineering and nanotechnology, University of Queensland. The cryovials were transferred to New Zealand on dry ice. The cells were inoculated immediately on arrival. 50 mL sf900II SFM was added into a sterile 250 mL cell culture flask. The cyroflex from cryovials were cut off and the cells were thawed carefully by hand, making sure that the lid of the cryovial was always intact

during the thawing process. The thawed cells were transferred (~1 mL) into the 50 mL SFM. The flasks were incubated at 28˚C, 120 rpm. The cells were monitor for recovery after 4 days. The cell density and viability was determined. The cells were passaged (sub-cultured) regularly.

B) Subculture of cells

The insect cells were sub-cultured in Sf900II SFM. The SFM was pre-warmed to room temperature. The cell density and viability of the existing cultures were determined. Sf9 cells were seeded at, $1x10^6$ cells/mL, while the High-Five cells were seeded at $2x10^5$ cells/mL. In both cases the culture volume was 50mL. The caps of the 250 mL flask were loosened (to facilitate oxygen) and incubated at 28˚C at 120 rpm. It is essential that the cells are in log phase at the time of infection. The cells used for the experiment should come from a culture in mid-exponential growth phase. Hence, the cells were sub-cultured twice every week (Monday & Friday). In order to understand the growth cycle of the insect cells, both the cell lines were inoculated into fresh media and were allowed to grow over a period of 7 days without sub-culturing. The cell densities and viability were monitored every 24 h and a growth curve was plotted.

C) Freezing of cells

The cryovials were labeled with freezing number, date, cell line and medium. The freezing medium (SFM+15% DMSO) was filter sterilized using 0.22 µm filter into 50 mL falcon tube and stored at 4˚C. The cell density and viability of culture was determined. The cells were at exponential growth phase with 95% viability. The cells were spun down at low speed (1500 rpm for 5 min) and the supernatant was removed and filter sterilized through 0.22 µm filter into another sterile 50 mL falcon tube (conditioned media). The cell pellets were re-suspended in cold freezing medium. Equal volume of sterile conditioned medium was added to the concentrated cells.1mL of concentrated cells was transferred into labeled cryovials. The cryovials were stored at –80˚C. Liquid nitrogen storage is highly recommended for storing cell stocks.

4.4.7 Transfection (FlashBAC BEVS)

A) Seeding of cells

Three wells were set up for infection in a six-well plate. One well was used as control,

second well was used for wild-type NA infection and the third well was used for H274Y NA infection. 6 x 10^5 Sf9 cells/mL was seeded in 2 mL of Sf900II medium per well in a six-well plate. The plate was gently moved side to side for even distribution and the plate was incubated at 28˚C for 1 h to allow cells to attach to the plate surface.

B) Transfection mix preparation

Mixture A:	
flashBAC DNA (100 ng)	5 µL
Transfer vector DNA (500 ng)	5 µL
Grace's medium	100 µL
Mixture B:	
Cellfectin	6 µL
Grace's medium	100 µL

Then 105 µL of Mixture A was mixed with 106 µL of Mixture B. This is called the transfection mix. The transfection mix was incubated at room temperature for 30 min. 800 µL Grace's medium was added to the transfection mix. 1 mL of Grace's medium was used as the transfection mix for the control well.

C) Transfection

The six well plate was removed from the incubator and the media was removed, quickly 2mL of Grace's medium was added (care was taken in not allowing the cells to dry out). The medium was removed and 1mL of transfection mix was added to the well in a dropwise manner. The cells were incubated at 28˚C for 5 h. After 5 h the transfection mix was removed and 2 mL of Sf900II medium supplemented with antibiotics and antimycotics (100X) was added. The plate was placed in plastic container with moist paper towels and incubated 28˚C for 7 days. The cells were monitored at 5 day post infection (dpi), increased cell diameter, increased size of cell nuclei, and detachment were observed. At 7 dpi, the cells were harvested. 2 mL medium from the 6-well plate was transferred to a sterile 10 mL tube. P1 budded virus (BV) was harvested by centrifugation at 1500 rpm for 5 min. The supernatant was transferred to a fresh 10 mL tube. The tube was labelled and stored at 4˚C. This was the P1 BV stock.

4.4.8 BV Amplification

A) P2 BV Amplification

800 µL of P1 BV cell culture supernatant was added to passage of cells to make a P2 BV culture. P2 BV was monitored 2 days after infection. The cells had 88% viability and hence it was left for another day. On the 3rd day the viability had decreased to 78% (<80%), thus the cells were ready for harvest. The cells were harvested by centrifuging the entire culture in a sterile 50 mL tube (1500 rpm, 5 min). The supernatant was transferred into a fresh sterile 50mL tube, labelled and stored at 4˚C immediately. This was the P2 BV stock.

B) P3 BV Amplification

10 µL of P2 BV cell culture supernatant was added to passage of cells to make a P3 BV culture. P3 BV was monitored 2 days after infection. The cells had 81% viability and hence it was left for another day. On the 3rd day the viability had decreased to 74% (<80%), thus the cells were ready for harvest. The cells were harvested by centrifuging the entire culture in a sterile 50 mL tube (1500 rpm, 5 min). The supernatant was transferred into a fresh sterile 50 mL tube, labelled and stored at 4˚C immediately. This was the P3 BV stock.

C) Protein expression

Sf9 and High-Five cells were seeded at 3 x 10^6 cells/mL and 1.5 x 10^6 cells/mL respectively. For a Sf9 culture 1.5 mL of P3 BV was added per 50 mL and for a High-Five culture 0.75 mL P3 BV was added per 50 mL. The flasks were incubated at 28˚C, 120 rpm. Cultures were sampled every 24 h for 4 days. The samples were spun down for 5 min at maximum speed in a micro-centrifuge and the supernatant and cell pellet were stored separately in 4˚C.The samples were the used for SDS-PAGE and western blot assay.

4.4.9 Western blotting

A) Sodium dodecyl sulfate polyacrylamide gel electrophoresis (SDS-PAGE)

Samples of each of the recombinant cell lysates were separated by sodium SDS-PAGE using an Invitrogen Novex mini cell. Samples were mixed with β-mercaptoethanol and SDS then heated and centrifuged at 11,000 rpm for 40 s before being loaded into the gel.

The electrophoresis was run at 200V for 45min. After electrophoresis, the gel was stained in staining solution (0.22% Coomassie Brilliant Blue R-250, 50% methanol, 10% glacial acetic acid) for 40 min with gentle agitation. The gel was detained in destaining solution (20% methanol, 10% glacial acetic acid) with gentle agitation. The gel image was documented using the GE image-quant LAS 500 gel documentation unit.

B) Semi dry electrophoretic transfer

For electroblotting the protein bands were separated using SDS-PAGE (staining and destaining not performed for electroblotting). Electroblotting was performed using Trans-Blot®SD semi-dry electrophoretic transfer cell. Twelve sheets of Whatman filter paper and 1 sheet of nitrocellulose membrane (pore size 0.2 m) were cut to the size of the PAGE gel and soaked in transfer buffer for 45 min. Six filter papers were placed onto the platinum anode. A test tube was rolled over the surface of the filter paper to remove all air bubbles. The pre-wetted nitrocellulose membrane was placed on top of the filter paper. Again a test tube was rolled over the surface to remove all air bubbles. The SDS-PAGE was carefully placed on top of the transfer membrane. The gel was aligned to the centre of the membrane. A test tube was rolled over the surface to remove all air bubbles. The remaining six filter papers were placed on top of the gel. A test tube was rolled over the surface to remove all air bubbles. The cathode was placed onto the stack. The power supply was turned on and the gel was transferred to the membrane for 30 min at 25V.

C) Antibody staining

The membrane was blocked for 1 h at room temperature using blocking buffer. The membrane was incubated with Influenza A H1N1 (Swine Flu 2009) NA / neuraminidase antibody, overnight at 4˚C. The antibody was diluted in blocking buffer (1:1000). The membrane was washed thrice (15 min each wash) with PBST. The membrane was incubated with labelled secondary antibody (mouse IgG secondary antibody HP conjugate) for 1 h at room temperature. The antibody was diluted in blocking buffer (1:10,000). The membrane was washed thrice (15 min each wash) with PBST. The secondary antibody was allowed to develop a chemiluminescent signal with ECL western blotting detection agents. The signal was documented using GE image-quant LAS 500 gel documentation unit.

4.4.10 Protein purification

A) Cell Lysis

Cell lysis was performed using the protocol described by (slightly modified) Dalakouras et al. (2006). Recombinant insect cells were harvested and suspended in 4 mL of lysis buffer. 400 µL of protease inhibitor cocktail was added, to the cell suspension, just before sonication. The cells were sonicated on ice to release proteins. The final cell lysate was centrifuged at 12,000 rpm for 15 min at 4˚C and to separate the soluble and insoluble fraction. The supernatant containing the soluble proteins were collected and used as a source of NA.

B) Anion exchange chromatography

Anion exchange chromatography was carried out on an AKTA Explorer 10 chromatography system. A 1 mL Resource™ Q anion exchange column was equilibrated with Buffer A. Sample was injected onto the column through an injection loop and washed through with buffer A for 5 column volumes (CV). Bound proteins were eluted with Buffer B (gradient elution for 20 CV). UV absorbance at 280 nm and 215 nm was measured using an AKTA UV-900 unit. The flow through and eluted fractions were collected using an AKTA Frac-900 unit. The fractions were subjected to western blot analysis to detect the presence of influenza NA. The fractions with positive western blot signal were combined for further analysis and purification.

C) Size exclusion chromatography

Size exclusion chromatography was carried out on an AKTA Explorer 10 chromatography system. A 24 mL Superdex S200 10/300 GL size exclusion column was equilibrated Buffer C. The anion exchange combined fractions was injected onto the column through an injection loop and washed through with buffer C. UV absorbance at 280 nm and 215 nm was measured using an AKTA UV-900 unit. Fractions were collected using an AKTA UV-900 unit. The fractions were subjected to SDS-PAGE and dot blot analysis to detect the presence of influenza NA.

4.4.11 Activity Assay

Recombinant samples were sent away for external testing to Dr Richard Hall at Environmental Science & Research (ESR) at the National Centre for Biosecurity &

Infectious Disease (NCBID), Wallaceville, NZ. The samples were tested for NA activity using a fluorometric assay originally described by Potier et al. (1979).Virus samples from ESR were used as positive and negative control for the assay. The nomenclature of the control virus are described as type, location isolated, strain number, year of first isolation, subtype (for example : A/Fukui/45/2004 (H3N2)).

4. 5 Results and discussion

4.5.1 Cloning of NA into pBac 1 vector

A) Cloning

The NA wild-type gene (1466 bp) was amplified by PCR from pFastBac construct containing NA. The primers used for the PCR reaction had homologous regions corresponding to pBac vector. The PCR product was run on 0.8% agarose gel and a band of 1466 bp was obtained (Figure 4-3) and gel-purified. The concentration of the gel-purified DNA was measured at 54 ng/µL. The PCR product was then cloned into pBac1 vector using the *in-vivo* cloning method.

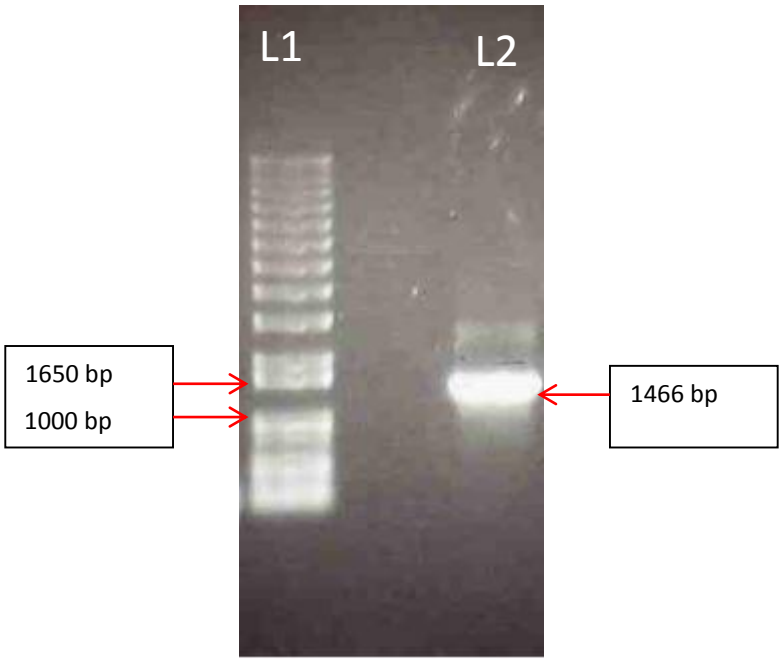

Figure 4-3: 0.8% Agarose gel (stained with SYBR safe) analysis of the PCR product (L2).The ba corresponding to 1466 bp is the GOI (NA wild type). L1) 1 kb plus DNA ladder (Invitrogen).

B) Colony PCR

Colony PCR of the clones C1-C6 was performed to verify the presence of the NA sequence with pBac-NAf and pBac-NAr primers and Taq DNA polymerase. The amplified fragment (1466 bp) was seen only in one clone (Figure 4-4). This indicated the presence of the NA in that particular clone (C2). The negative control for colony PCR was the plasmid pBac1 without the GOI.

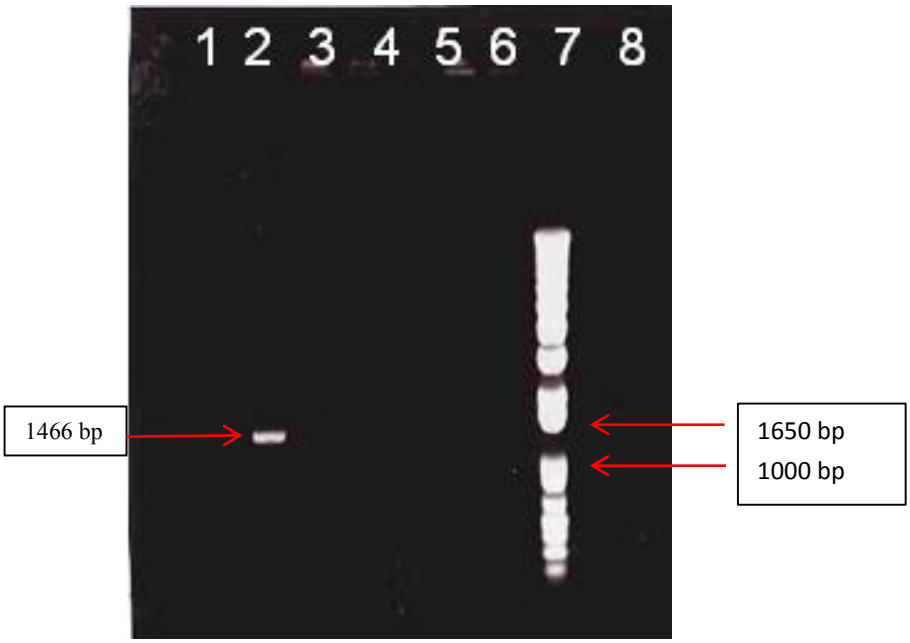

Figure 4-4: Colony PCR amplified fragments of NA on 1% agarose gel with pBac-NAf and pBac-NAr primers and Taq DNA polymerase. Lane: 1-6) C1-C6, 7) 1 kb plus DNA ladder (Invitrogen) and 8) negative control (plasmid pBac1).

C) Restriction digestion

Double digestions of pBac1-NA were performed with the restriction endonucleases BamH I and Xho I. Two fragments corresponding to pBac 1 vector (5292 bp) and NA (1466 bp) were obtained after digestion, as shown in Figure 4-5. This indicated the presence of the NA in colony 2.The undigested sample had only one fragment corresponding to pBac 1- NA (6725).

D) DNA sequencing of the pBac-NA

DNA sequencing of clone 2 was performed with the primer pBac1-NAf for plus strand

determination and the sequencing result was positive. The clone was again checked through DNA sequencing with the primer (1629 DWN primer) that recognized the sequence in the vector (Figure 4-2). Based on the positive sequencing results, clone 2 was used for infecting the insect cells. Also, clone 2 was used for SDM to obtain the H274Y mutant.

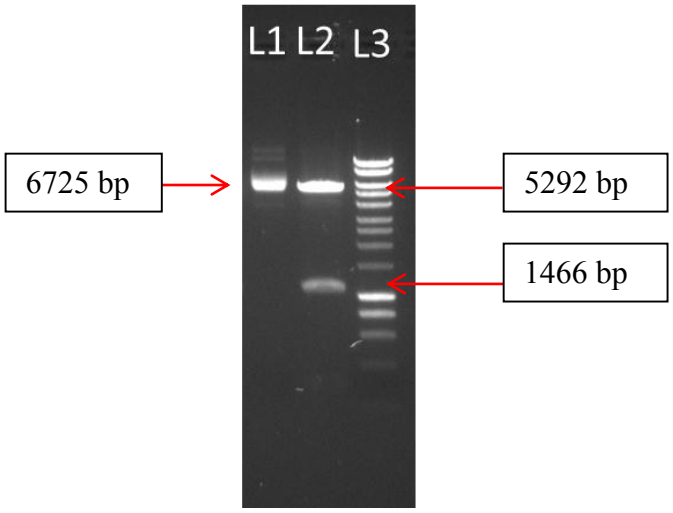

Figure 4-5: Double digestions of pBac-NA, (L1) undigested DNA containing a single band corresponding to pBac-NA (6725), (L2) double digested DNA containing two fragments corresponding to pBac 1 vector (5292 bp) and NA (1466 bp) and (L3) 1kB plus DNA ladder (Invitrogen) on 1% agarose gel.

4.5.2 Site directed mutagenesis (SDM)

A) Restriction digestion

A double restriction digestion analysis was performed on clone 2 of pBac1-NA mutant with the restriction endonucleases BamH I and Xho I. Two fragments corresponding to pBac 1 vector (5292 bp) and NA mutant (1466 bp) were obtained after digestion, as shown in Figure 4 6. This indicated the presence of the NA. The undigested sample had only one fragment corresponding to pBac 1- NA mutant (6725 bp).

B) DNA sequencing of pBac-NA mutant

The overnight cultures grown from the three colonies that were transformed (into XL1-Blue competent cells) after SDM were minipreped and were sent for sequencing. The sequencing analysis of the mutation at position 274, which was towards the end of the

protein sequence, was performed with the reverse primer alone. From the sequencing result it was confirmed that clone 2 was clean and carried the desired mutation. Hence, clone 2 was again sequenced with the forward primer. This confirmed that the colony was perfectly clean and carried only the desired mutation at position 274.

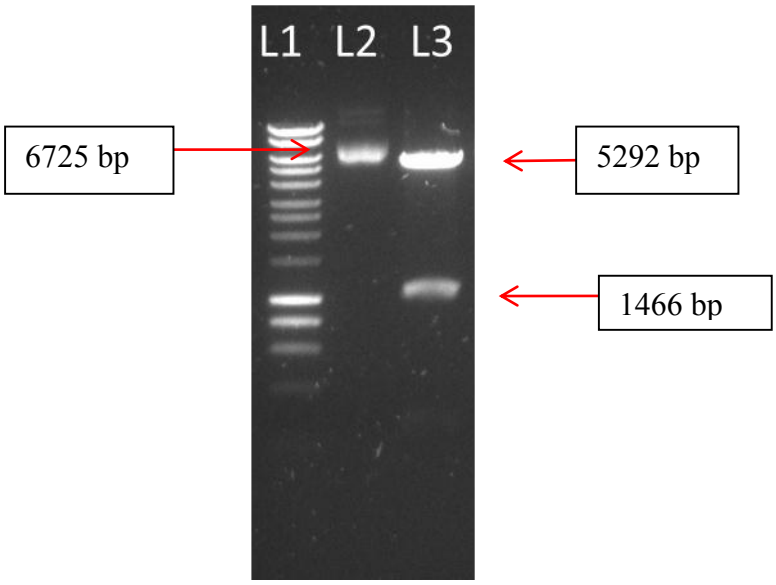

Figure 4-6: Double digestions of pBac-NA H274Y, (L1) 1 kb plus DNA ladder (Invitrogen), (L2) undigested DNA containing a single band corresponding to pBac-NA mutant (6725) and (L3) double digested DNA containing two fragments corresponding to pBac 1 vector (5292 bp) and NA mutant (1466 bp) on 1% agarose gel.

4.5.3 Insect cell culture

Sf9 cells and High-Five cells were cultured in sf900 II SFM for 168 h (7 days). One mL samples were collected every 24 h to determine the cell density and viability (Figure 4-7). For the sf9 cells it was observed that cell densities increased exponentially over the first four days. This indicated the growth phase of the cells. The cell density reached a maximum of 1.2 x 10^7 cells/mL. On days five and six the cell density reached a plateau (stationary phase). The sf9 cell viability remained above 96% until day five, after which a gradual decrease in cell viability was noticed. The viability dropped to 78% at the end of day seven. This indicated that the cells had reached their death phase. For the High-Five cells, the exponential phase lasted for three days, with the cell density reaching a maximum of 5.4 x 10^6 cells/mL. The stationary phase was observed on day 4, after which the viability dropped significantly (88%) and the cells entered the death phase. The viability decreased to less than 70% on day seven. For subsequent sub-culturing of cells,

it was essential that the cells were in the exponential phase. From the cell growth curve analysis (Figure 4-7), it was determined that the optimum time for sub-culture for both the cell lines were between days three and four.

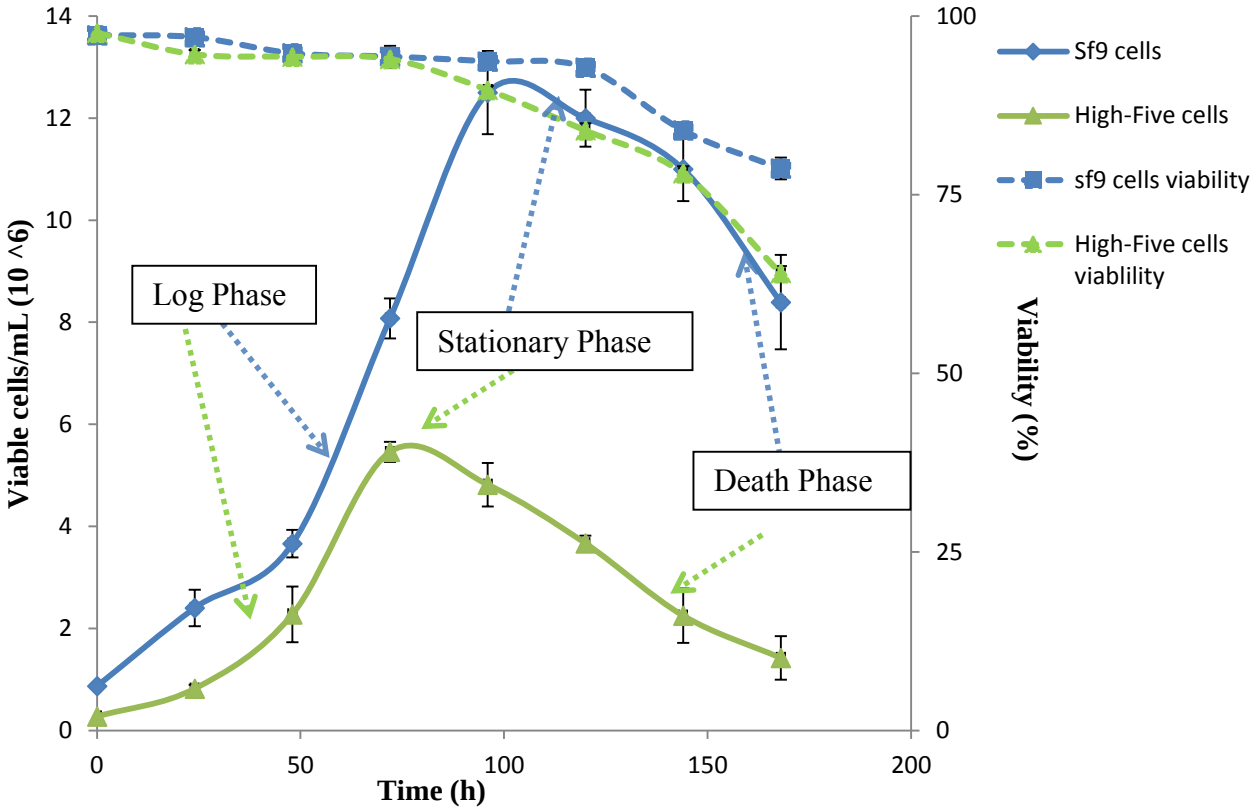

Figure 4-7: Growth curve analysis for sf9 cells and High-Five cells. One mL sample was collected after every 24 h and cell density and viability was measured (triplicates). All data points shown in the graph are mean ± standard deviation (S.D.) of the triplicate measurements.

4.5.4 Transfection of insect cells

A) Isolation of P1 viral stock

Transfection of Sf9 insect cells (6 x 10^5 cells/mL, viability > 97%) was performed in an un-supplemented Grace's Medium in a 6-well tissue culture plate as described in section 4.4.7. Six µL of Cellfectin® reagent was used for mediating the transfection. After 5 h of transfection, the cells were cultured in 2 mL Sf900II medium supplemented with antibiotics and antimycotics (100X) for 7 days at 28˚C. Infection was monitored after 5 dpi. When compared to the non-transfected cells, the transfected cells showed increase

in cell diameter, cessation of cell growth and detachment from plate surface. These were signs of late and very late infection. P1 viral stock was isolated and collected after 7 dpi.

B) Preparation of P2 and P3 viral stocks

The collected P1 viral stock was a low-titer stock and therefore, the stock was amplified to obtain high-titer P2 and P3 stocks. The stocks were amplified as described in section 4.4.8. When compared to the non-transfected cells, the trasnfected cells decreased in cell viability. Once the viability decreased below 80%, (Figure 4-8) the P2 and P3 virus stocks were harvested.

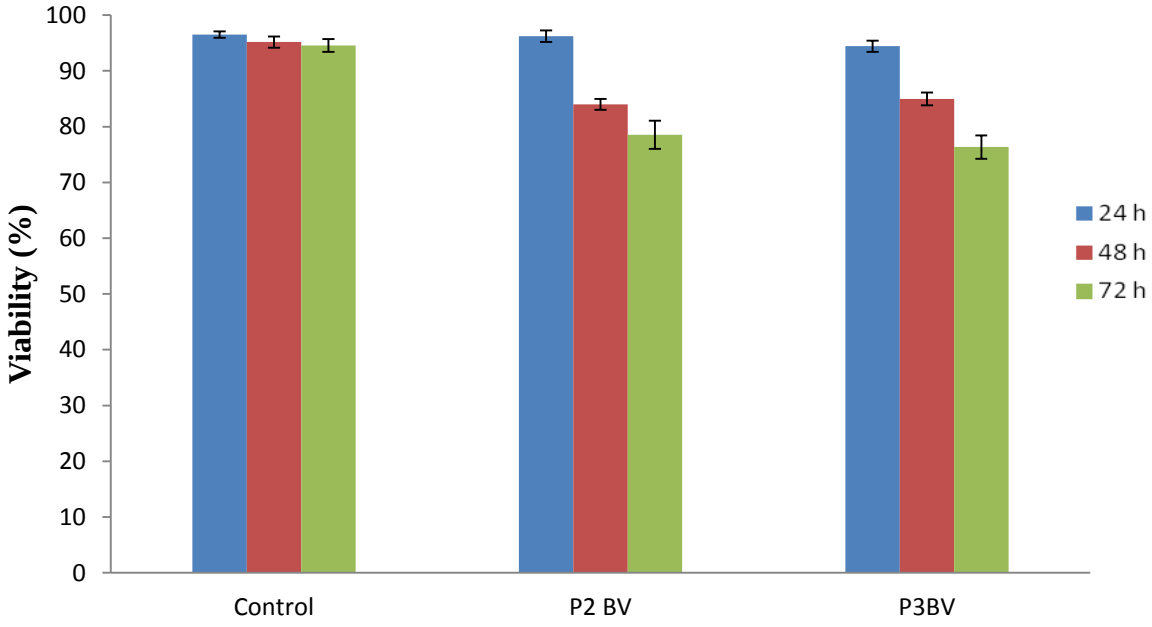

Figure 4-8: Monitoring cell viability for P2 and P3 viral stock. One mL sample was collected after every 24 h and cell viability was measured (triplicates). The viability data shown in the graph are mean ± S.D. of the triplicate measurements.

4.5.5 Expression analysis

A) Cell density and viability

The expression condition of the recombinant influenza NA was optimized by using two different cell lines (sf9 and High-Five cells). Sf9 and High-Five cells were seeded at 3 x 10^6 cells/mL and 1.5 x 10^6 cells/mL respectively for protein expression. The expression was set up by adding P3 viral stocks to the cells (as described in 4.4.8). Sf9 and High-

Five cells with the same seeding density of 3 x 10^6 cells/mL and 1.5 x 10^6 cells/mL (no P3 stock added) were used as control. A time course expression analysis was performed for 24, 48, 72 and 96 h post-infection. One mL sample was collected every 24 h. The cell morphology, viability and cell density were monitored during the time course. From the bar graph (Figure 4-9 & Figure 4-10) it was observed that the cell viability of the infected cells were lower than the respective controls. However, once infected with P3 viral stock, the viability should drop to around 80% by 24 h. In this case the viability was still 90% for the infected cells. Moreover, from the growth curves (Figure 4-11 & Figure 4-12) it was observed that the cells were still growing up to 48 h post infection. This indicated that the not all cells were infected. The uninfected cells continued to grow, thereby not allowing the cell density and viability to drop as expected. This could have been because of poor quality of the recombinant baculocvirus (P3 BV) used for infection.

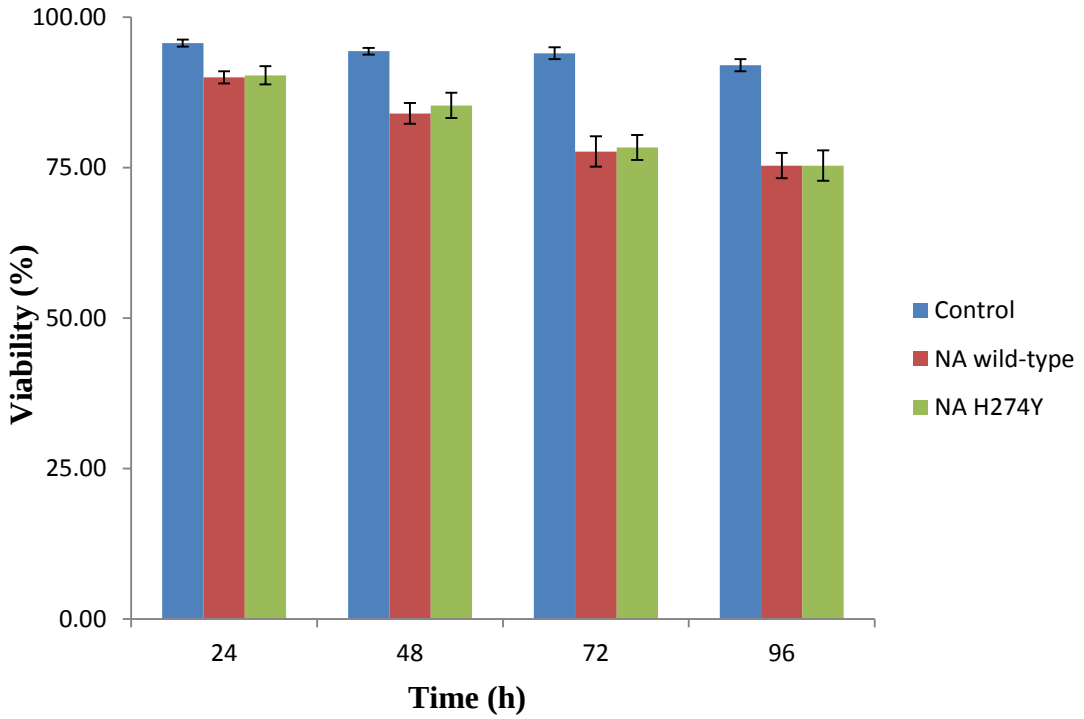

Figure 4-9: Time course analysis (cell viability) in High-Five cells. One mL samples were collected every 24 h. Cell viability was measured (triplicates). The viability data shown in the graph are mean ± S.D. of the triplicate measurements.

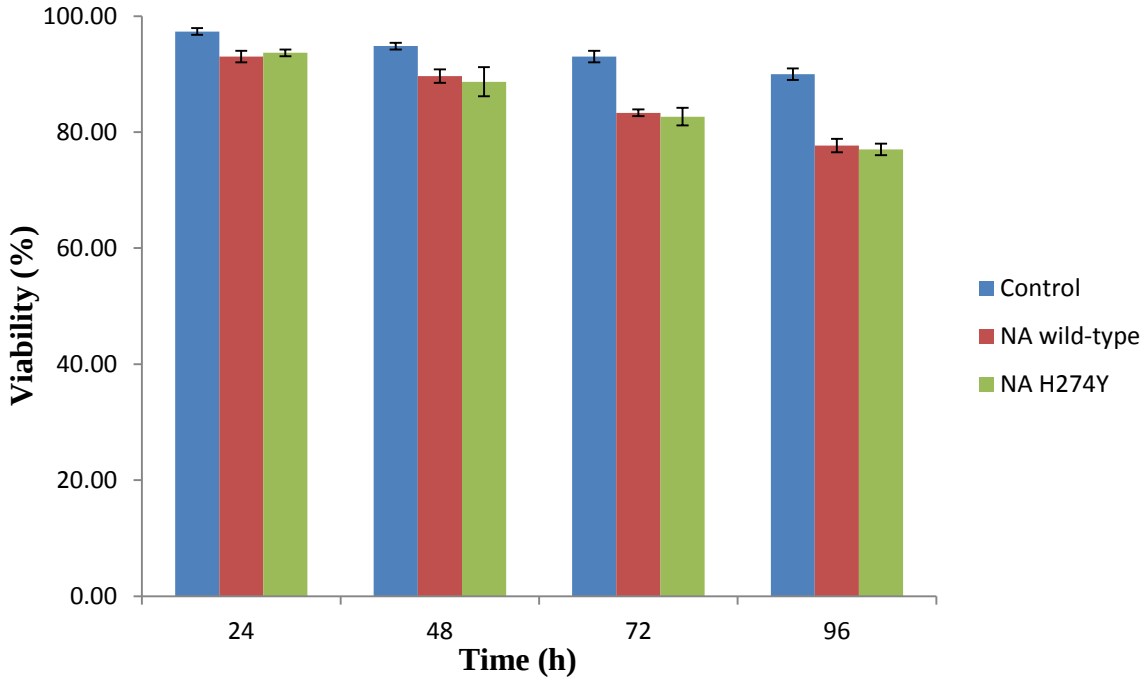

Figure 4-10: Time course analysis (cell viability) in sf9 cells. One mL samples were collected every 24 h. Cell viability was measured (triplicates). The viability data shown in the graph are mean ± S.D. of the triplicate measurements.

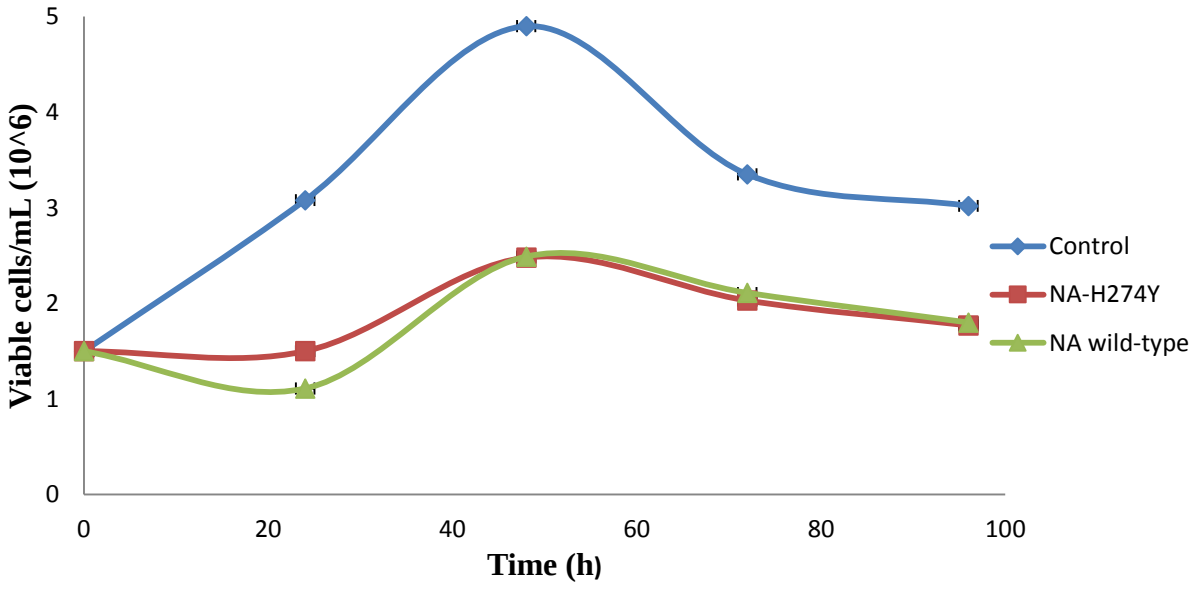

Figure 4-11: Time course analysis (growth curve plot) in High-Five cells. One mL samples were collected every 24 h. Cell densities were measured (triplicates) a growth curve chart has been plotted. The cell denstiy data shown in the graph are mean ± S.D. of triplicate measurements.

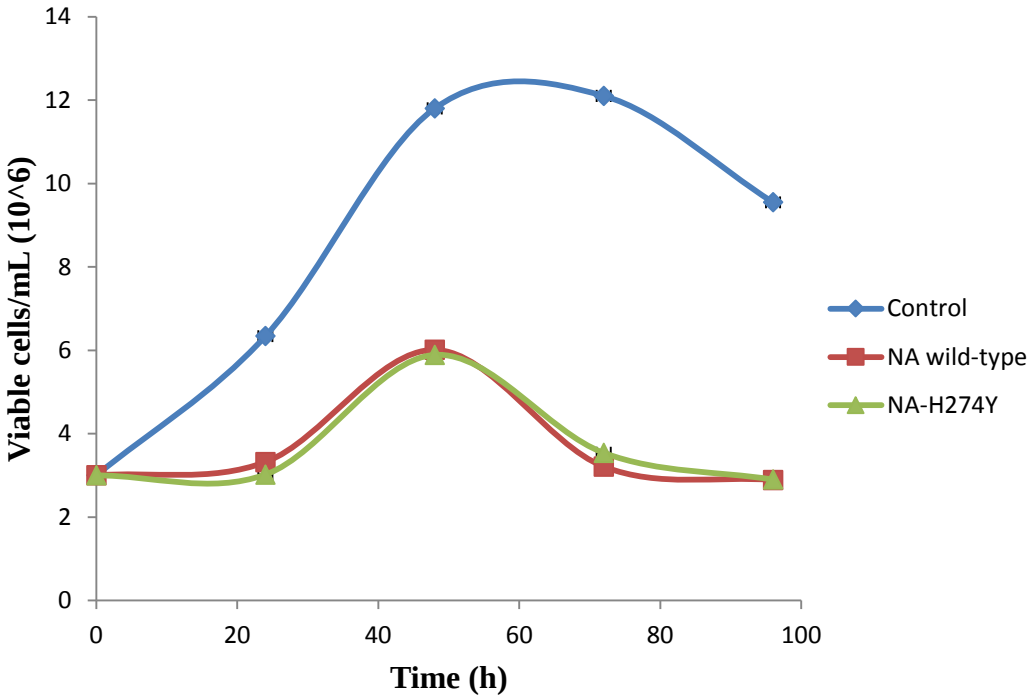

Figure 4-12: Time course analysis (growth curve plot) in sf9 cells. One mL samples were collected every 24 h. Cell densities were measured (triplicates) a growth curve chart has been plotted. The cell denstiy data shown in the graph are mean ± S.D. of triplicate measurements.

B) Cell morphology

Change in cell morphology was an essential factor for monitoring insect cell infection. The infected cells gradually showed changes in cell morphology, such as, an increase in cell diameter, increase in cell nucleus and cessation of cell growth. When the cells were subjected to a trypan blue viability test, the viable cells remained colourless, while dead cells were blue. This is because the cell membranes of the viable cells remained intact and did not allow the trypan blue to enter the cells, whereas dead cells were stain because of damaged cell membranes. From the cell images (Figure 4-14 & Figure 4-13) it was observed that infection has started spreading gradually. Both the cell lines followed a similar trend. For the first 24 h, very few cells were infected, due to which the cell density and viability did not drop as expected (Figure 4-9 & Figure 4-10). After 72 h post infection most of the high five cells had been infected. This had resulted in more cell death which in turn had dropped the viability below 80%. The sf9 cells on the other hand showed a similar drop in viability only after 96 h post infection.

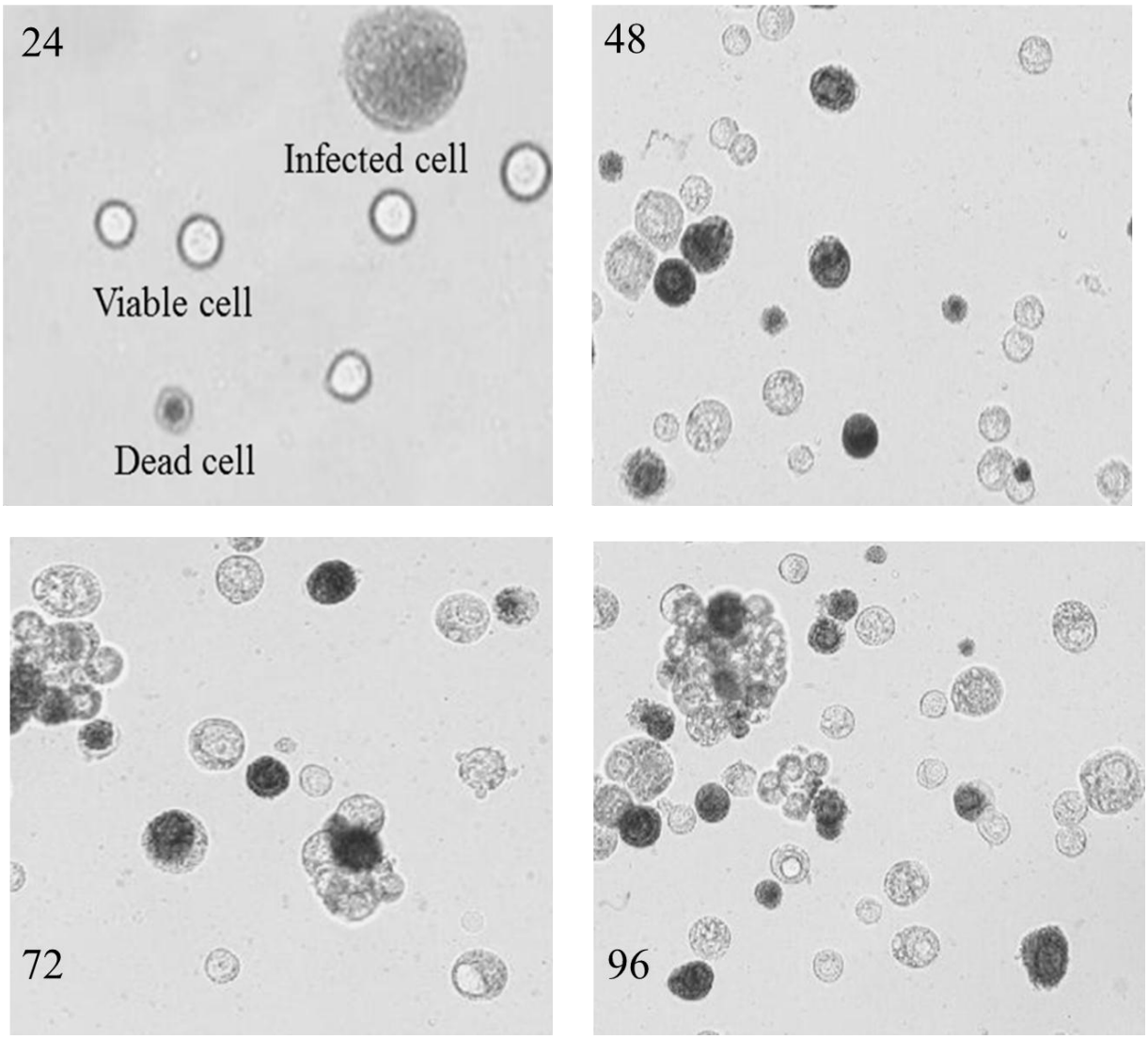

Figure 4-13: High-Five cells transfected with the recombinant baculovirus of influenza NA. Changes in cell morphology were observed every 24 h under a microscope at 40X magnification.

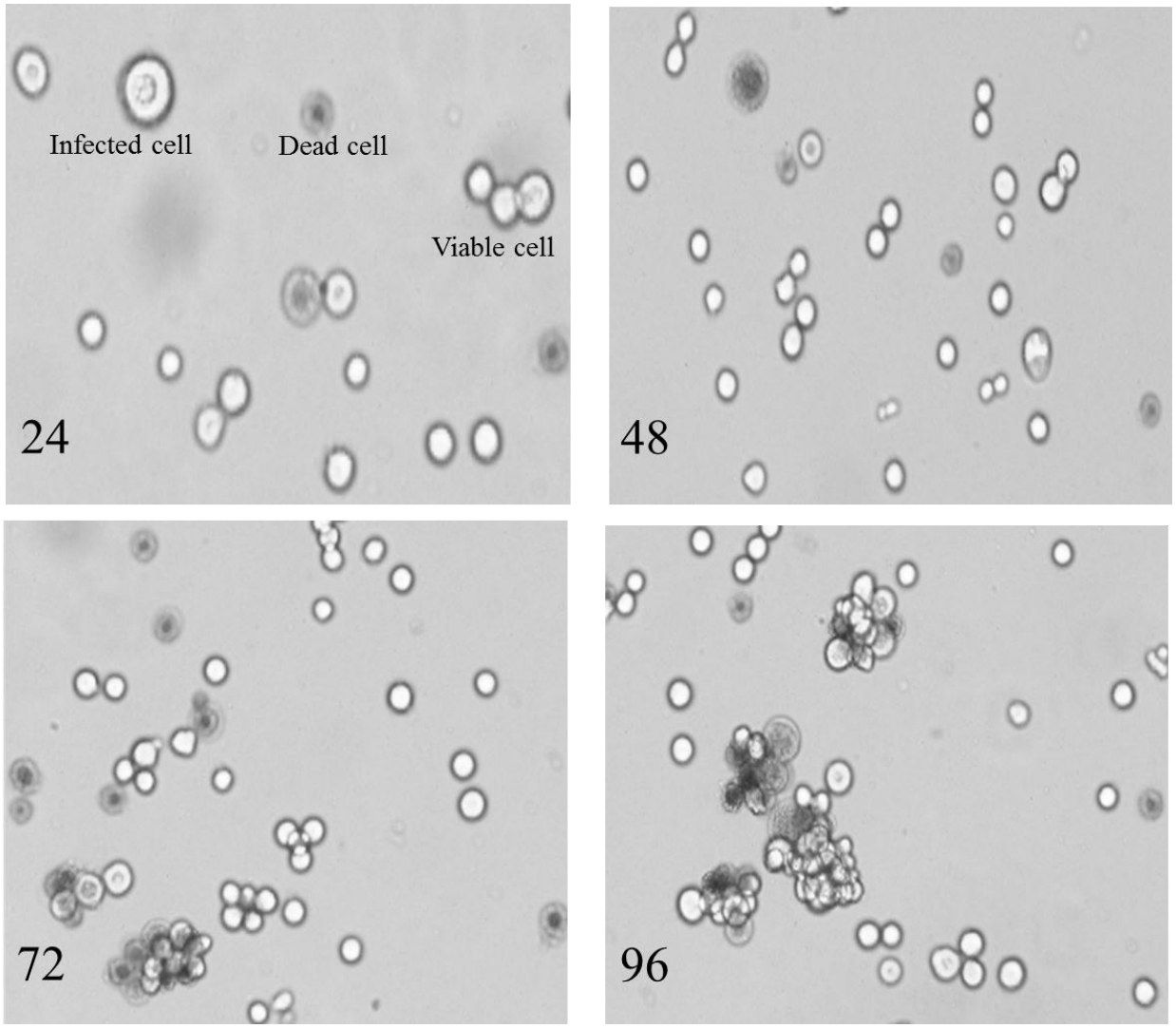

Figure 4-14: Sf9 cells transfected with the recombinant baculovirus of influenza NA. Changes in cell morphology were observed every 24 h under a microscope at 40X magnification.

C) Sodium dodecyl sulfate polyacrylamide gel electrophoresis (SDS-PAGE)

Influenza NA forms a tetrameric structure, which is the only enzymatically active form of NA. The molecular weight of active (tetrameric) NA is approximately 240 kDa. However, it has been reported that, SDS-PAGE analysis in the presence of β-mercaptoethanol resulted only in a 55 kDa band (Wu et al. 2009; Deroo et al. 1996). This is because under reducing conditions the protein was denatured and di-sulphide bonds were disrupted. Hence, the tetrameric NA was converted to a monomeric form. Similar observations were made in this thesis work. From the SDS-PAGE analysis (Figure 4-15) it was very difficult to see a prominent 55 kDa band. As only few insect cells were infected, when the cells were lysed for releasing the proteins, the majority of the proteins were host cell proteins with very minor anounts of NA. Hence, it was difficult to follow the protein on the SDS-PAGE. Therefore a western blot analysis was performed to confirm the presence of NA.

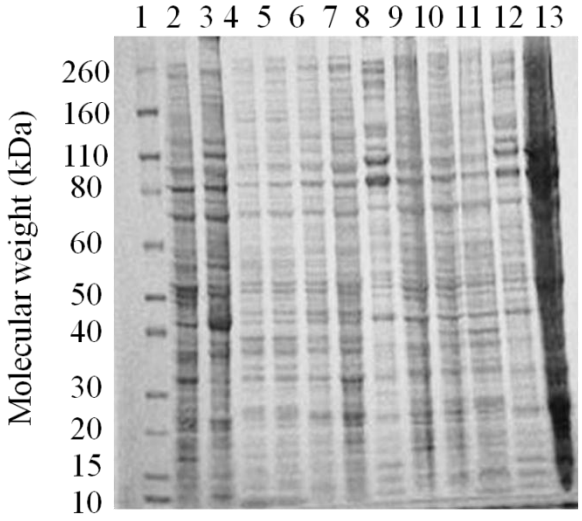

***Figure 4-15**: SDS-PAGE analysis of the time course of expression of influenza NA in Sf9 and High-Five insect cells, under reducing condition and stained with coomassie blue. L1) Ladder, L2) Sf9 cell pellet (control 72 h), L3) Sf9 cell pellet (control 96 h), L4) Sf9 cell pellet (NA-WT 72 h), L5) Sf9 cell pellet (NA-WT 96 h), L6) Sf9 cell pellet (NA-H274Y 72 h), L7) Sf9 cell pellet (NA-H274Y 96 h), L8) High-Five cell pellet (control 48 h), L9) High-Five cell pellet (control 72 h), L10) High-Five cell pellet (NA-WT 48 h), L11) High-Five cell pellet (NA-WT 72 h), L12) High-Five cell pellet (NA-H274Y 48 h), L13) High-Five cell pellet (NA-H274Y 72 h).*

D) Western-blotting

Western-blotting analyses was performed to confirm the presence of influenza NA in the High-Five and sf9 samples collected at different time intervals (24 h, 48 h and 72 h post infection for High-Five cells and 72 h and 96 h post infection for sf9 cells). The samples were blotted to the nitrocellulose membrane after separation by SDS-PAGE as described in 4.4.9. The western blot image (Figure 4-16) confirmed the presence of NA (both wild-type and H274Y mutant) in all the samples. A predominant band was seen at 55 kDa for both the cell lines. The High-Five cells expressed NA from 24 h post infection. The expression was at its peak at 72 h post infection. This was in good agreement with the above discussed results. There was a significant drop in cell viability (Figure 4-9 & Figure 4-11) after 72 h post infection for High-Five cells. Moreover, the cell image (Figure 4-13) also confirmed that most of the cells were infected only after 72 h post infection. The level of expression in sf9 cells was relatively low. The expression reached a maximum only at 96 h post infection. This was also in good agreement with the above discussed results. As seen in the viability graph (Figure 4-10), the cell viability drops below 80% only after 96 h post infection for sf9 cells. Hence, the western blot band intensity was stronger after 96 h post infection. Western blotting has proved to be a useful tool for detecting the presence of NA in the cell culture samples. From this blot, it was concluded that High-Five cells expressed NA relatively more NA than sf9 cells. It was also concluded that 72 h post infection was the optimum time for harvesting the cells for further analysis.

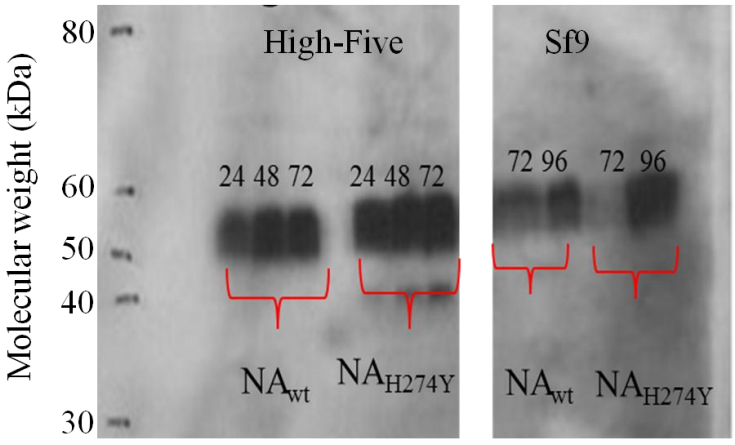

***Figure 4-16**: Western blotting analysis of the time course of expression of influenza NA in Sf9 and High-Five insect cells, detected with the monoclonal influenza A H1N1 (swine flu 2009) NA / neuraminidase antibody.*

4.5.6 Purification

A) Cell Lysis

Cells were lysed as described in 4.4.10.A. The soluble and insoluble fractions were analysed using western blot (Figure 4-17) to confirm the presence of NA. The majority of the protein was found in the soluble fractions. Although the insoluble fractions also contained NA, the amount was comparatively lesser than the amount found in the soluble fractions. The Soluble fractions were used as a source of NA.

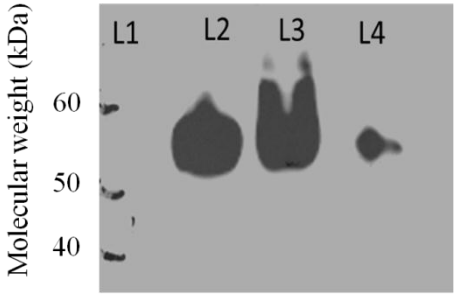

Figure 4-17: Western blotting analysis of soluble and insoluble cell lysate fractions detected with the monoclonal influenza A H1N1 (swine flu 2009) NA / neuraminidase antibody. L1) ladder, L2) total protein, L3) soluble fraction and L4) insoluble fraction.

B) Anion exchange chromatography- gradient elution

Anion exchange purification of influenza NA wild type expressed in High-Five insect cells was performed with a 1 mL Resource Q column as described in section 4.4.10. Figure 4-18 showed that majority of the contaminants (host cell proteins) did not bind to the column at pH 6.0, while the target protein NA bound to the column. The bound proteins were eluted with an increasing salt gradient (0% to 100% buffer B). Western blot results (Figure 4-20) confirmed that NA was not present in the flow through fractions. The fractions corresponding to the peak indicated in Figure 4-18, showed positive western blot band at 55 kDa. Anion exchange chromatography proved to be a very useful first step purification technique to remove major host cell proteins from the cell extract. The fractions with the positive western blot band were pooled and further purified using SEC.

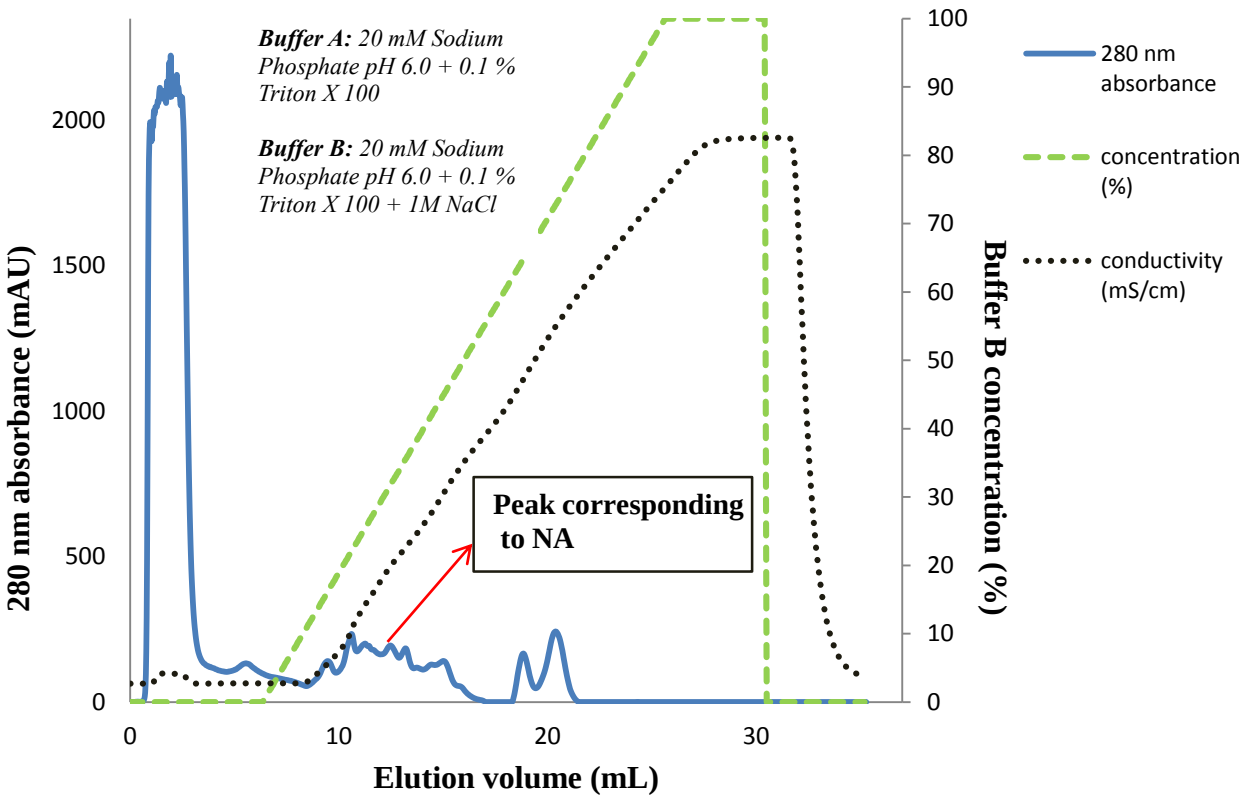

Figure 4-18: Anion exchange chromatogram for NA wild type on 1 mL Resource™ Q anion exchange column at pH 6.0. Bound proteins were eluted using increasing salt gradient for 20 column volumes (CV). The flow through and elution fractions were collected tested for the presence of influenza NA.

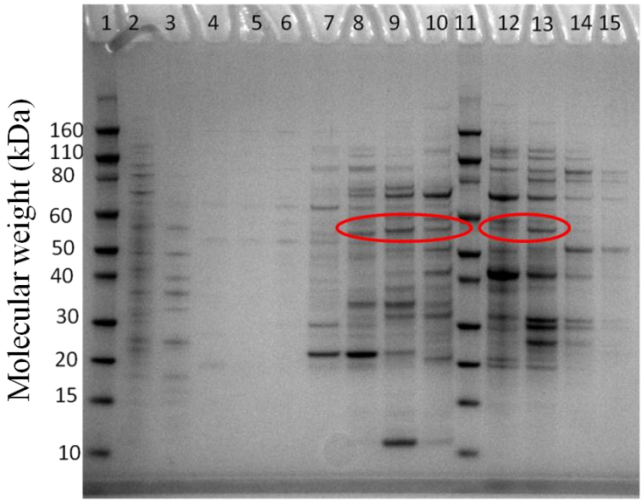

Figure 4-19: SDS-PAGE analysis of anion exchange chromatography fractions. L1 & 11) ladder, L2) injected sample, L3) flow through, L4-10 & L12-15) elution fractions.

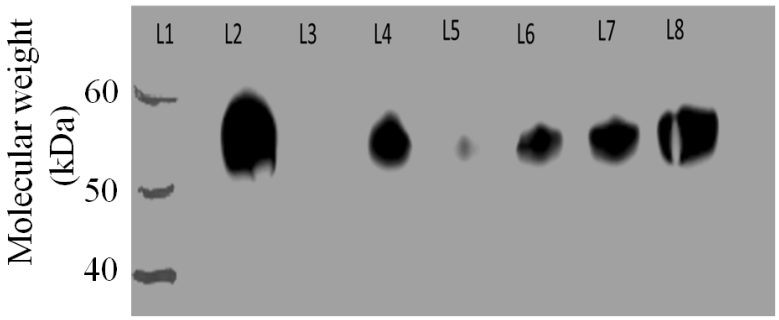

Figure 4-20: Western blotting analysis of anion exchange chromatography fractions (flow through and elution), detected with the monoclonal influenza A H1N1 (swine flu 2009) NA / neuraminidase antibody. L1) ladder, L2) injected sample, L3) flow through, L4-8) fractions corresponding to fractions highlighted in Figure 4-19.

C) Size exclusion chromatography

Using a superdex 200 gel filtration column, the combined anion exchange fractions were purified based on their size. The active terameric NA has a molecular weight of 240 kDa, hence, it can be easily separated from smaller contaminants using SEC. Considering the huge size of NA, it was expected to elute in the early fractions. The fractions corresponding to the peak indicated in Figure 4-21, were analysed on SDS-PAGE (Figure 4-22), it was observed that one fraction showed a single band at 55 kDa (NA). Moreover, the other fractions had NA along with other contaminants. The single fraction containing NA was highly diluted and hence, the band on the SDS-PAGE was very faint. Fraction in L2 to L5 (Figure 4-22) were tested for the presence of NA using dot blot. The dot blot analysis was performed instead of western blot, because the SDS-PAGE bands were very faint. Moreover, dot blot analysis can be performed slight quicker that the western blot. The dot blot (Figure 4-23) showed positive signals for these fractions. Although SEC was successfully used to purify NA, the samples were not used for further analysis (activity assay and SPR). This was because the SEC fractions were very dilute. Hence, the anion exchange fractions were used for developing the SPR assay.

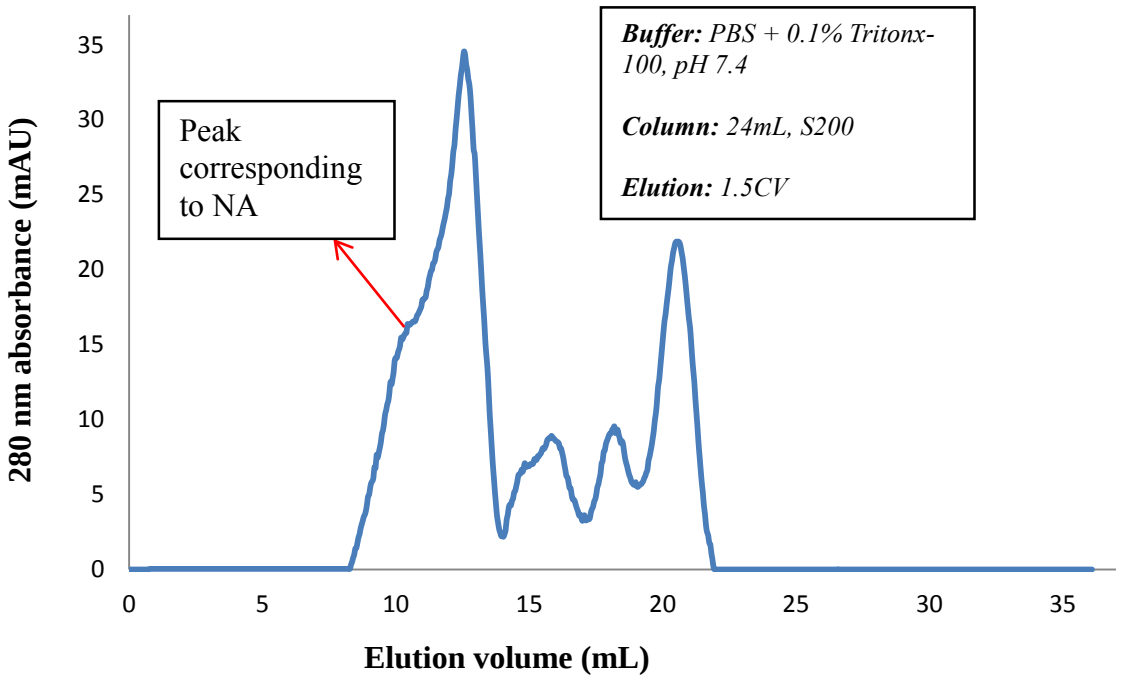

Figure 4-21: Size exclusion chromatogram for superdex 200 gel filtration column. Proteins were separated based on their size. The fractions were collected tested for the presence of influenza NA.

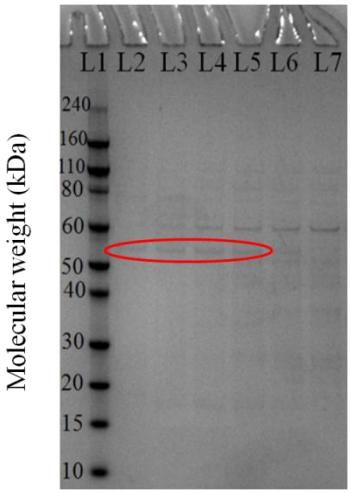

Figure 4-22: SDS-PAGE analysis of the SEC purified influenza NA under reducing conditions and commassie staining. L1) ladder, L2-7) fractions corresponding to peak indicated in the SEC chromatogram (Figure 4-21). L2 has a single band at 55 kDa corresponding to NA. This band is also present in L3-5 along with a 60 kDa contaminant.

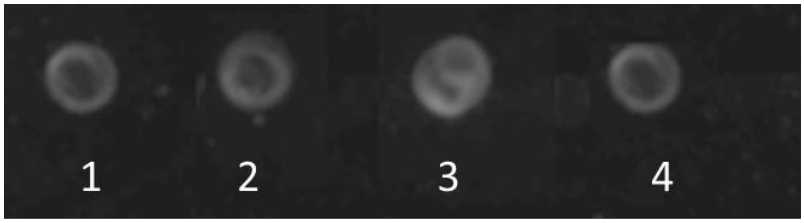

Figure 4-23: Dot blot analysis of SEC fractions, detected with the monoclonal influenza A H1N1 (swine flu 2009) NA / neuraminidase antibody (same fractions as L2-5 in Figure 4-22) for confirming the presence of NA.

D) Anion exchange chromatography- step elution

Based on the anion exchange elution profile (gradient elution), a step elution method was developed. In the gradient elution NA eluted at 23 mS/cm (conductivity). This corresponds to approximately 50% of buffer B concentration. The concentration of buffer B was increased stepwise. The first step was 25% of buffer B, which removed some of the contaminants. The next step was 60% of buffer B. NA was expected to elute off under this concentration. The third step was 100% buffer B, which removed other proteins bound to the column. The step elution was faster to run, and the target protein eluted in a smaller overall volume than with gradient elution. Figure 4-24 shows two overlaid chromatogram of anion exchange chromatography on recombinant NA wild type and NA H274Y eluted with a increasing salt concentration (step elution). The sample was injected using a 2 mL sample injection loop, the injected samples were the respective cell lysates. Both cell lysates behaved similarly at pH 6.0. Flow through and elution samples were collected for each of the protein for analysis. A dot blot analysis was performed on NA wild type to determine the presence of NA in the fractions. The dot blot result (Figure 4-25) showed positive signal for fractions eluted at 60% buffer B concentration. Later the fractions with positive signals for the wild type protein were pooled. For NA H274Y protein, exactly the same fractions were pooled, because both the chromatograms were identical. Both pooled fractions were then analysed on a western blot. Figure 4-26 showed a 55 kDa band for the wild type and H274Y samples. The band for H274Y sample showed a stronger signal when compared to the band for the wild type protein. This indicated that the concentration of the mutant was higher in the lysate than the wild type protein. This was in good agreement with the chromatogram (Figure 4-24), where the

absorbance at 280 nm for the mutant protein was slightly higher than the wild type protein.

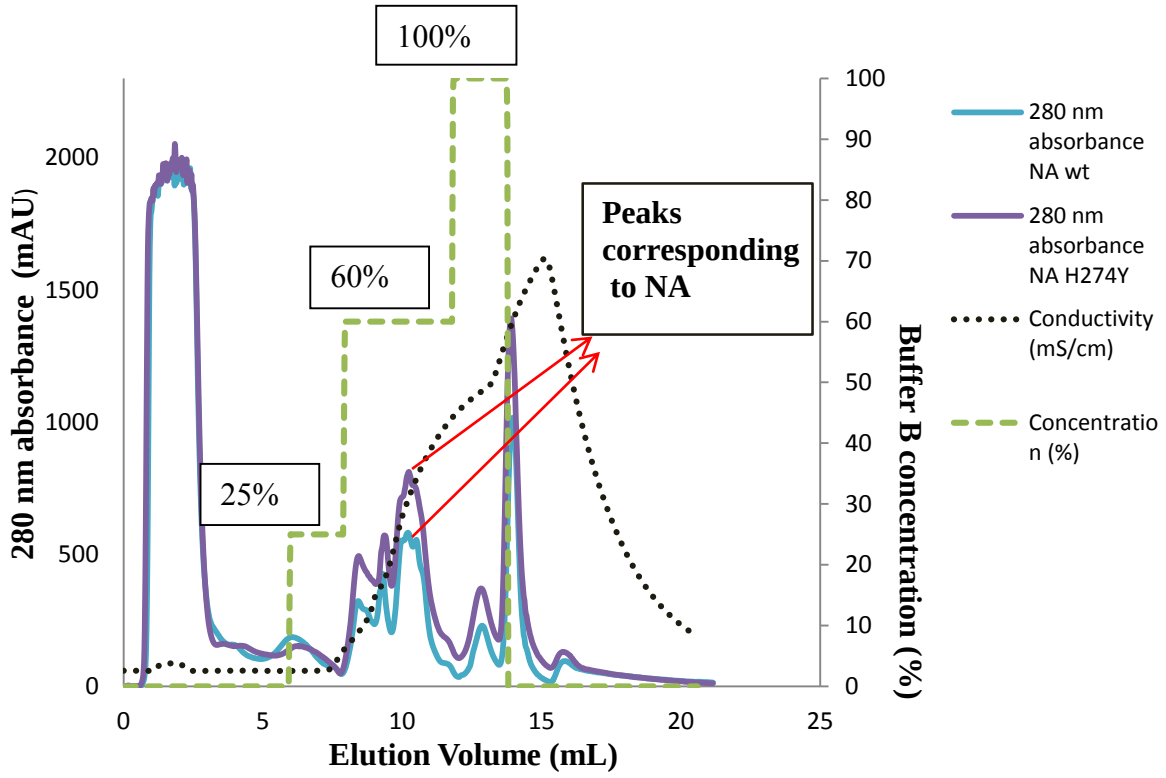

Figure 4-24: Overlaid chromatogram of anion exchange chromatography, on NA wild type and NA H274Y cell lysated, on 1mL Resource™ Q anion exchange column at pH 6.0. Bound proteins were eluted using increasing salt concentration (step elution). The flow through and elution fractions were collected and analysed.

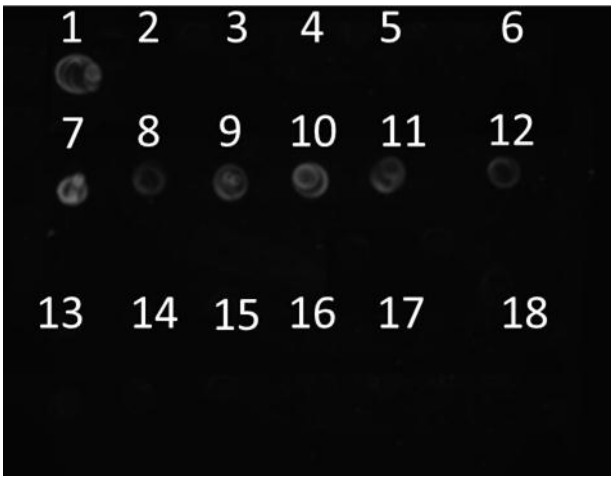

Figure 4-25: Dot blot analysis of anion exchange chromatography run on NA wild type (step elution). 1) injected sample, 2-6) fractions eluted at 25% buffer B, 7-12) fractions eluted at 60% buffer B and 13-18) fractions eluted at 100% buffer B.

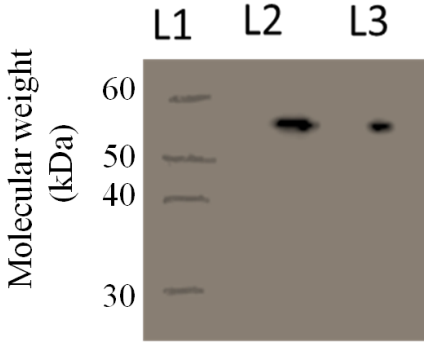

Figure 4-26: Western blotting analysis of pooled anion exchange chromatography fractions for NA wild type and NA H274Y mutant, detected with the monoclonal influenza A H1N1 (swine flu 2009) NA / neuraminidase antibody. L1) ladder, L2) NA H274Y and L3) NA wild type.

4.5.7 Activity assay

Recombinant influenza NA (wild type and H274Y) was tested for activity using a fluorometric assay, described by Potier et al. (1979). The preliminary results are presented in Figure 4-27 & Figure 4-28 (cell pellets and cell culture supernatant respectively). Both the wild type and H274Y mutant showed high enzyme activity for cell pellets. The cell culture supernatant also showed activity. This indicated that a little amount of NA has been secreted into the cell culture supernatant. For the soluble cell sample, the activity assay looked saturated for the first three dilution factors and gradually decreased with the increase in dilution factor. The activity for the wild type and

H274Y mutant were very similar. This meant that the mutation had not affected the activity of the protein. The positive control used in this assay was influenza virus from environmental science & research (ESR), while two negative controls were used. ESR negative control was the assay buffer without the virus and the High-Five control was the cells which were not infected with recombinant baculovirus.

4.5.4 Inhibition assay

Sensitivity of influenza viruses to the antiviral drugs (oseltamivir and zanamivir) were determined by fluorometric neuraminidase-inhibition assay. The 50% inhibitory concentration (IC_{50}) was determined using a log-dose–response curve-fit in GraphPad PRISM (v5.04) (Figure 4-29 & Figure 4-30). The IC_{50} value represents (Table 4-9 & Table 4-10) the concentration at which antiviral drugs inhibits neuraminidase activity by 50%.

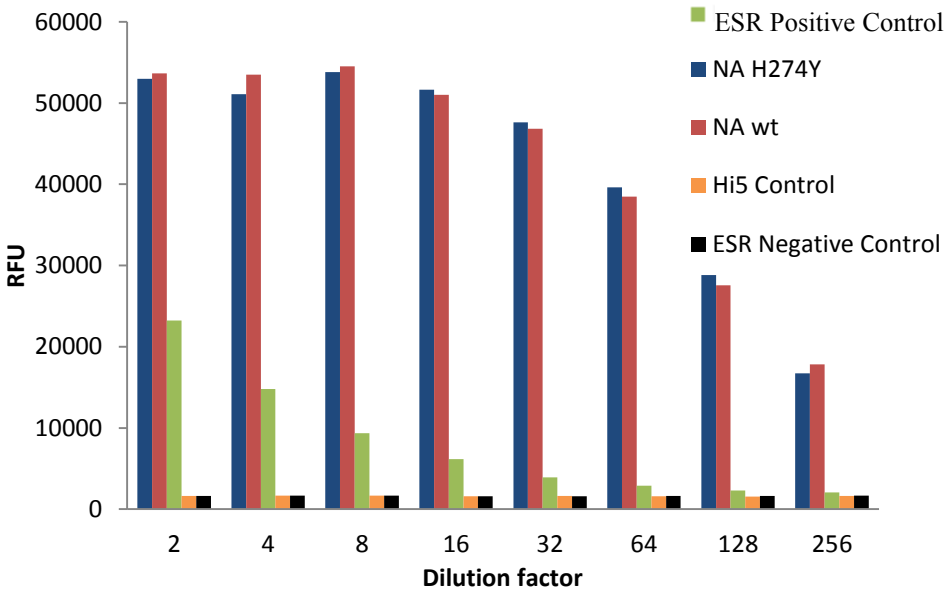

Figure 4-27: Activity assay for recombinant High-Five cell pellets. The assay was performed at Environmental Science & Research (ESR) at the National Centre for Biosecurity & Infectious Disease (NCBID).

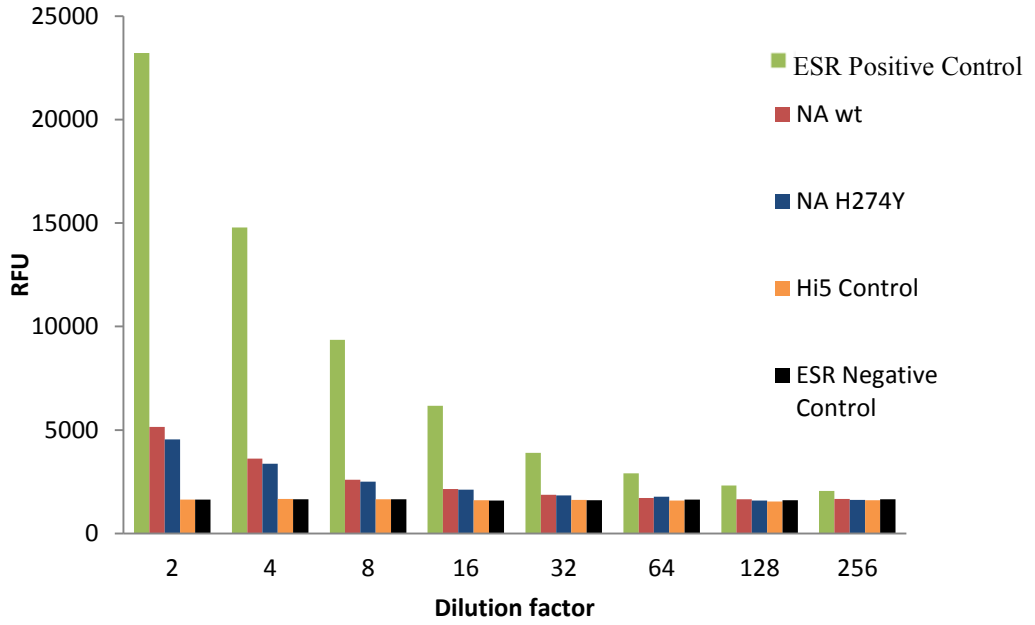

Figure 4-28: Activity assay for cell culture supernatant. The assay was performed at Environmental Science & Research (ESR) at the National Centre for Biosecurity & Infectious Disease (NCBID). The supernatant activity levels observed were not as high as seen for the cell pellets. This suggested that most of the proteins were cell associated while the remaining was secreted into the cell culture supernatant.

A) Oseltamivir

A/Fukui/45/2004 (H3N2) (E119V) & A/Victoria/124/2005 (H1N1) (H274Y) were positive controls (the viruses that are resistant to oseltamivir) used in the activity assay. A/Fukui/20/2004 (H3N2) (wild type) was used as a negative control (the virus that is sensitive to oseltamivir) in the activity assay. The respective IC_{50} values are given in Table 4-9. Clearly the wild type (0.59 nM) was sensitive to oseltamivir, while the H274Y mutant (349.43 nM) was resistant to oseltamivir, even though both the proteins had similar activity. This result was consistent with the data reported by Collins et al. (2008), suggesting that the binding affinity of the H274Y mutant for oseltamivir had reduced significantly. The H274Y mutant disrupts the binding pocket of group 1 NA's (N1, N4, N5 and N8) and not group 2 NA's (N2, N3, N6, N7 and N9). The proper folding of the protein brings amino acid at 252 exactly below the amino acid at 274. Group 1 NA's already possess a bulky tyrosine residue at 252. For these NA's to further accommodate a tyrosine at 274 requires alterations in the binding pocket, which disrupts the salt bridge formation required for stabilizing oseltamivir binding. In contrast the group 2 NA's have a smaller threonine residue at position 252, which allows the protein to accommodate

tyrosine at 274 without altering the binding of oseltamivir (Russell et al. 2006; Collins et al. 2009). The NA present in the ESR positive control (H1N1) used in this inhibition falls under group 1 classification, hence the H274Y mutation has affected oseltamivir binding affinity. The NA present in Fukui resistant (H3N2) strain falls under group 2 and the E119V mutation has been reported to show resistance to the oseltamivir, although the mechanism by which the mutation confers resistance is still not clear (McKimm-Breschkin 2000; Yen et al. 2005).

B) Zanamivir

A/Philippines/1279/2006 (H1N1) (Q136K) was the positive control (the virus that is resistant to zanamivir) used in the activity assay. A/Philippines/1279/2006 (H1N1) (wild type) was negative control (the virus that is sensitive to zanamivir) used in the activity assay. The respective IC_{50} values are given in Table 4-10. In this case, both the wild type (0.26 nM) and the H274Y mutant (0.44 nM) were sensitive to zanamivir. This result indicated that zanamivir was a more potent inhibitor than oseltamivir for H274Y mutant. This result was also consistent with the data reported by Collins et al. (2008). Zanamivir possess the same glycerol moiety at C6 as sialic acid. Hence, a mutation in the binding pocket is less likely to develop resistance to the drug without weakening its binding with sialic acid (Collins et al. 2009). This has allowed H274Y mutant to remain sensitive to zanamivir. The Q136K resistant control used in this assay is not involved with the binding pocket of the protein. Q136K mutation has been reported to show resistance to the zanamivir. The amino acid Q at 136 forms hydrogen bonds with R156 and D151, both of which interact with the guanidine group of zanamivir. Mutation Q136K, does not allow R156 and D151 to interact with zanamivir. This mutation is irrelevant for sialic acid binding because sialic acid does not possess a guanidine group (Hurt et al. 2009). Hence, zanamivir developed resistance to Q136K.

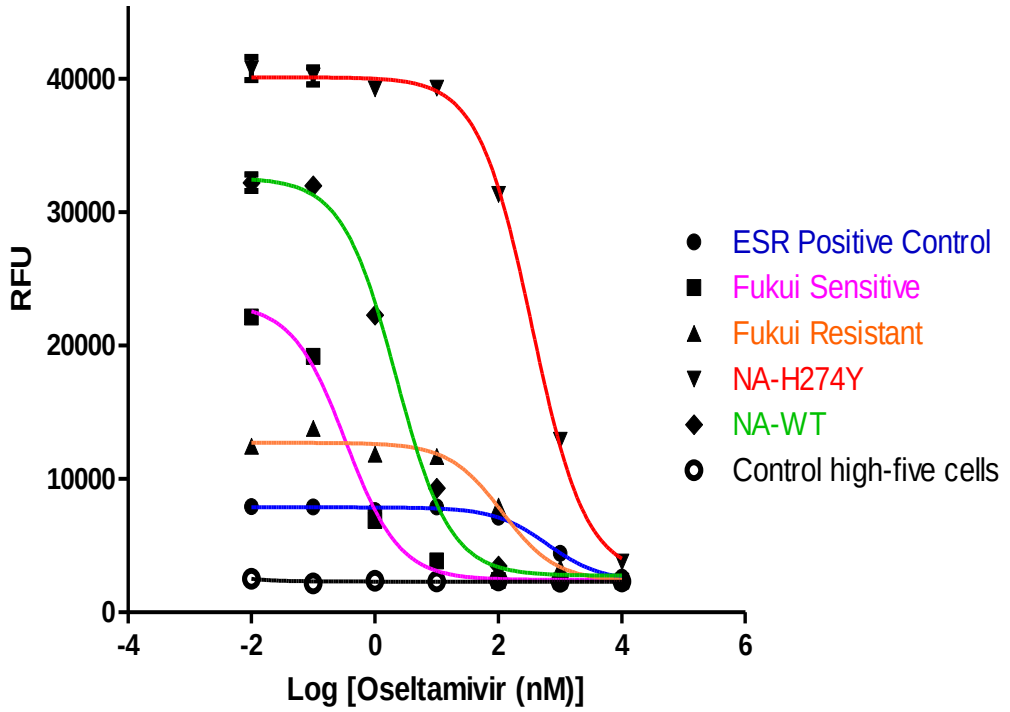

Figure 4-29: Determination of IC_{50} values for oseltamivir with recombinant NA wild type and H274Y. The recombinant NA's (wild type and H274Y) and the original viruses were incubated with increasing concentrations of oseltamivir. Data presented are mean ± S.D. of duplicate measurements for recombinant NA. The assay was performed at Environmental Science & Research (ESR) at the National Centre for Biosecurity & Infectious Disease (NCBID).

Table 4-9: Determination of IC_{50} values for oseltamivir

Sample Group	**Sample**	**NA mutation**	**IC_{50} value***	**Phenotype**
ESR control virus	A/Victoria/124/2005 (H1N1)	274Y	560.20	Resistant
	A/Fukui/20/2004 (H3N2)	119E	0.32	Sensitive
	A/Fukui/45/2004 (H3N2)	119V	103.20	Resistant
Recombinant samples generated in BIC laboratory, Christchurch	Control High-Five cells	-	-	No activity
	NA-Wildtype	274H	0.59	Sensitive
	NA-H274Y	274Y	349.43	Resistant

50% Inhibitory concentration; n = 2 for recombinant NA generated in BIC laboratory, Christchurch.

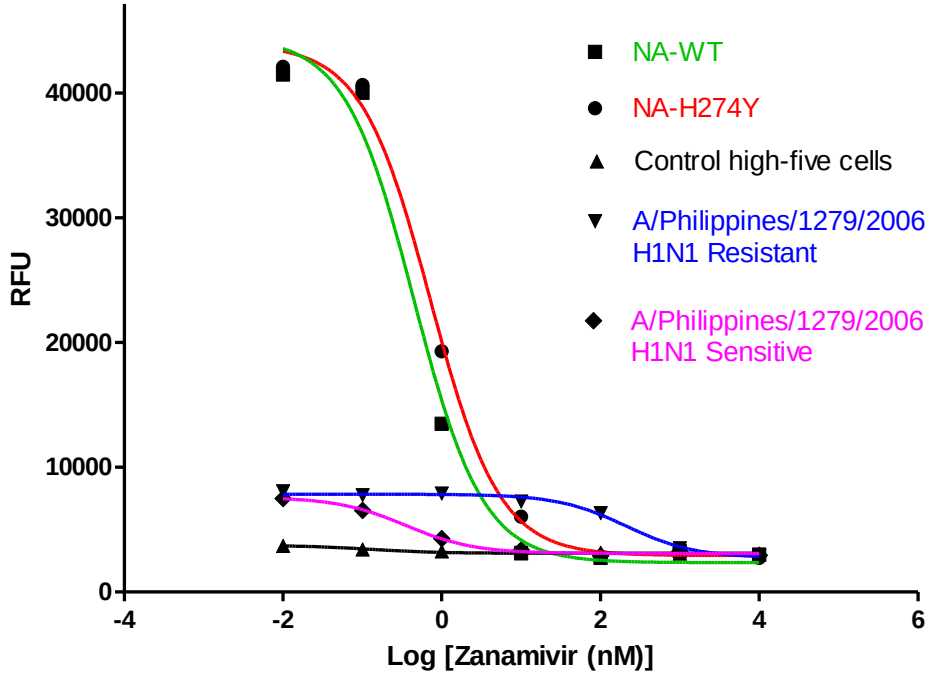

Figure 4-30: Determination of IC_{50} values for zanamivir with recombinant NA wild type and H274Y. The recombinant NA's (wild type and H274Y) and the original viruses were incubated with increasing concentrations of zanamivir. Data presented are mean ± S.D. of duplicate measurements for recombinant NA. The assay was performed at Environmental Science & Research (ESR) at the National Centre for Biosecurity & Infectious Disease (NCBID).

Table 4-10 Determination of IC_{50} values for zanamivir

Sample Group	Sample	NA mutation	IC_{50} value*	Phenotype
ESR control virus	A/Philippines/1279/2006 (H1N1)	136K	178.36	Resistant
	A/Philippines/1279/2006 (H1N1)	136Q	0.25	Sensitive
Recombinant samples generated in BIC laboratory, Christchurch	Control High-Five cells	-	-	No activity
	NA-Wildtype	274H	0.26	Sensitive
	NA-H274Y	274Y	0.44	Sensitive

50% Inhibitory concentration; n = 2 for recombinant NA generated in BIC laboratory, Christchurch.

4.5.5 Activity assay for ion exchange combined fractions

The dot blot (Figure 4-25) and western blot (Figure 4-26) analyses for the pooled ion exchange fractions confirmed the presence of NA. As discussed above, NA must be in tetramer form to be active. Irrespective of the form NA took after purification, the protein would appear as a 55 kDa band on SDS-PAGE. Hence, an activity assay was required to confirm the presence of tetramer and test if the samples retained the activity after ion exchange purification.

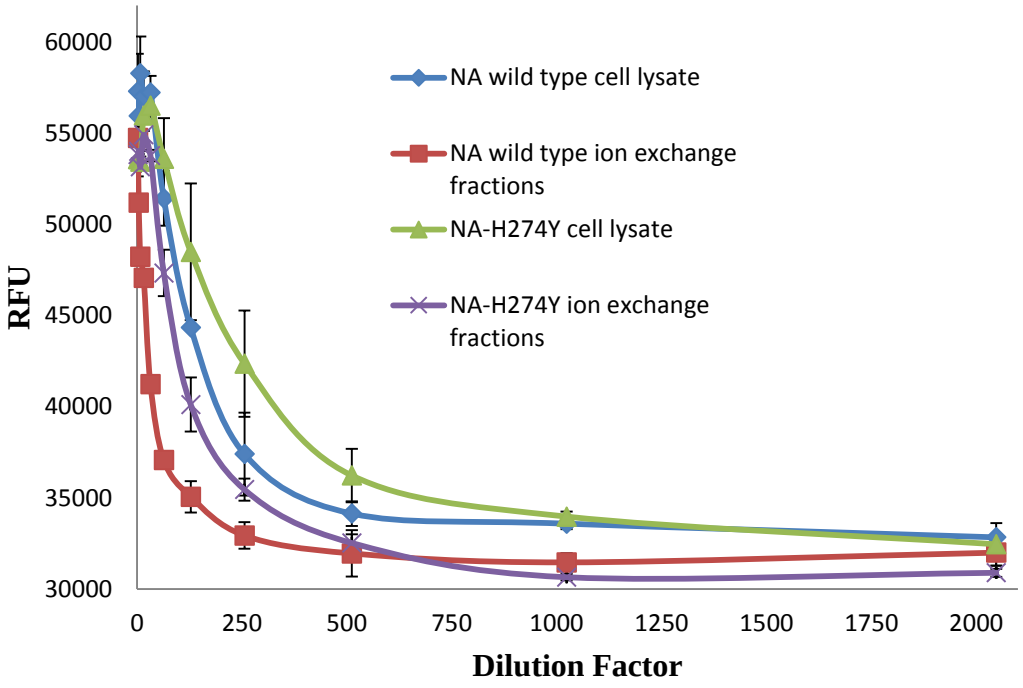

Figure 4-31: Activity assay for ion exchange pooled fractions. Serial dilutions of the load sample for the chromatography (NA wild type and H274Y cell lysates) and the fractions pooled after chromatography were tested for the activity. All Data presented are mean ± S.D. of duplicate measurements.

Figure 4-31 showed that all four samples (chromatography load samples and pooled fractions) were active. The activity for H274Y mutant was relatively higher than the wild type. This could be because the concentration of the mutant in the sample was higher than the wild type. The difference in the activity for the wild type and mutant can be correlated with the overlaid chromatogram peaks (Figure 4-24), where the mutant had

higher 280 absorbance than the wild type. This also correlates well with the western blot result (Figure 4-26), where the mutant had a stronger intensity than the wild type. All three results (chromatogram, western blot and activity assay) suggested that the mutant concentration was higher in the lysate than that of the wild type. Ion exchange purified NA was used for SPR assay development. The SPR assay to measure the kinetics of zanamivir and NA (wild type and H274Y mutant) interactions are described in detail in chapter 5. The SPR assay results were compared with results obtained from NA activity assay reported in this chapter and molecular docking results reported in Chapter 3.

4. 6 Conclusions

In summary, this chapter describes the cloning, expression and purification of influenza neuraminidase wild type and H274Y mutant using baculovirus expression system. NA was expressed at very low levels in insect cells. This could be because of the poor quality of the baculovirus generated or low virus titre used for BV amplification. Since the expression level was very low, it was difficult to follow the protein on an SDS-PAGE. Hence, a western blot was required to confirm the expression of NA. Standard purification techniques such as anion exchange and size exclusion chromatography were used to purify the protein. Standard fluorometric activity assay was performed on the recombinant proteins. Both the wild type and the mutant showed similar level of activities (53,650 and 52,992 RFU respectively). In addition, the recombinant NA was used in an inhibition assay. The inhibition assays were compared based on the calculated IC_{50} values. The wild type protein was found to be sensitive to oseltamivir (IC_{50} = 0.59 nM) and the H274Y mutant protein was resistant to oseltamivir (IC_{50} = 349.43 nM). In contrast, both wild type (IC_{50} = 0.26 nM) and H274Y mutant (IC_{50} = 0.44 nM) proteins were sensitive to zanamivir. This indicated that zanamivir was a more potent inhibitor than oseltamivir, for treating H274Y mutant. This is in good agreement with the literature. The recombinantly generated NA was used for SPR assay development. Chapter 5 describes the SPR assay in detail.

5. Surface plasmon resonance assay development

5.1 Introduction

The need for a simple and a reliable assay to monitor influenza anti-viral drug resistance has increased due to the high levels of inconsistency exhibited by the MUNANA assay and the short half-life of the sensitive chemiluminescent (1, 2-dioxetane derivative of sialic acid, NA-STAR) assay (Wetherall et al. 2003). This chapter describes the development of a simple, label-free, real-time surface plasmon resonance assay to measure the kinetics of zanamivir and NA (wild type and H274Y mutant) interactions. Synthesis of zanamivir-spacer conjugate, immobilization of the conjugate to the sensor chip and SPR interaction analysis are discussed in detail in this chapter. The current enzymatic assays are performed at pH 6.0 and at 37°C. The SPR experiments were designed to be carried out at pH 6.0 and at 35°C (maximum temperature that can be achieved in SPR auto sampler). Moreover, this chapter also describes the development of inhibition assays to monitor NI drug resistance. The proposed SPR assay results were compared with results obtained from the fluorescently labelled NA activity assay (Chapter 4), molecular docking results (Chapter 3) and kinetics data reported in the literature.

5.2 Materials and methods

5.2.1 Instrumentation

A ProteOn XPR36 protein interaction system (Bio-Rad Laboratories, Hercules, CA, USA) was used for the SPR assay development. Ideally, in a single experiment, the ProteOn XPR36 system has the ability to monitor 36 interactions simultaneously. Instrument Control and data analysis were carried out using the ProteOn Manager Software Version 3.0.

5.2.2 Reagents

Amine coupling reagents 1-ethyl-3-(3-dimethylaminopropyl) carbodiimide-HCl (EDAC, 0.4 M), sulfo-N-hydroxysuccinimide (NHS, 0.1 M), ethanolamine-HCl (1.0 M, pH 8.5) and GLC biosensor chips were purchased from Bio-Rad Laboratories.

Regeneration buffer (10 mM glycine-HCl, pH 3.0), immobilization buffer (20 mM sodium phosphate, pH 8.0) and running buffer (20 mM sodium phosphate, 300 mM sodium chloride, 0.1% triton-100, pH 6.0) were prepared in the laboratory using analytical grade chemicals purchased from Sigma Aldrich (St. Louis, MO, USA).

5.2.3 **Zanamivir-spacer conjugate synthesis**

Compound 1 (286 mg, 0.5 mmol) was dissolved in pyridine (1.5 mL) under nitrogen (N2). 4-dimethylaminopyridine (DMAP, 152 mg, 2.5 eq.) and 4-nitrophenyl chloroformate (121 mg, 1.2 eq.) were added before leaving to stir for 3 hours. After 3 hours N-Boc-1,6-hexanediamine (0.13 mL, 1 eq.) was added before leaving the reaction to stir overnight. After 16 h the reaction was diluted with ethyl acetate (EtOAc, 20 mL) and extracted with HCl (2M, 40 mL). The aqueous phase was then extracted with EtOAc (2 x 20 mL) and the combined organic layers were dried by adding excess magnesium sulfate (MgSO4) and concentrated under vacuum. The structure of the product was confirmed by high resolution mass spectra (electrospray ionization/time-of-flight) (HRMS ESI/TOF) [HRMS (ESI-TOF): calculated for C36H58N6O15H+: 815.4033, measured: 815.4040 (MH+)].

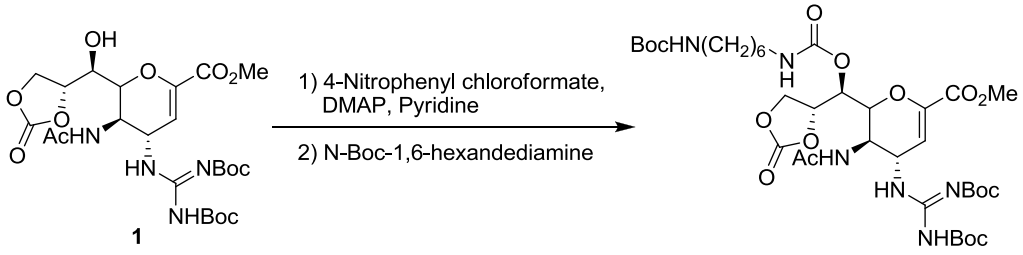

Figure 5-1: Synthetic chemistry step 1 - Synthesis of* N*-Boc-1,6-hexanediamine-zanamivir conjugate (Image drawn using Chemdraw Ultra 6.0).

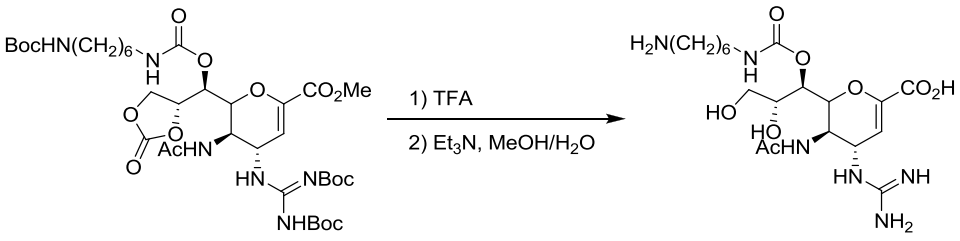

Figure 5-2: Synthetic chemistry step 2 - Boc protection removal using trifluoroacetic acid (TFA) (Image drawn using Chemdraw Ultra 6.0).

The residue from the previous reaction (Figure 5-1) was dissolved in trifluoroacetic acid (TFA, 5 mL) under N_2 and was left to stir. After 1 h the reaction was concentrated under vacuum and redissolved in 50% methanol (40 mL). After the addition of triethylamine (10 mL) the reaction was left to stir for 6 hours. After 6 hours the reaction was concentrated under vacuum and freeze dried to return a yellow viscous gel like substance (Figure 5-2). The structure of the product (1,6-hexanediamine-zanamivir conjugate) was confirmed by mass spectrometry [HRMS (ESI-TOF): calculated for $C_{19}H_{34}N_6O_8H^+$: 475.2509, measured: 475.2511 (MH^+)].

5.2.4 **Ligand preparation**

The synthesized ligand mixture was highly viscous. Hence, two strategies were examined in preparing ligand mixture for immobilization (Table 5-1).

Table 5-1: Ligand preparation strategies

Strategy	**Preparation method**
Strategy 1	25 mg of ligand mixture was dissolved in 1 mL of immobilization buffer. The solution was spun down at 13000 rpm for 5 min at 4°C. 300 µL of this sample was tested for immobilization.
Strategy 2	50 mg of ligand mixture was dissolved in 1 mL of immobilization buffer. The solution was spun down at 13000 rpm for 20 min at 25°C. 500 µL of this solution was mixed with 500 µL of immobilization buffer and spun down at 13000 rpm for 20 min at 25°C. 300 µL of this sample was tested for immobilization.

5.2.5 **Biosensor surface preparation**

Immobilization was carried out at 35°C using a standard amine coupling technique following the manufacturer's instructions. Channels 1 and 2 were activated simultaneously with a mixture of EDAC and NHS (1:1 v/v, 30 µL/min, 5 min) followed by ligand (running buffer and zanamivir reaction mixture in channel 1 and 2 respectively) and, finally, unreacted surface ester groups were deactivated with ethanolamine-HCl (1M, pH 8.5, 30 µL/min, 5 min). Channel 1 was used as the reference channel.

5.2.6 **Analyte sample preparation**

The final NA concentration was determined from quantitative densitometry analysis (Appendix C). Pure bovine serum albumin (BSA, monomer) was used as a standard for densitometry analysis. A series of NA sample diluted in SPR running buffer were used as analyte for SPR assay development. The starting enzyme concentrations used in the assay were 5.2 nM and 6.1 nM for the wild-type and H274Y mutant respectively.

5.2.7 **Surface plasmon resonance biosensor assay**

Six analyte samples were injected simultaneously for 300 s (25 µl/min) over the immobilized ligand channels at 35°C. The binding responses were acquired for 300 s association and 600 s dissociation. The sensor surface was regenerated between experiments by two quick injections of regeneration buffer (18 s, 100 µL/min) to remove NA bound to zanamivir. The reference subtracted SPR signal corresponds to the binding of the analyte to the immobilized ligand. The generated data points were analysed using the ProteOn Manager™ Software tools. The SPR curves were fitted to a simple Langmuir 1:1 model and a Langmuir 1:1 model with drift to obtain kinetic parameters. The goodness of the fit was determined from the residuals and χ^2 values (the average of the squared differences between the measured data point and the fit).

5.2.8 **Inhibition assay**

25 mM master stock of each neuraminidase inhibitor (NI) and sialic acid were prepared. 500 µL aliquots of 100 µM working stocks were prepared from the master stock. NI for SPR assays were prepared as described in Table 5-2. SPR inhibition experiments were performed at 35°C using the same running buffer as mentioned above. 150 µL of fixed concentration (6 nM) NA was mixed with 150 µL of increasing concentrations of 2X inhibitor (Table 5-2). The mixture was incubated for 30 min at 35°C inside the SPR auto sampler chamber. The effect of inhibitor on SPR response was monitored using the same assay conditions as described above. For a clear robust analysis, the analytes were injected in a randomized order. In a few experiments, the analytes were also randomized in subsequent injections. For example, see Table 5-3. The processed SPR data was analysed to determine 50% inhibitory concentration ($IC_{50\text{-}spr}$) using a log-dose–response curve-fit in GraphPad PRISM (v5.04). The $IC_{50\text{-}spr}$ value represents the concentration at which inhibitor and sialic acid inhibits neuraminidase binding to the immobilized ligand by 50%.

Table 5-2 NI sample preparation for SPR inhibition assay

Dilution	Inhibitor mix	Inhibitor concentration before assay (2X) (nM)	Inhibitor concentration in assay (nM)
1	20 µL working stock + 980 µL running buffer (RB)	2,000	1,000
2	100 µL dilution 1 + 900 µL RB	200	100
3	100 µL dilution 2+ 900 µL RB	20	10
4	100 µL dilution 3 + 900 µL RB	2	1
5	100 µL dilution 4 + 900 µL RB	0.2	0.1

Table 5-3: Zanamivir inhibition assay - shuffling and reshuffling order of analytes.

Channel number	Inhibitor concentration in injection 1 (nM)	Inhibitor concentration in injection 2 (nM)	Inhibitor concentration in injection 3 (nM)
1	1	1	0
2	0.1	0.1	0.1
3	0	0	1
4	10	10	10
5	1000	1000	100
6	100	100	1000

5.3 Results and discussion

5.3.1 Ligand immobilization

Coupling a ligand via primary amine groups to an activated SPR chip surface occurs spontaneously. This direct coupling method is easy to execute. However, the immobilized ligand could be tethered in random orientations. This has a significant effect on the analyte binding because the random orientation of the ligand could possibly limit the access to the ligand binding site and hence can lead to a complex kinetic behaviour (Fee 2013). Therefore, designing suitable immobilization chemistry was absolutely critical and challenging. To obtain a more uniform surface orientation of ligand, the ligand was initially tethered to a spacer molecule. The ligand-spacer conjugate was then immobilized to the SPR chip surface. However, altering the chemical structure of the ligand molecule for immobilization could significantly interfere with analyte binding. Among the various spacer molecules tested by McKimm-Breschkin et al. to immobilize zanamivir on a microsphere, 1, 6-hexanediamine was reported as an appropriate spacer molecule to tether zanamivir and not to lose its anti-viral activity (McKimm-Breschkin et al. 2003). Hence 1, 6-hexanediamine was tethered to the inhert 7-hydroxyl group of zanamivir and this conjugate was then immobilized on to the SPR sensor chip. This allowed a more uniform surface orientation of ligand by exposing the active part for the drug for analyte binding.

The ligand prepared with both strategies described in Table 5-1 were tested independently on two different GLC sensor chips. The ligand was immobilized on channel 2 of the GLC sensor chip. Channel 1 was prepared as a reference channel. A typical immobilization procedure involved activation of the sensor surface, followed by ligand coupling and then deactivation of excess reactive surface groups. After the ligand coupling and deactivation steps, the final ligand immobilization responses (ΔRU) were determined. The ΔRU for strategy 2 was observed to be twice that of strategy 1. Since the ligand mixture was highly viscous, spinning at 25°C allowed proper solubilisation of the mixture. This in turn increased binding of the ligand on the sensor chip.

The analyte detection depends on the amount of ligand immobilized on the sensor surface. From the preliminary experiments (data not shown), although both strategies

showed analyte binding, it was determined that the ligand prepared using strategy 2 was more stable and gave reproducible results. After initial investigations strategy 2 was concluded to be optimal and was used for subsequent immobilizations on GLC sensor chip surfaces. Chip surface channels were washed 3 times with regeneration buffer for 18 s before injecting analytes. This practice enhanced assay reproducibility by removing any loosely bound ligand.

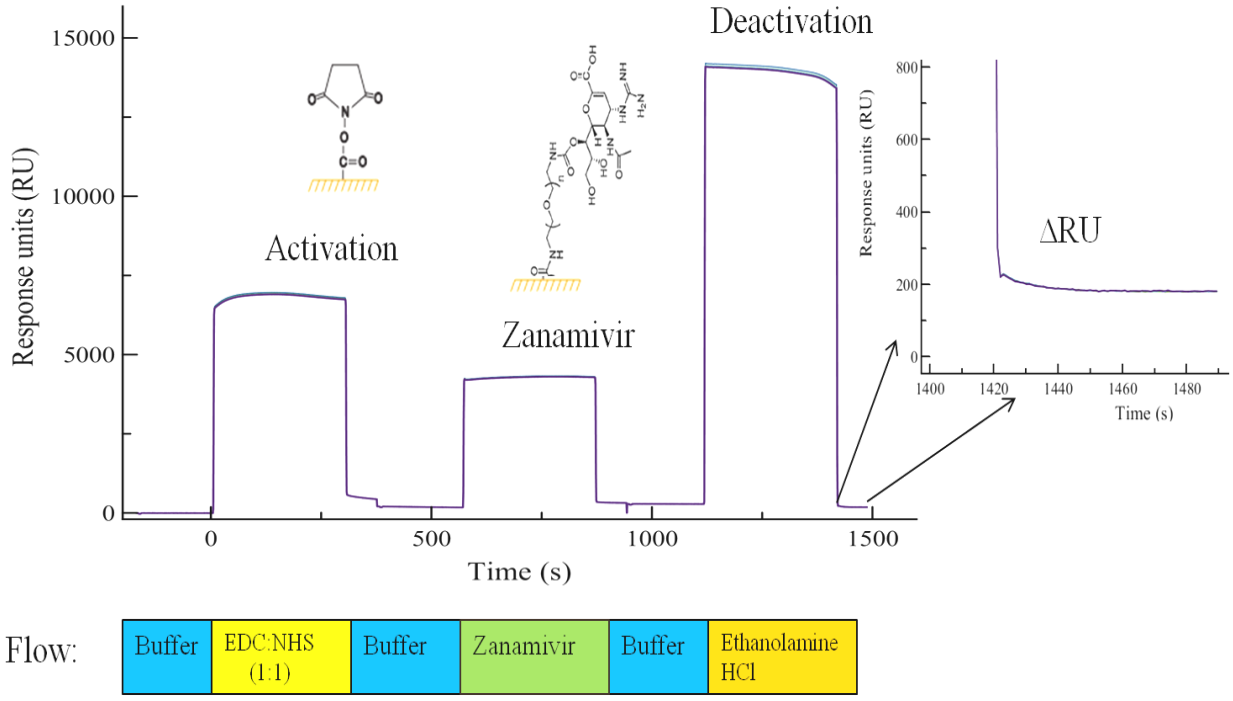

Figure 5-3: Immobilization of zanamivir-spacer conjugate using strategy 1. The figure shows activation of the chip surface with a mixture of EDAC and NHS, followed by zanamivir-spacer conjugate and capping of un-reacted surface ester groups with ethanolamine-HCl. The final ligand immobilized level (ΔRU) was 190 RU.

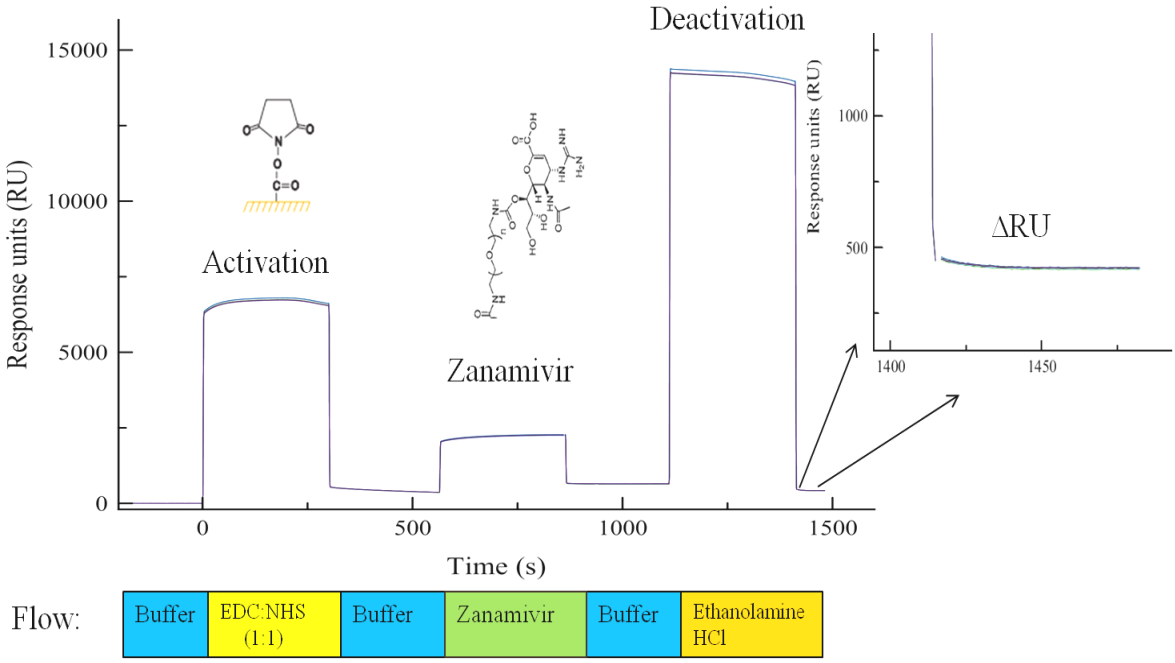

Figure 5-4: Immobilization of zanamivir-spacer conjugate using strategy 2. The figure shows activation of the chip surface with a mixture of EDAC and NHS, followed by zanamivir-spacer conjugate and capping of un-reacted surface ester groups with ethanolamine-HCl. The final ligand immobilization level (ΔRU) was 431 RU.

Preliminary SPR experiments (Appendix D) were performed with NA cell culture supernatant as analyte that showed positive binding response. Moreover, the cell culture supernatant from High-Five control (cells which were not infected with recombinant baculovirus) did not show any signs of binding to the immobilized ligand.

5.3.2 SPR interaction analysis

As shown in Figure 5-5 and Figure 5-6, the immobilized ligand in channel 2 showed specific binding of influenza NA. The SPR signals were observed to decrease with a decrease in concentration of the analyte. Similar concentration-dependent signal decreases were observed with the H274Y mutant. With the start of the injection of analyte, gradual increase in SPR signal was observed in both cases. At the end of the injection very slow dissociation phase was observed and the analyte did not dissociate completely from the ligand. This indicated that the analyte had bound strongly to the immobilized ligand. Thus the sensor surface was regenerated twice with regeneration

buffer. A drop in pH was expected to change the conformation of bound NA, thereby releasing NA from the NA-zanamivir complex formed on the chip surface.

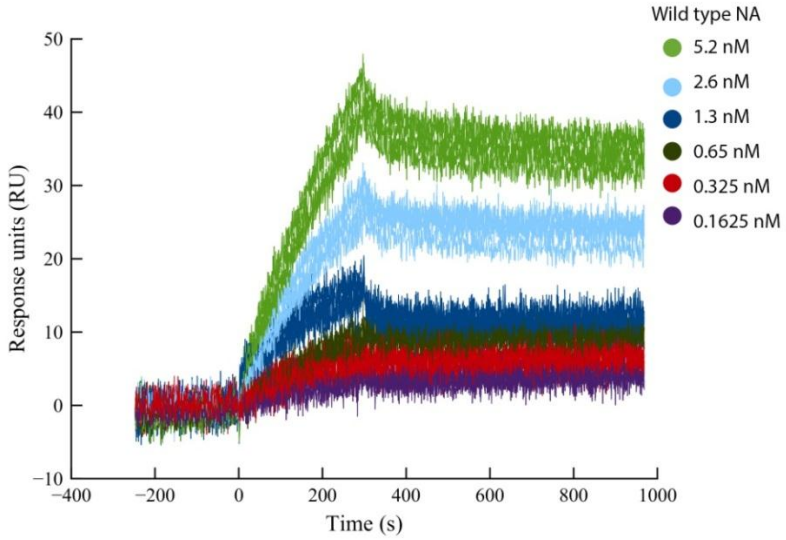

Figure 5-5: Reference-subtracted SPR sensograms showing binding curves for various concentrations of NA wild-type protein (5.2 nM to 0.1625 nM) with zanamivir-spacer conjugate immobilized on the chip surface.

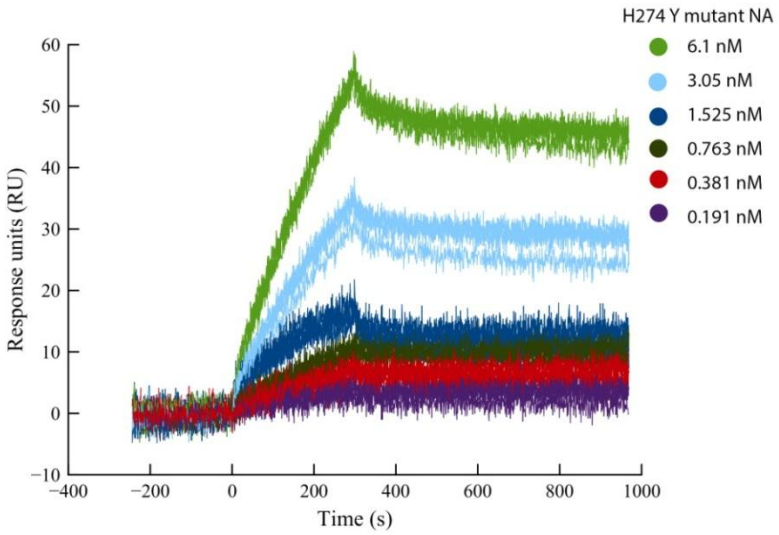

Figure 5-6: Reference-subtracted SPR sensograms showing binding curves for various concentrations of NA H274Y protein (6.1 nM to 0.191 nM) with zanamivir-spacer conjugate immobilized on the chip surface.

To study the association (k_a) and dissociation (k_d) rate constants between wild-type and H274Y influenza NA, sensograms were obtained with different concentrations of the proteins. The analyte samples were injected in a shuffled order. The experiment was

repeated 5 times in each case. The binding curves were fitted to the 1:1 Langmuir binding model (Figure 5-7 and Figure 5-8) and 1:1 Langmuir binding model with drift (Figure 5-9 and Figure 5-10) using ProteOn Manager™ Software tools. Both the models assume that analyte and the ligand are homogenous and the binding events are independent. From the first visual inspection it was observed that for both models the lines of the resulting fit passed through the experimental data. However, when the results were analysed further with the residuals, the following observations were made. For the top two concentrations, the fitted line passed slightly below the experimental curves for the mutant, while they passed exactly through the middle of the experimental curves for the wild-type. The fitted line for the third concentration passed above the curves in the dissociation phase for both proteins. The three low concentrations fitted very well for both proteins. The goodness of the fit was then examined by χ^2 (Table 5-4). For a good fit, χ^2 is expected to be less than 10% of R_{max}. Global fitting of the data using the 1:1 model resulted in a good fit for the H274Y mutant yielding a χ^2 value of < 10% of R_{max}. However, this value was found to be slightly >10% for the wild type protein indicating that the fit was not as good as the mutant. This could be because of slight baseline drift observed in the dissociation phase. Unlike the 1:1 Langmuir binding model, 1:1 Langmuir binding model with drift takes the baseline drift into consideration. The 1:1 model with drift resulted in χ^2 values < 10% in both the cases. This suggested the 1:1 model with drift fitted the curves reasonably better than 1:1 model without drift. Hence, the kinetic parameters obtained from 1:1 model with drift was used for method validation.

The k_a value for wild-type protein was observed to be twice that of H274Y, indicating that the wild-type protein had a slightly stronger affinity to the immobilized ligand than the mutant. However, there is not much difference in the k_d values for both proteins. This suggests that once the protein attached itself to the ligand both the proteins interacted in a similar manner. This also showed that the H274Y mutant that blocks movement of Glu276 on oseltamivir binding has no effect on zanamivir binding, because zanamivir does not induce the conformational change of Glu276. Hence the H274Y mutant did not have a major impact on zanamivir interaction. This was in good agreement with the results of Hurt et al. (2009). Table 5-4 summarizes the dissociation constant of both proteins. This result also suggested that the mutation has not had a significant impact on zanamivir binding.

Table 5-4: SPR kinetic parameters obtained using ProteOn Manager™ Software tools

Curve fitting model	**Protein**	**k_a (1/Ms)**	**k_a error (1/Ms)**	**k_d (1/s)**	**k_d error (1/s)**	**K_D (nM)**	**R_{max} (RU)**	**R_{max} error (RU)**	**χ^2 (RU)**
Langmuir 1:1	Wild-type	1.05×10^{6}	4.86×10^{3}	2.15×10^{-4}	3.56×10^{-6}	0.205	48.16	1.5×10^{-1}	5.88
	H274Y	5.32×10^{5}	3.17×10^{3}	2.92×10^{-4}	3.11×10^{-6}	0.55	85.60	3.84×10^{-1}	6.86
Langmuir 1:1 with drift	Wild-type	8.01×10^{5}	5.63×10^{3}	4.13×10^{-4}	4.58×10^{-6}	0.516	56.28	3.28×10^{-1}	5.01
	H274Y	4.36×10^{5}	3.91×10^{3}	3.87×10^{-4}	3.91×10^{-6}	0.88	98.62	6.78×10^{-1}	6.50

The kinetic parameters were determined from five independent measurements. k_a and k_d are the association and dissociation rate constants, respectively. The goodness of the fit was then examined by χ^2 value (the average of the squared differences between the measured data point and the fit).

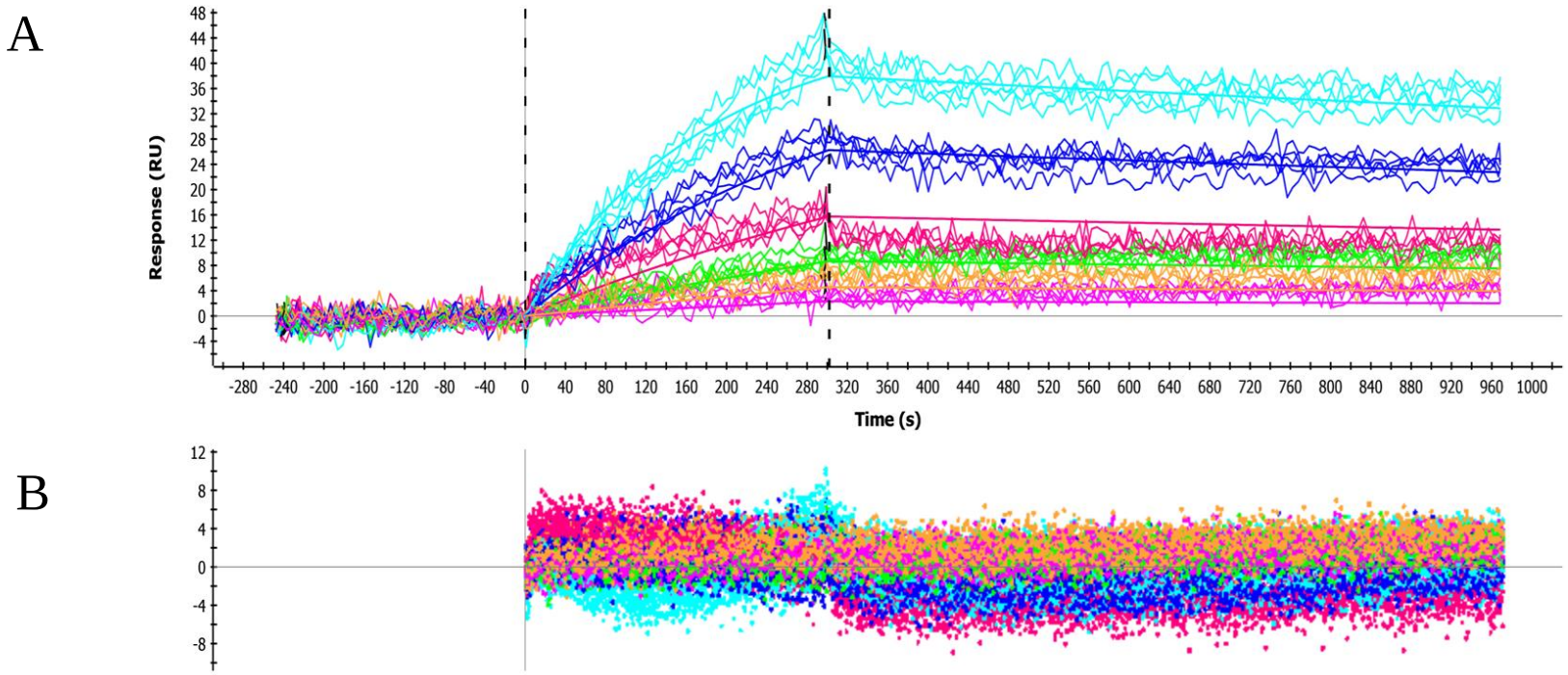

Figure 5-7: Wild-type NA SPR binding curve fitting using Langmuir 1:1 model. A) The data presented here are of five independent experiments for six concentrations (5.2 nM, 2.6 nM, 1.3 nM, 0.65 nM, 0.325 nM and 0.1625 nM) yielding identical results. The fitted lines (solid lines) pass through the experimental curves. B) The residuals, showing the goodness of the fit with the original experimental data.

A

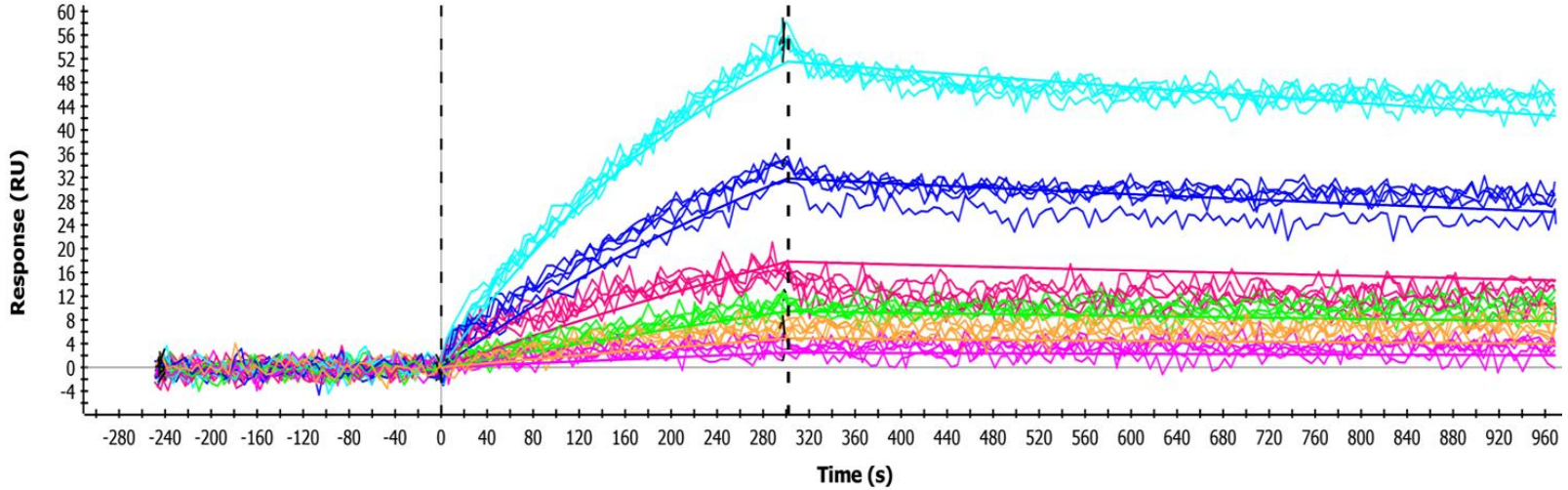

B

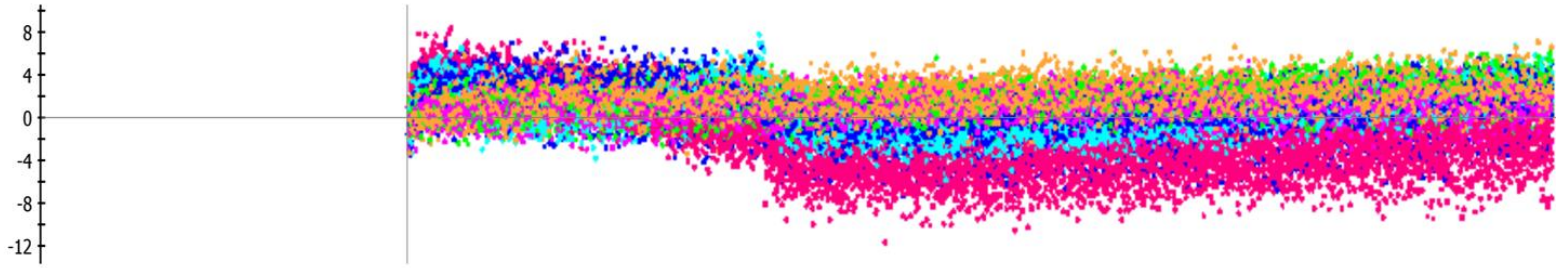

Figure 5-8: H274Y NA SPR binding curve fitting using Langmuir 1:1 model. A) The data presented here are of five independent experiments for six concentrations (5.2 nM, 2.6 nM, 1.3 nM, 0.65 nM, 0.325 nM and 0.1625 nM) yielding identical results. The fitted lines (solid lines) pass through the experimental curves. B) The residuals, showing the goodness of the fit with the original experimental data.

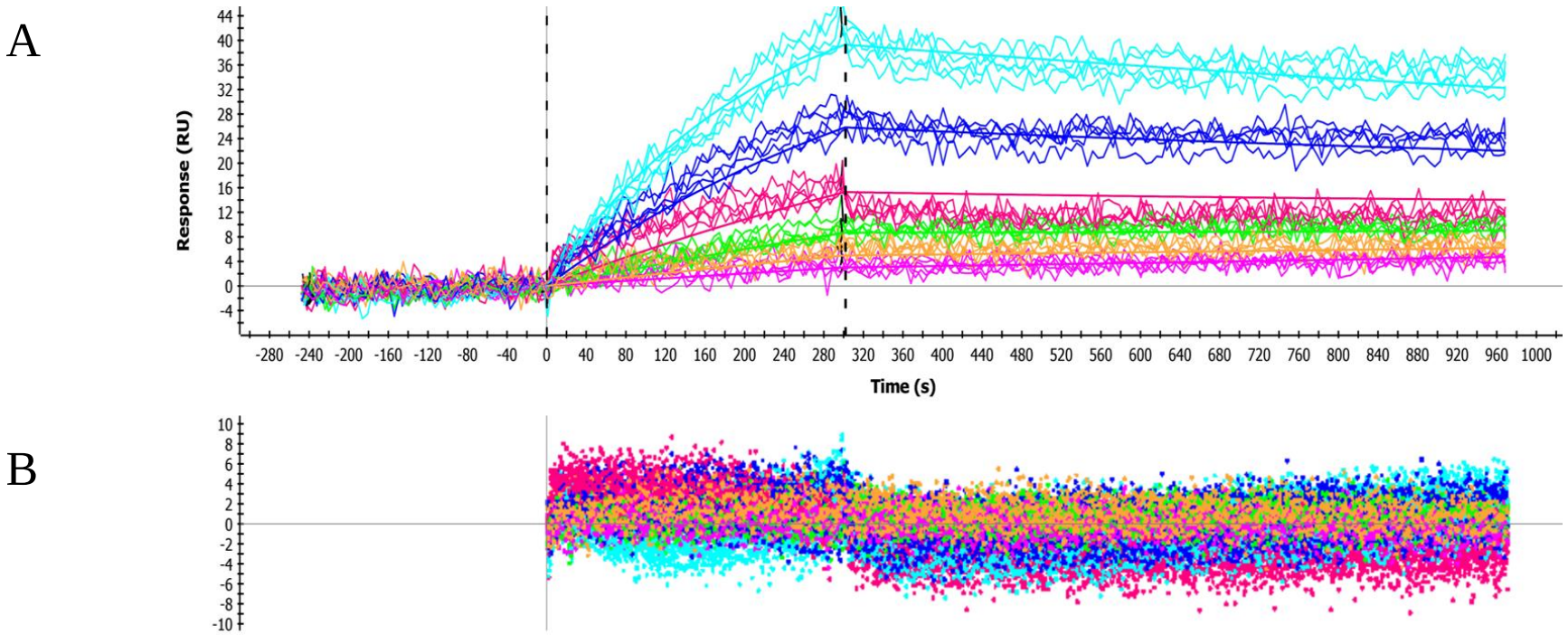

Figure 5-9: Wild-type NA SPR binding curve fitting using Langmuir 1:1 model with drift. A) The data presented here are of five independent experiments for six concentrations (5.2 nM, 2.6 nM, 1.3 nM, 0.65 nM, 0.325 nM and 0.1625 nM) yielding identical results. The fitted lines (solid lines) pass through the experimental curves. B) The residuals, showing the goodness of the fit with the original experimental data.

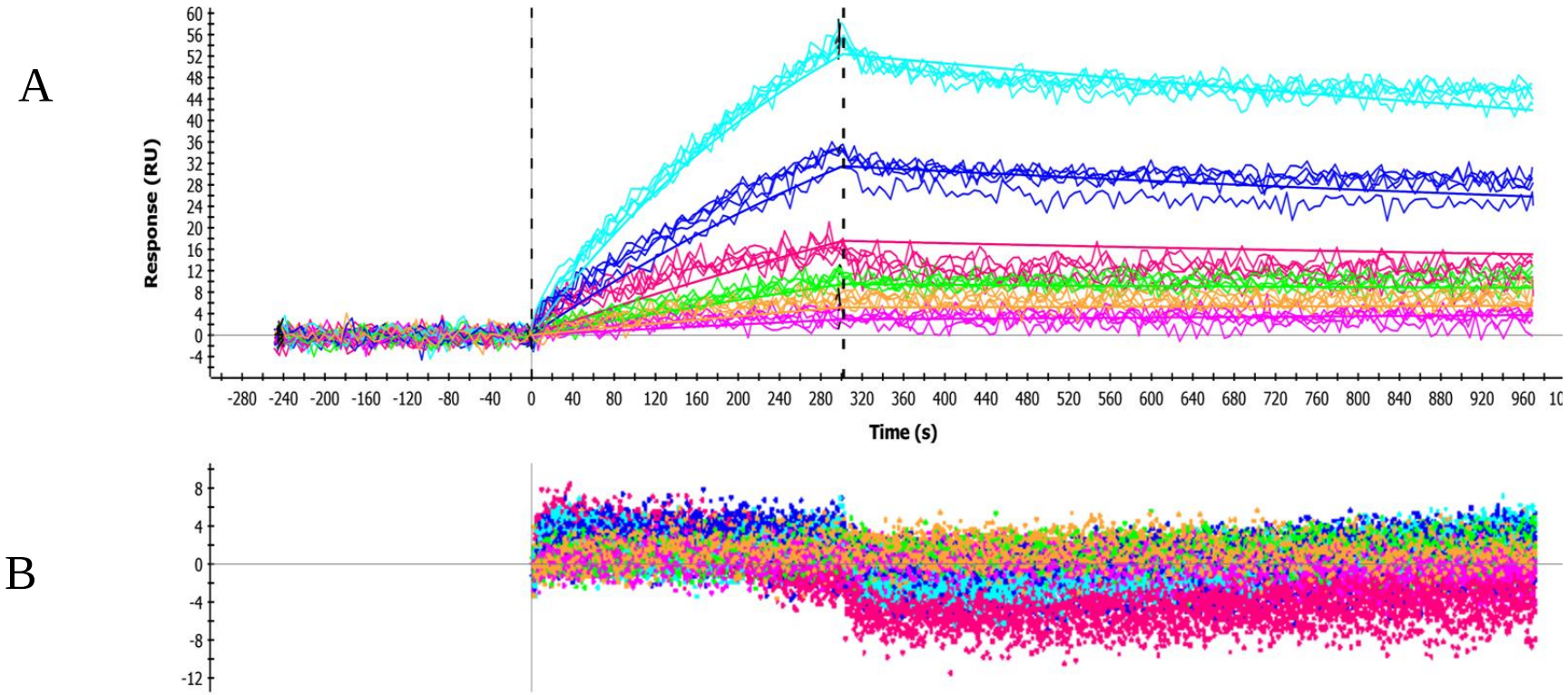

Figure 5-10: H274Y NA SPR binding curve fitting using Langmuir 1:1 model with drift. A) The data presented here are of five independent experiments for six concentrations (5.2 nM, 2.6 nM, 1.3 nM, 0.65 nM, 0.325 nM and 0.1625 nM) yielding identical results. The fitted lines (solid lines) pass through the experimental curves. B) The residuals, showing the goodness of the fit with the original experimental data.

5.3.3 Inhibition assay

Following the kinetics measurements, it was decided to investigate if this assay could be extended to an inhibition binding assay. The immobilized zanamivir-spacer conjugate was considered as a bio-specific ligand for the wild type and mutant proteins. The effects of three inhibitors (sialic acid, zanamivir, oseltamivir) on NA binding to the immobilized ligand were studied. Reference-subtracted SPR sensograms for various concentrations of inhibitors in the presence of a fixed concentration of NA wild type and mutant (6 nM) were monitored. Incubating NA with varying concentrations of inhibitor, lead to the formation of NA-inhibitor complex. Concentration of inhibitor and affinity between NA and inhibitor were the two important driving forces for an NA-inhibitor complex formation. As more of this complex was formed, a decrease in the availability of free NA in the sample was expected. This in turn resulted in a drop in RU signal. Hence the effect of the inhibitor was determined from the drop in RU signal.

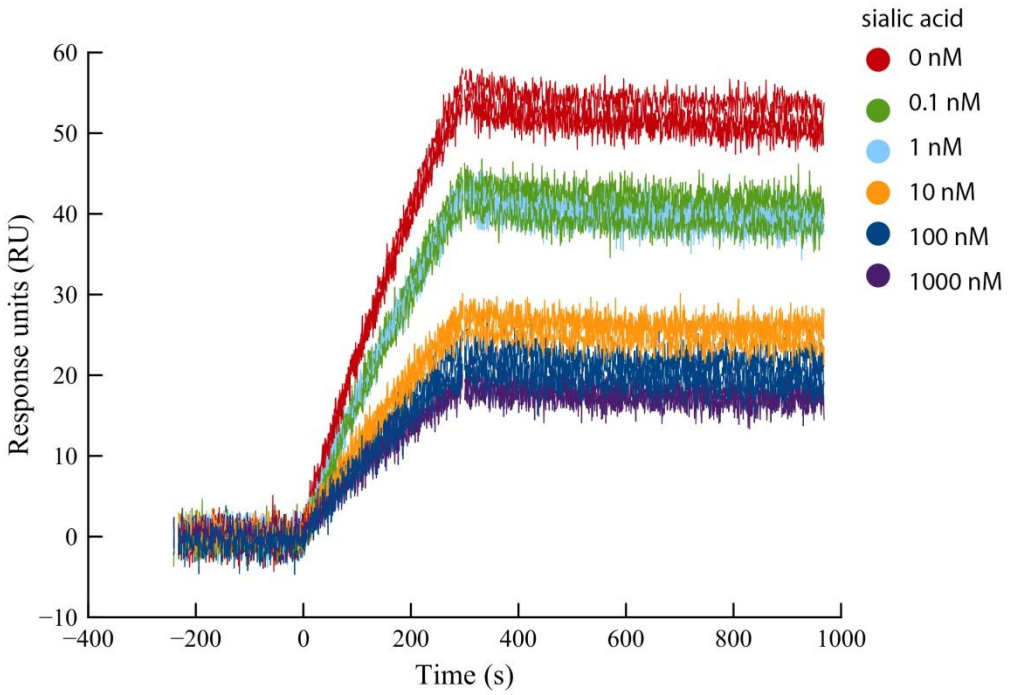

Figure 5-11: Reference-subtracted SPR sensograms showing binding curves for 6 nM NA wild-type protein incubated with various concentrations of sialic acid (0 nM to 1000 nM).The data presented here correspond to three independent experiments. The samples were injected in a shuffled order.

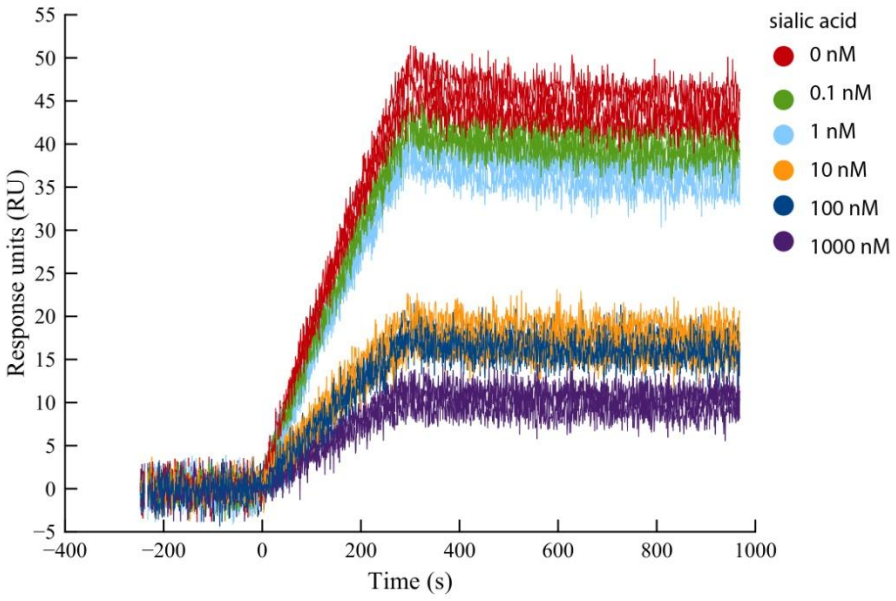

Figure 5-12: Reference-subtracted SPR sensograms showing binding curves for 6 nM NA H274Y protein incubated with various concentrations of sialic acid (0 nM to 1000 nM).The data presented here correspond to three independent experiments. The samples were injected in a shuffled order.

For sialic acid inhibition assay, there was a significant drop in RU when the concentration of sialic acid was increased from 1 nM to 10 nM. With further increase in sialic acid concentration, a further drop in RU was expected. However, further increase of sialic acid to 100 nM and 1000 nM did not alter the binding response significantly (Figure 5-11 and Figure 5-12).

For zanamivir inhibition assay, there was a drop of ~ 20 RU even for 0.1 nM. There was also a further decrease in RU when zanamivir concentration was increased from 1 to 10 nM. Similar to sialic acid results, further increase of zanamivir to 100 nM and 1000 nM did not affect the binding significantly (Figure 5-13 and Figure 5-14). This trend with sialic acid and zanamivir was observed for both NA isoforms. While monitoring oseltamivir inhibition assay a significant difference in trend between the wild-type and mutant protein were observed. In the wild-type protein, a gradual drop in RU was seen with the increase in oseltamivir concentration from 0 nM to 100 nM. A further increase from 100 nM to 1000 nM did not affect the binding response (Figure 5-15). However for the mutant the binding response was not altered up to 100 nM of oseltamivir. A significant drop in RU was observed only when oseltamivir was increased from 100 nM to 1000 nM (Figure 5-16).

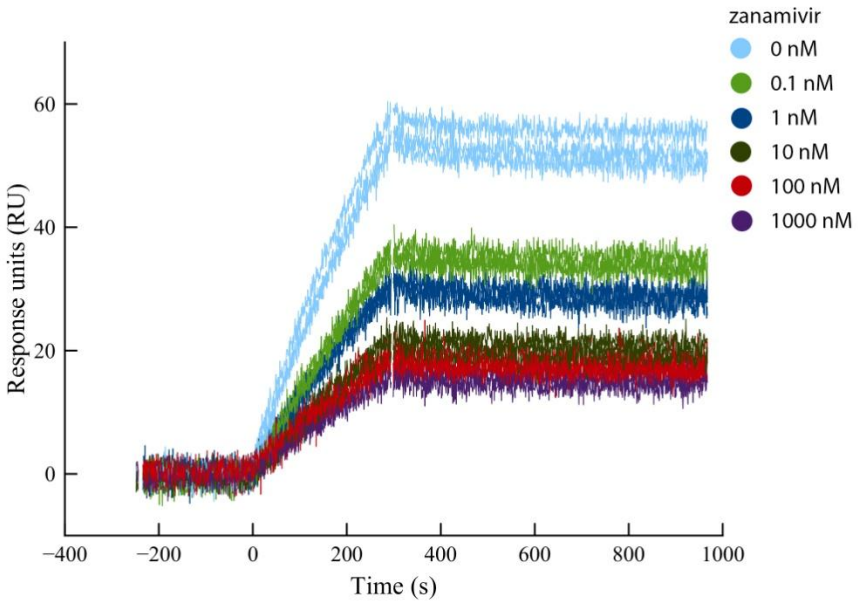

Figure 5-13: Reference-subtracted SPR sensograms showing binding curves for 6 nM NA wild-type protein incubated with various concentrations of zanamivir (0 nM to 1000 nM).The data presented here correspond to three independent experiments. The samples were injected in a shuffled order. The samples were also reshuffled in-between experiments (see methods section).

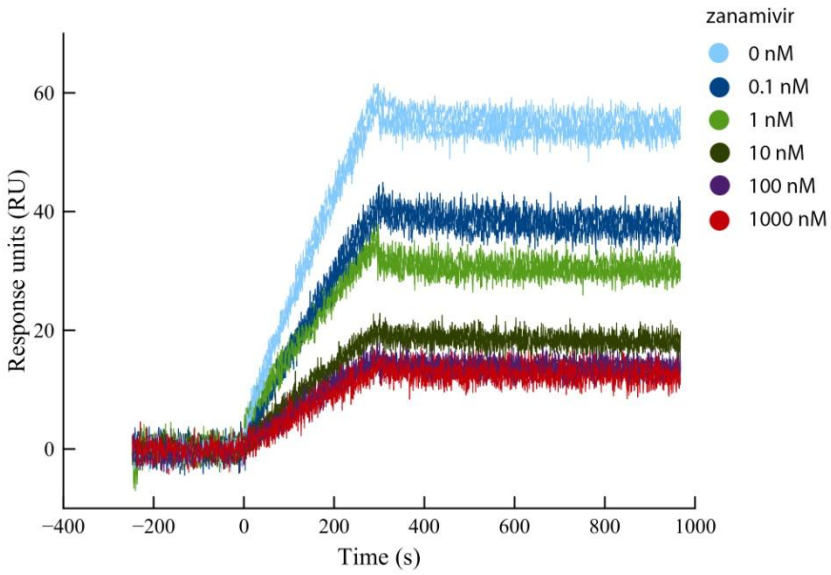

Figure 5-14: Reference-subtracted SPR sensograms showing binding curves for 6 nM NA H274Y protein incubated with various concentrations of zanamivir (0 nM to 1000 nM).The data presented here corresponds to three independent experiments. The samples were injected in a shuffled order. The samples were also reshuffled in-between experiments (see methods section).

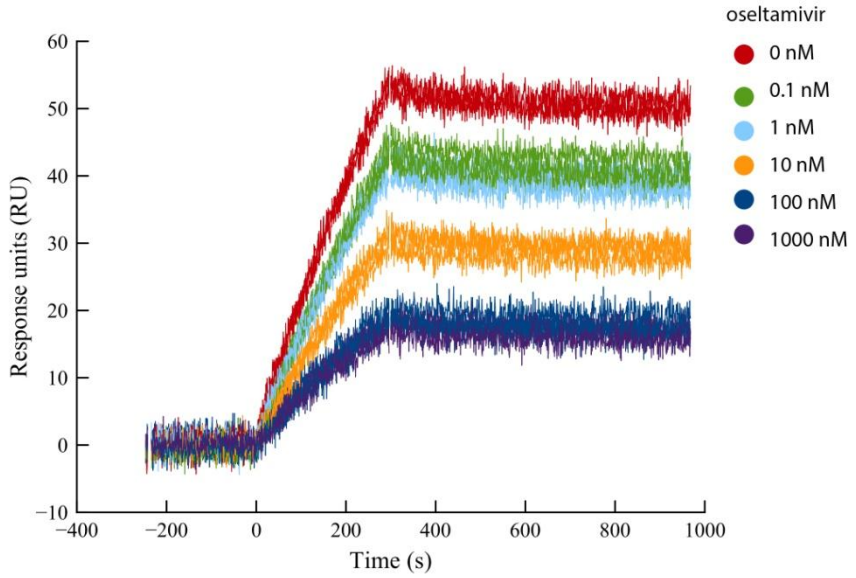

Figure 5-15: Reference-subtracted SPR sensograms showing binding curves for 6 nM NA wild-type protein incubated with various concentrations of oseltamivir (0 nM to 1000 nM).The data presented here correspond to three independent experiments. The samples were injected in a shuffled order.

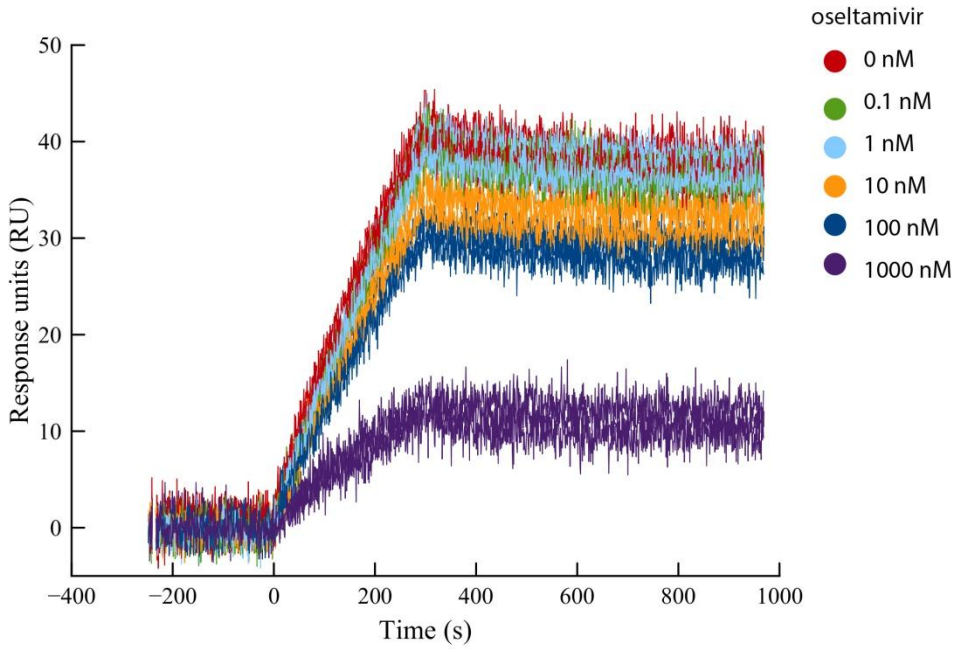

Figure 5-16: Reference-subtracted SPR sensograms showing binding curves for 6 nM NA H274Y protein incubated with various concentrations of oseltamivir (0 nM to 1000 nM).The data presented here correspond to three independent experiments. The samples were injected in a shuffled order.

$IC_{50\text{-spr}}$ values were determined to evaluate and quantitatively compare the inhibitory effect of each inhibitor on the binding interaction of NA isoforms with the bio specific ligand on the SPR chip. The reference subtracted RU values at the end of analyte injection were obtained from the SPR binding experiments. $IC_{50\text{-spr}}$ values were determined using a log-dose–response curve-fit in GraphPad PRISM (v5.04) (Figure 5-17).

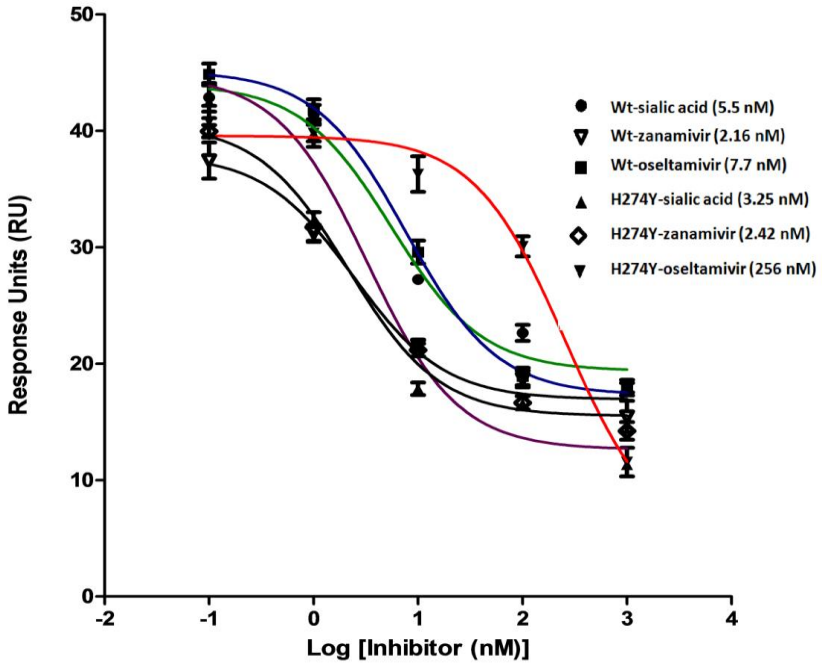

Figure 5-17: Determination of $IC_{50\text{-}SPR}$ values for sialic acid, zanamivir and oseltamivir with recombinant NA wild type and H274Y. The recombinant NA's (wild type and H274Y) were incubated with increasing concentrations of inhibitors. Respective $IC_{50\text{-}SPR}$ values are also presented in this graph. The data presented are mean ± S.D. of triplicate measurements for recombinant NA.

The measured kinetic parameters suggested that the H274Y mutation had not affected the efficacy of zanamivir. This finding was consistent with the data reported by Collins et al. (2008) and $IC_{50\text{-spr}}$ values determined from the SPR inhibition assay. Zanamivir possess the same glycerol moiety at C6 as sialic acid. Hence, a mutation interfering with the glycerol side chain interaction is less likely to develop resistance to the drug without weakening its binding with sialic acid (Collins et al. 2009). This has allowed zanamivir to remain sensitive to the H274Y mutant. Any mutation that can affect the binding of the guanidine group in zanamivir is more likely to cause resistance to

zanamivir, as seen in Q136K (Hurt et al. 2009).

While comparing $IC_{50\text{-spr}}$ values obtained from oseltamivir inhibition assays, there was a significant difference between the wild type (7.7 nM) and H274Y mutant (256 nM), even though both the proteins had similar $IC_{50\text{-spr}}$ values for sialic acid and zanamivir. This result was consistent with the data reported by Collins et al. (2008), suggesting that the binding affinity of the H274Y mutant for oseltamivir had reduced significantly. This was because, when oseltamivir binds to the wild-type protein, the Glu276 rotates and forms a salt bridge with Arg224. The presence of His at 274 (found adjacent to Glu276) is very critical for Glu276 to rotate and form the new binding pocket (and form the salt bridge) during oseltamivir binding. However, when the His at 274 has been mutated to Tyr, the Tyr pushes Glu 276 further into the binding pocket, thereby preventing this conformational change (Russell et al. 2006; Collins et al. 2009).

5.3.4 Comparison with experimental data from the literature

The kinetic parameters obtained for NA-zanamivir interaction from the SPR assay were compared with inhibition kinetic data reported by Collins et al. (2008). Collins et al. reported that the experimental inhibition constant (K_i) in their work was the dissociation constant for the antiviral drugs and it was therefore used to compare the dissociation constant obtained from SPR assay (Table 5-5). However, it should be noted that it is not possible to provide direct, quantitative comparisons between the two results because the experimental conditions and environment were different. Collins et al. used zanamivir in solution, while zanamivir was immobilized to a sensor chip in the SPR assay. Hence, a comparison was made between calculated relative K_i and K_D values (H274Y/wild-type).

Table 5-5: Comparison of kinetic parameters.

Protein	**Literature (Collins et al. 2009) K_i (nM)**	**SPR assay K_D (nM)**
Wild-type	0.1	0.52
H274Y	0.19	0.89
Relative binding(H274Y/ Wild-type)	1.9	1.7

Table 5-6: Zanamivir inhibition assay data comparison

	(Mitnaul et al. 1996)		(Relenza ™ : Laboratory manual, 2000)		(Bantia et al. 2000)		(McKimm-Breschkin et al. 1998)		Current SPR assay		MUNANA enzyme assay (Chapter 4)	
Protein	IC_{50}	Relative IC_{50}	IC_{50}	Relative IC_{50}	IC_{50}	Relative IC_{50}	IC_{50}	Relative IC_{50}	IC_{50}	Relative IC_{50}	IC_{50}	Relative IC_{50}
Wild-type	2	1	0.9	1	1.5	1	1.5	1	2.16	1	0.26	1
H274Y	2.5	1.3	1	1.1	1.8	1.2	2	1.3	2.4	1.11	0.24	1.7

Table 5-7: Oseltamivir inhibition assay data comparison

	(Mitnaul et al. 1996)		(Relenza ™ : Laboratory manual, 2000)		(Bantia et al. 2000)		(McKimm-Breschkin et al. 1998)		Current SPR assay		MUNANA enzyme assay (Chapter 4)	
Protein	IC_{50}	Relative IC_{50}	IC_{50}	Relative IC_{50}	IC_{50}	Relative IC_{50}	IC_{50}	Relative IC_{50}	IC_{50}	Relative IC_{50}	IC_{50}	Relative IC_{50}
Wild-type	2	1	0.9	1	2	1	0.9	1	7.7	1	0.59	1
H274Y	>1000	>500	800	890	450	225	350	390	256	33.3	349.43	592.5

The relative binding values suggested that the current SPR assay yielded similar results to the existing labelled enzymatic assay. The SPR inhibition assays were also compared to inhibition assay data reported in the literature (Table 5-6 and Table 5-7) and the enzymatic assays performed with the recombinant NA samples used for SPR analysis. All comparisons were made between relative IC_{50} values obtained from respective assays. From Table 5-6 it was observed that zanamivir inhibition assay results were highly consistent across all assays. This was because the MUNANA activity assay has been highly consistent when a particular mutant was sensitive to the antiviral drug. However, the inconsistency in the assay had been observed only in drug resistant viruses (Table 5-7). The relative IC_{50} values for oseltamivir inhibition did not match as well as zanamivir inhibition data. However, all the assays suggest that there was a large difference in IC_{50} values between the wild-type NA and H274Y mutant NA, indicating that H274Y is resistant to oseltamivir.

While comparing the SPR inhibition results with the docking results from chapter 3, a similar trend was observed. The computed MM-GB/SA values for sialic acid and zanamivir did not have a significant effect due to the H274Y mutation. This showed that wild-type NA and H27Y mutant had similar binding affinities for sialic acid and zanamivir. Oseltamivir showed a significant decrease in the binding affinity for H274Y mutant when compared with the wild-type. This was because of the prevention of the conformational associated with Glu276 that was vital for oseltamivir activity. This was consistent with the SPR inhibition assay results. However, as discussed in chapter 3, the modelling program did not produce docked structures similar to crystal structures. Hence, the computed energy values may just be coincidentally similar to the SPR experimental data.

In this thesis, an SPR biosensor assay for reliable influenza antiviral drug resistance was developed. This assay can be further extended to study more NA mutations and new antiviral drugs. The SPR biosensor assay has the potential to replace low consistency labelled enzymatic assays.

5.4 Conclusions

In summary, this chapter describes the development of an SPR assay for accurate monitoring of influenza antiviral drug resistance. A spacer molecule (1, 6-hexanediamine) was site specifically tethered to the inert 7-hydroxyl group of

zanamivir. The tethered zanamivir was immobilized on to an SPR GLC chip to obtain 431 final immobilized RU. Preliminary SPR experiments showed that immobilized zanamivir retained its anti-viral activity. The reference subtracted binding responses obtained for NA wild-type and H274Y mutant were analysed using the ProteOn Manager™ Software tools. The SPR curves were fitted to a simple Langmuir 1:1 model and a Langmuir 1:1 model with drift to obtain kinetic parameters. The goodness of the fit was determined from the residuals and χ^2 values. The kinetic parameters obtained for NA-zanamivir interaction from the SPR assay were compared to inhibition kinetic data reported in the literature. The relative binding values obtained from literature and current SPR assay (1.9 and 1.7 respectively) suggested that the current SPR assay yielded similar results to the existing labelled enzymatic assay. In addition, an SPR inhibition assay was also developed. The immobilized zanamivir was considered as a bio-specific ligand to NA isoforms. Three inhibitors (sialic acid, zanamivir and oseltamivir) were tested. The calculated $IC_{50\text{-}spr}$ values were compared and it was observed that wild type protein was sensitive (IC50 = 7.7 nM) and H274Y mutant protein (IC50 = 256 nM) was resistant to oseltamivir. On the other hand, both wild type (IC50 = 2.16 nM) and H274Y mutant (IC50 = 2.4 nM) proteins were sensitive to zanamivir. It was also found that both wild type (IC50 = 5.5 nM) and H274Y mutant (IC50 = 3.25 nM) proteins were sensitive to sialic acid. The viral proteins remained sensitive to sialic acid because sialic acid is the natural receptor. Among the two antiviral drugs, it was observed that zanamivir is a more potent inhibitor than oseltamivir for treating the H274Y mutant. This statement is again in good agreement with the literature and the MUNANA activity assay reported in chapter 4 of this thesis (Collins et al. 2009).

To my knowledge, this is the first SPR biosensor assay to monitor influenza antiviral drug resistance. There is a tremendous scope to extend this study to more mutants and new antiviral drugs. This could pave the way for a reliable SPR biosensor assay to replace low consistency labelled enzymatic assays.

6. Conclusions and recommendations for future work

6.1 Introduction

The outbreak of pandemic influenza and its ability to spread rapidly makes it a potential and severe threat to public health. The antiviral drugs such as oseltamivir and zanamivir are neuraminidase (NA) inhibitors (NI), which bind more tightly to NA than its natural substrate, sialic acid. However, the virus can acquire resistance to antiviral drugs by developing single point mutations (such as H274Y & N294S), thus in some cases the drugs may not be as effective as expected. The high level of inconsistency exhibited by MUNANA assays and the short half-life of the chemiluminescent (1,2-dioxetane derivative of sialic acid, NA-STAR) assay for monitoring drug resistance lead to the need for a simple, label-free, reliable assay. This study set out to develop a reliable label-free surface plasmon resonance assay to monitor NI drug resistance. The important findings of this thesis are chapter specific and are discussed below.

6.2 Molecular docking

The binding affinities, ΔG and MM-GB/SA values for wild-type NA interactions show that both the antiviral drugs studied interact strongly with the wild-type protein. The marked changes observed in predicted binding affinities, ΔG and MM-GB/SA values for the H274Y and N294S interactions may explain reduced antiviral efficacies. The ΔG values for all antiviral interactions with mutant NA forms are reduced in magnitude, thereby indicating that they are less favourable than interactions with the wild-type protein. A similar trend was observed with MM-GB/SA results. Moreover, replacing the His at 274 prevented the formation of a salt bridge with Glu 276, which appears to be a conformational feature that is critical for oseltamivir interactions. Amongst all of the computed values, MM-GB/SA is the closest to the experimental data. In several cases, the interactions between the anti-viral drugs and NA mutants were markedly less favourable than those between sialic acid and the same mutants, indicating that these mutations could confer anti-viral resistance. However, when the docked structures were compared with PDB crystal structures, it was observed that the

modelling program did not produce docked structures similar to crystal structures. Hence the computed ΔG values may just be coincidentally similar with the experimental ΔG values. Docking programs widely used to study the best conformation a protein can take to accommodate a ligand. However, they lack the ability to simulate the relevant macromolecular movement (such as, protein side chain and backbone movement, key catalytic residue movements) that help the protein to maintain this confirmation for accommodating a ligand. This calls for a more reliable experimental validation.

Recommendations for future work

- It docking programs are widely used for predicting protein-ligand interactions. This is because a protein may take different confirmations because of point mutations. The protein structures used for docking may not necessarily match experimental structures. This is a significant limitation observed in docking programs. Alternatively, molecular dynamics (MD) simulations can be used to study the interactions of antiviral drugs to NA isoforms. MD simulations are more advantageous than simple docking studies. Docking studies describes the best conformation a protein can take to accommodate a ligand, while MD simulations have the ability to simulate the relevant macromolecular movement (such as, protein side chain and backbone movement, key catalytic residue movements) that help the protein to maintain this confirmation for accommodating a ligand. However, MD studies can also produce some extreme conformations that might not match with experimental structures. Hence it is important to validate the MD studies by comparing the binding mode of the MD structure with the known crystal structure.

6.3 Expression and purification of influenza neuraminidase

Influenza NA wild-type and H274Y mutant was expressed in BEVS in high-five insect cells. The expressed proteins were partially purified using standard purification techniques such as anion exchange and size exclusion chromatography. Because the quality of the baculovirus generated was poor or low virus titre used for BV amplification, NA was expressed at very low levels and it was difficult to detect the protein on SDS-PAGE gels. Hence, a western blot was required to confirm the

expression of NA. However, the level of expression was sufficient for SPR analysis. A standard fluorometric activity assay was performed on the recombinant proteins. Both the wild type and the mutant showed similar level of activities. In addition, the recombinant NA was used in an inhibition assay. The inhibition assays were compared based on the calculated IC_{50} values. The wild type protein was found to be sensitive to oseltamivir (IC_{50} = 0.59 nM) and the H274Y mutant protein was resistant to oseltamivir (IC_{50} = 349.43 nM). In contrast, both wild type (IC_{50} = 0.26 nM) and H274Y mutant (IC_{50} = 0.44 nM) proteins were sensitive to zanamivir. This indicated that zanamivir was a more potent inhibitor than oseltamivir, for treating H274Y mutant. This is in good agreement with the literature.

Recommendations for future work

- Attempts may be made to improve the quality of the baculovirus generated using sf9 cells. Sf9 cells are more robust and stable than high-five cells. Hence using sf9 cells for baculovirus amplification will yield a good quality recombinant baculovirus. The multiplicity of infection (MOI) can be varied to increase the quality of baculovirus. This baculovirus can then be used for protein expression in either high-five cells or sf9 cells.
- Experts in baculovirus protein expression at the Protein Expression Facility at the University of Queensland have recently found indications that reducing the expression temperature to 21°C allows high level protein expression in insect cells (unpublished work). If these indications turn out to be confirmed, 21°C expression temperature could be used for expressing NA.
- There is scope for producing more mutants that are known to be resistant to antiviral drugs. Large scale protein expression and purification of these mutants can be attempted.

6.4 Surface plasmon resonance assay development

An SPR assay for accurate monitoring of influenza antiviral drug resistance has been developed. A spacer molecule (1, 6- hexanediamine) was site-specifically tethered to the inert 7-hydroxyl group of zanamivir. The tethered zanamivir was immobilized onto an SPR GLC chip to obtain a final immobilization response of 431 RU. Preliminary SPR experiments showed that immobilized zanamivir retained its antiviral activity. The

reference subtracted binding responses obtained for NA wild-type and H274Y mutant were analysed using the ProteOn Manager™ Software tools. The SPR curves were fitted to a simple Langmuir 1:1 model and a Langmuir 1:1 model with drift to obtain kinetic parameters. The goodness of the fit was determined from the residuals and χ^2 values. The kinetic parameters obtained for NA-zanamivir interaction from the SPR assay were compared to inhibition kinetic data reported in the literature. The relative binding values obtained from literature and the current SPR assay (1.9 and 1.7 respectively) suggests that the current SPR assay yields similar results to the already existing labelled enzymatic assay. In addition, an SPR inhibition assay was developed. The immobilized zanamivir was considered as a bio-specific ligand to NA isoforms. Three inhibitors (sialic acid, zanamivir and oseltamivir) were tested. The calculated IC50-spr values were compared and it was observed that wild type protein was sensitive (IC50 = 7.7 nM) and H274Y mutant protein (IC50 = 256 nM) was resistant to oseltamivir. On the other hand, both wild type (IC50 = 2.16 nM) and H274Y mutant (IC50 = 2.4 nM) proteins were sensitive to zanamivir. It was also found that both wild type (IC50 = 5.5 nM) and H274Y mutant (IC50 = 3.25 nM) proteins were sensitive to sialic acid. The viral proteins remained sensitive to sialic acid because sialic acid is the natural receptor. Among the two antiviral drugs, it was observed that zanamivir is a more potent inhibitor than oseltamivir for treating the H274Y mutant.

To my knowledge, this is the first SPR biosensor assay to monitor influenza antiviral drug resistance. There is a tremendous scope to extend this study to more mutants and new antiviral drugs. This could pave the way for a reliable SPR biosensor assay to replace the current enzymatic assays.

Recommendations for future work

- Kinetic parameters for a zanamivir resistant mutant such as Q136K can be measured using the proposed SPR assay. A decrease in affinity is expected for this mutant. It will be interesting to see by how much the kinetic parameters change for this mutant and also to see if it is comparable with the literature.
- Immobilizing sialic acid to the SPR chip surface can be attempted. The substrates for current enzymatic assays for monitoring drug resistance are either a chemiluminescent substrate (NA-STAR) or a fluorescent labelled substrate (MUNANA). Both substrates have the labelled material tethered to C-2-

hydroxyl group of sialic acid. Attaching a tether at this position has not affected the ability of sialic acid to bind NA. This group in sialic acid could be explored to tether the spacer molecule required for SPR immobilization (Figure 6-1). Once sialic acid is immobilized it can be used in the inhibition assay to quantitatively compare the inhibitory effects of antiviral drugs for a wide range on NA mutants.

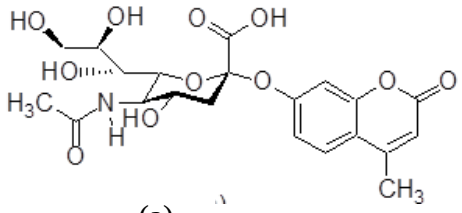

(a)

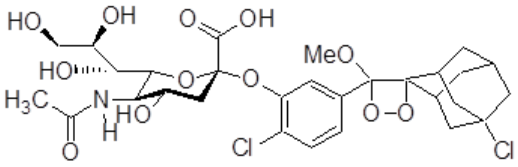

(b)

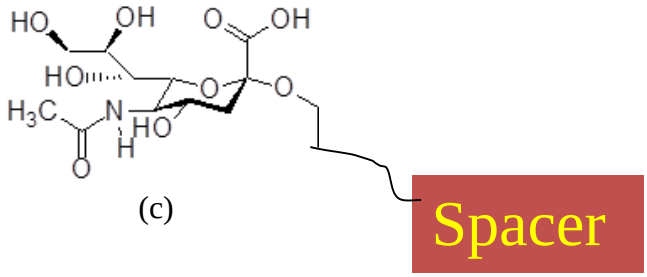

(c)

Figure 6-1: Structures of sialic acid derivatives a) MUNANA substrate used in fluorescent assay b) 1,2-dioxetane derivative of sialic acid used in chemiluminescent assay c) proposed structure for future SPR assay development.

- A second generation zanamivir is being developed. This is a dimer in which two molecules of zanamivir are linked via their 7-hydroxyl groups by an appropriate spacer molecule. This dimer potentially has two advantages. The dimer could increase NA binding by 100-fold over zanamivir because the dimer-drug will bind to 2 adjacent neuraminidase active sites at the same time. Moreover, this

could also increase the bioavailability of the drug, allowing the drug to be retained in the body for up to a week. Zanamivir is being administered as two doses/day for a period of 5 days. This could be replaced by one dose of the dimer every 5 days. This next generation drug can be immobilized on to a SPR sensor chip and its efficiency can be very quickly tested against various isoforms of NA using the proposed SPR assay.

References

Abdulhalim I, Zourob M, Lakhtakia A (2008) Surface plasmon resonance for biosensing: A mini-review. Electromagnetics 28 (3):29.

Amano Y, Cheng Q (2005) Detection of influenza virus: traditional approaches and development of biosensors. Analytical and Bioanalytical Chemistry 381 (1):156-164.

Ayres MD, Howard SC, Kuzio J, Lopezferber M, Possee RD (1994) The complete DNA-sequence of autographo-californica nuclear polyhedrosis-virus. Virology 202 (2):586-605.

Baac H, Hajos JP, Lee J, Kim D, Kim SJ, Shuler ML (2006) Antibody-based surface plasmon resonance detection of intact viral pathogen. Biotechnology and Bioengineering 94 (4):815-819.

Babu YS, Chand P, Bantia S, Kotian P, Dehghani A, El-Kattan Y, Lin TH, Hutchison TL, Elliott AJ, Parker CD, Ananth SL, Horn LL, Laver GW, Montgomery JA (2000) BCX-1812 (RWJ-270201): Discovery of a novel, highly potent, orally active, and selective influenza neuraminidase inhibitor through structure-based drug design. Journal of Medicinal Chemistry 43 (19):3482-3486.

Bianchi N, Rutigliano C, Tomassetti M, Feriotto G, Zorzato F, Gambari R (1997) Biosensor technology and surface plasmon resonance for real-time detection of HIV-1 genomic sequences amplified by polymerase chain reaction. Clinical and Diagnostic Virology 8 (3):199-208.

Biswas SK, Boutz PL, Nayak DP (1998) Influenza virus nucleoprotein interacts with influenza virus polymerase proteins. Journal of Virology 72 (7):5493-5501.

Blick TJ, Tiong T, Sahasrabudhe A, Varghese JN, Colman PM, Hart GJ, Bethell RC, McKimmBreschkin JL (1995) Generation and characterization of an influenza virus neuraminidase variant with decreased sensitivity to the neuraminidase-specific inhibitor 4-guanidino-Neu5Ac2en. Virology 214 (2):475-484.

Boltovets PM, Snopok BA, Boyko VR, Shevchenko TP, Dyachenko NS, Shirshov YM (2004) Detection of plant viruses using a surface plasmon resonance via complexing with specific antibodies. Journal of Virological Methods 121 (1):101-106.

Carrat F, Flahault A (2007) Influenza vaccine: The challenge of antigenic drift. Vaccine 25 (39-40):6852-6862.

Castrucci MR, Bilsel P, Kawaoka Y (1992) Attenuation of influenza-A virus by insertion of a foreign epitope into the neuraminidase. Journal of Virology 66 (8):4647-4653.

Chong AKJ, Pegg MS, Taylor NR, Vonitzstein M (1992) Evidence for a sialosyl cation transition-state complex in the reaction of sialidase from influenza-virus. European Journal of Biochemistry 207 (1):335-343.

Chung JW, Kim SD, Bernhardt R, Pyun JC (2005) Application of SPR biosensor for medical diagnostics of human hepatitis B virus (hHBV). Sensors and Actuators B-Chemical 111:416-422.

Collins PJ, Haire LF, Lin YP, Liu J, Russell RJ, Walker PA, Martin SR, Daniels RS, Gregory V, Skehel JJ, Gamblin SJ, Hay AJ (2009) Structural basis for oseltamivir resistance of influenza viruses. Vaccine 27 (45):6317-6323.

Collins PJ, Haire LF, Lin YP, Liu J, Russell RJ, Walker PA, Skehel JJ, Martin SR, Hay AJ, Gamblin SJ (2008) Crystal structures of oseltamivir-resistant influenza virus neuraminidase mutants. Nature 453 (7199):1258-1261.

Colman PM (1994) Influenza-virus neuraminidase - structure,antibodies, and inhibitors. Protein Science 3 (10):1687-1696.

Colman PM (2002) Neuraminidase inhibitors as antivirals. Vaccine 20:S55-S58.

Colman PM (2009) New Antivirals and Drug Resistance. Annual Review of Biochemistry 78:95-118.

Colman PM, Varghese JN, Laver WG (1983) structure of the catalytic and antigenic sites in influenza-virus neuraminidase. Nature 303 (5912):41-44.

Colman PM, Ward CW (1985) Structure and diversity of influenza-virus neuraminidase Current Topics in Microbiology and Immunology 114:177-255.

Dalakouras T, Smith BJ, Platis D, Cox MMJ, Labrou NE (2006) Development of recombinant protein-based influenza vaccine Expression and affinity purification of H1N1 influenza virus neuraminidase. Journal of Chromatography A 1136 (1):48-56.

De Clereq E, Neyts J (2007) Avian influenza A (H5N1) infection: targets and strategies for chemotherapeutic intervention. Trends in Pharmacological Sciences 28 (6):280-285.

Deroo T, Min Jou W, Fiers W (1996) Recombinant neuraminidase vaccine protects against lethal influenza. Vaccine 14 (6):561-569.

Douglas RG (1990) Drug-therapy-prophylaxis and treatment of influenza. New England Journal of Medicine 322 (7):443-450.

Eckert DM, Kim PS (2001) Mechanisms of viral membrane fusion and its inhibition. Annual Review of Biochemistry 70:777-810.

Fee CJ (2013) Biosensors: Surface Plasmon Resonance *in* J. Gerrard (Ed.), *Protein Nanotechnology: Protocols, Instrumentation, and Applications.* Humana Press, Springer Science + Business Media, USA.ISBN - 10: 162703353X

Ferraris O, Lina B (2008) Mutations of neuraminidase implicated in neuraminidase inhibitors resistance. Journal of Clinical Virology 41 (1):13-19.

Fouchier RAM, Schneeberger PM, Rozendaal FW, Broekman JM, Kemink SAG, Munster V, Kuiken T, Rimmelzwaan GF, Schutten M, van Doornum GJJ, Koch G, Bosman A, Koopmans M, Osterhaus ADME (2004) Avian influenza A virus (H7N7) associated with human conjunctivitis and a fatal case of acute respiratory distress syndrome. Proceedings of the National Academy of Sciences of the United States of America 101 (5):1356-1361.

Gubareva LV, Kaiser L, Hayden FG (2000) Influenza virus neuraminidase inhibitors. Lancet 355 (9206):827-835.

Gubareva LV, Matrosovich MN, Brenner MK, Bethell RC, Webster RG (1998) Evidence for zanamivir resistance in an immunocompromised child infected with influenza B virus. Journal of Infectious Diseases 178 (5):1257-1262.

Harris A, Cardone G, Winkler DC, Heymann JB, Brecher M, White JM, Steven AC (2006) Influenza virus pleiomorphy characterized by cryoelectron tomography. Proceedings of the National Academy of Sciences of the United States of America 103 (50):19123-19127.

Hasegawa H, Ichinohe T, Tamura S, Kurata T (2007) Development of a mucosal vaccine for influenza viruses: preparation for a potential influenza pandemic. Expert Review of Vaccines 6 (2):193-201.

Hidari K, Shimada S, Suzuki Y, Suzuki T (2007) Binding kinetics of influenza viruses to sialic acid-containing carbohydrates. Glycoconjugate Journal 24 (9):583-590.

Hink WF (1970) Established insect cell line from cabbage looper, trichoplusia-ni. Nature 226 (5244):466-467.

Hink WF (1973) Plaque assay of an insect virus in a cabbage-looper (TN-368) cell line. In Vitro-Journal of the Tissue Culture Association 8 (5):412-413.

Hirst GK (1941) The agglutination of red cells by allantoic fluid of chick embryos infected with influenza virus. Science 94:22-23.

Hitchman RB, Possee RD, King LA (2009) Baculovirus Expression Systems for Recombinant Protein Production in Insect Cells. Recent Patents on Biotechnology 3:46-54.

Homola J, Yee SS, Gauglitz G (1999) Surface plasmon resonance sensors: review. Sensors and Actuators B: Chemical 54 (1–2):3-15.

Huang JG, Lee CL, Lin HM, Chuang TL, Wang WS, Juang RH, Wang CH, Lee CK, Lin SM, Lin CW (2006) A miniaturized germanium-doped silicon dioxide-based surface plasmon resonance waveguide sensor for immunoassay detection. Biosensors & Bioelectronics 22 (4):519-525.

Ilyushina NA, Bovin NV, Webster RG, Govorkova EA (2006) Combination chemotherapy, a potential strategy for reducing the emergence of drug-resistant influenza A variants. Antiviral Research 70 (3):121-131.

Invitrogen (Instruction manual) Guide to Baculovirus Expression Vector Systems (BEVS) and Insect Cell Culture Techniques. Instruction manual.

Ives JAL, Carr JA, Mendel DB, Tai CY, Lambkin R, Kelly L, Oxford JS, Hayden FG, Roberts NA (2002) The H274Y mutation in the influenza A/H1N1 neuraminidase active site following oseltamivir phosphate treatment leave virus severely compromised both in vitro and in vivo. Antiviral Research 55 (2):307-317.

Kim CU, Lew W, Williams MA, Liu HT, Zhang LJ, Swaminathan S, Bischofberger N, Chen MS, Mendel DB, Tai CY, Laver WG, Stevens RC (1997) Influenza neuraminidase inhibitors possessing a novel hydrophobic interaction in the enzyme active site: Design, synthesis, and structural analysis of carbocyclic sialic acid analogues with potent anti-influenza activity. Journal of the American Chemical Society 119 (4):681-690.

Laver G, Garman E (2002) Pandemic influenza: its origin and control. Microbes and Infection 4 (13):1309-1316.

Le QM, Kiso M, Someya K, Sakai YT, Nguyen TH, Nguyen KHL, Pham ND, Ngyen HH, Yamada S, Muramoto Y, Horimoto T, Takada A, Goto H, Suzuki T, Suzuki Y, Kawaoka Y (2005) Avian flu - Isolation of drug-resistant H5N1 virus. Nature 437 (7062):1108-1108.

Lee HJ, Wark AW, Corn RM (2008) Enhanced bioaffinity sensing using surface plasmons, surface enzyme reactions, nanoparticles and diffraction gratings. Analyst 133 (5):596-601.

Lentz MR, Webster RG, Air GM (1987) Site-directed mutation of the active-site of influenza neuraminidase and implications for the catalytic mechanism. Biochemistry 26 (17):5351-5358.

Li SQ, Schulman J, Itamura S, Palese P (1993) Glycosylation of neuraminiidase determines the neurovirulence of influenza-A/WSN/33 virus. Journal of Virology 67 (11):6667-6673.

Liedberg B, Nylander C, Lundström I (1995) Biosensing with surface plasmon resonance — how it all started. Biosensors and Bioelectronics 10 (8):i-ix.

Liu CG, Eichelberger MC, Compans RW, Air GM (1995) Influenza type-A virus neuraminidase does not play a role in viral entry, replication.assembly, or budding. Journal of Virology 69 (2):1099-1106.

Maines TR, Lu XH, Erb SM, Edwards L, Guarner J, Greer PW, Nguyen DC, Szretter KJ, Chen LM, Thawatsupha P, Chittaganpitch M, Waicharoen S, Nguyen DT, Nguyen T, Nguyen HHT, Kim JH, Hoang LT, Kang C, Phuong LS, Lim W, Zaki S, Donis RO, Cox NJ, Katz JM, Tumpey TM (2005) Avian influenza (H5N1) viruses isolated from humans in Asia in 2004 exhibit increased virulence in mammals. Journal of Virology 79 (18):11788-11800.

Martinet W, Saelens X, Deroo T, Neirynck S, Contreras R, Jou WM, Fiers W (1997) Protection of mice against a lethal influenza challenge by immunization with yeast-derived recombinant influenza neuraminidase. European Journal of Biochemistry 247 (1):332-338.

Mather KA, White JF, Hudson PJ, McKimmbreschkin JL (1992) Expression of influenza neuraminidase in baculovirus-infected cells. Virus Research 26 (2):127-139.

Matrosovich M, Klenk HD (2003) Natural and synthetic sialic acid-containing inhibitors of influenza virus receptor binding. Reviews in Medical Virology 13 (2):85-97.

McDonald NJ, Smith CB, Cox NJ (2007) Antigenic drift in the evolution of H1N1 influenza A viruses resulting from deletion of a single amino acid in the haemagglutinin gene. Journal of General Virology 88:3209-3213.

McKimm-Breschkin JL (2000) Resistance of influenza viruses to neuraminidase inhibitors - a review. Antiviral Research 47 (1):1-17.

McKimm-Breschkin JL, Colman PM, Jin B, Krippner GY, McDonald M, Reece PA, Tucker SP, Waddington L, Watson KG, Wu WY (2003) Tethered neuraminidase inhibitors that bind an influenza virus: A first step towards a diagnostic method for influenza. Angewandte Chemie-International Edition 42 (27):3118-3121.

McKimm-Breschkin JL, Sahasrabudhe A, Blick TJ, McDonald M, Colman PM, Hart GJ, Bethell RC, Varghese JN (1998) Mutations in a conserved residue in the influenza virus neuraminidase active site decreases sensitivity to Neu5Ac2en-derived inhibitors. Journal of Virology 72 (3):2456-2462.

Miller LK, Lingg AJ, Bulla LA (1983) Bacterial, viral, and fungal insecticides. Science 219 (4585):715-721.

Mills CE, Robins JM, Lipsitch M (2004) Transmissibility of 1918 pandemic influenza. Nature 432 (7019):904-906.

Mitchell J (2010) Small Molecule Immunosensing Using Surface Plasmon Resonance. Sensors 10 (8):7323-7346.

Navratilova I, Myszka DG (2006) Investigating Biomolecular Interactions and Binding Properties Using SPR Biosensors. Surface Plasmon Resonance Based Sensors. In: Homola J, vol 4. Springer Series on Chemical Sensors and Biosensors. Springer Berlin Heidelberg, pp 155-176.

Nelson J, Couceiro SS, Paulson JC, Baum LG (1993) Influenza-virus strains selectively recognize sialyloligosacchardies on human respiratory epithelium-the role of the host-cell in selection of hemagglutinn receptor specificity Virus Research 29 (2):155-165.

Oakley AJ, Barrett S, Peat TS, Newman J, Streltsov VA, Waddington L, Saito T, Tashiro M, McKimm-Breschkin JL (2010) Structural and Functional Basis of Resistance to Neuraminidase Inhibitors of Influenza B Viruses. Journal of Medicinal Chemistry 53 (17):6421-6431.

Orozovic G, Orozovic K, Lennerstrand J, Olsen B (2011) Detection of Resistance Mutations to Antivirals Oseltamivir and Zanamivir in Avian Influenza A Viruses Isolated from Wild Birds. Plos One 6 (1).

Oshannessy DJ, Brighamburke M, Soneson KK, Hensley P, Brooks I (1993) Determination of rate and equilibrium binding constants for macromolecular interactions using surface-plasmon resonance – use of nonlinear least–square analysis-method. Analytical Biochemistry 212 (2):457-468.

Oxford JS, Bossuyt S, Eswarasaran R, Lambkin R (2002) Drugs to combat the epidemic and pandemic faces of influenza. Influenza 7:201-234.

Palese P, Tobita K, Ueda M, Compans RW (1974) Characterization of temperature sensitive influenza-virus mutants defective in neuraminidase Virology 61 (2):397-410.

Pennock GD, Shoemaker C, Miller LK (1984) Strong and regulated expression of E. coli beta-galactosidase in insect cells with a baculovirus vector. Molecular and Cellular Biology 4 (3):399-406.

Perez DR, Donis RO (2001) Functional analysis of PA binding by influenza a virus PB1: Effects on polymerase activity and viral infectivity. Journal of Virology 75 (17):8127-8136.

Pinto LH, Holsinger LJ, Lamb RA (1992) Influenza-virus M2 protein has ion channel activity. Cell 69 (3):517-528.

Potier M, Mameli L, Belisle M, Dallaire L, Melancon SB (1979) Fluorometric assay of neuraminidase with a sodium (-methylumbelliferyl-alpha-D-N-acetylneuraminate) substrate Analytical Biochemistry 94 (2):287-296.

Potter CW (2001) A history of influenza. Journal of Applied Microbiology 91 (4):572-579.

Rich RL, Myszka DG (2008) Survey of the year 2007 commercial optical biosensor literature. Journal of Molecular Recognition 21 (6):355-400.

Roberts NA (2001) Treatment of influenza with neuraminidase inhibitors: virological implications. Philosophical Transactions of the Royal Society of London Series B-Biological Sciences 356 (1416):1895-1897.

Rohrmann GF, Melgaard S, Beaudreau GS, Martignoni ME (1982) Characterization of DNA from 3 nuclear polyhedrosis viruses pathogenic for choristoneura sp. Journal of Invertebrate Pathology 40 (2):237-241.

Saito T, Kawano KJ (1997) Loss of glycosylation at Asn144 alters the substrate preference of the N8 influenza A virus neuraminidase. Journal of Veterinary Medical Science 59 (10):923-926.

Salahuddin P, Khan AU (2010) Structural and functional analysis of NS1 and NS2 proteins of H1N1 subtype. Genomics, proteomics & bioinformatics / Beijing Genomics Institute 8 (3):190-199.

Sauter NK, Glick GD, Crowther RL, Park SJ, Eisen MB, Skehel JJ, Knowles JR, Wiley DC (1992) Crystallographic detection of a 2nd ligand binding site in influenza-virus hemagglutinn. Proceedings of the National Academy of Sciences of the United States of America 89 (1):324-328.

Schmidt PM, Attwood RM, Mohr PG, Barrett SA, McKimm-Breschkin JL (2011) A Generic System for the Expression and Purification of Soluble and Stable Influenza Neuraminidase. Plos One 6 (2).

Schnell JR, Chou JJ (2008) Structure and mechanism of the M2 proton channel of influenza A virus. Nature 451 (7178):591-595.

Shtyrya MaB (2009) Influenza Virus Neuraminidase: Structure and Function. Acta Naturae 1 (2):26–32.

Shtyrya Y, Mochalova L, Voznova G, Rudneva I, Shilov A, Kaverin N, Bovin N (2009) Adjustment of receptor-binding and neuraminidase substrate specificties

in avian–human reassortant influenza viruses. Glycoconjugate Journal 26 (1):99-109.

Skehel JJ, Wiley DC (2000) Receptor binding and membrane fusion in virus entry: The influenza hemagglutinin. Annual Review of Biochemistry 69:531-569.

Smith BJ, Huyton T, Joosten RP, McKimm-Breschkin JL, Zhang JG, Luo CS, Lou MZ, Labrou NE, Garrett TPJ (2006) Structure of a calcium-deficient form of influenza virus neuraminidase: implications for substrate binding. Acta Crystallographica Section D-Biological Crystallography 62:947-952.

Smith BJ, McKimm-Breshkin JL, McDonald M, Fernley RT, Varghese JN, Colman PM (2002) Structural studies of the resistance of influenza virus neuramindase to inhibitors. Journal of Medicinal Chemistry 45 (11):2207-2212.

Smith FB (1995) The Russian Influenza in the United Kingdom, 1889–1894. Oxford Journals, Social History of Medicine Volume 8 (1): 55-73.

Smith GE, Fraser MJ, Summers MD (1983) Molecular engineering of the autographa-californica nuclear polyhedrosis-virus genome-deletion mutations within the polyhedrin gene. . Journal of Virology 46 (2):584-593.

Smith GE, Ju G, Ericson BL, Moschera J, Lahm HW, Chizzonite R, Summers MD (1985) Modification and secretion of human interleukin-2 produced in insect cells by a baculovirus expression vector.. Proceedings of the National Academy of Sciences of the United States of America 82 (24):8404-8408.

Štěpánek J, Vaisocherová H, Piliarik M (2006) Molecular Interactions in SPR Sensors. Surface Plasmon Resonance Based Sensors. In: Homola J (ed), vol 4. Springer Series on Chemical Sensors and Biosensors. Springer Berlin Heidelberg, pp 69-91.

Suzuki Y, Ito T, Suzuki T, Holland RE, Chambers TM, Kiso M, Ishida H, Kawaoka Y (2000) Sialic acid species as a determinant of the host range of influenza A viruses. Journal of Virology 74 (24):11825-11831.

Takahashi T, Suzuki T, Hidari K, Miyamoto D, Suzuki Y (2003) A molecular mechanism for the low-pH stability of sialidase activity of influenza A virus N2 neuraminidases. Febs Letters 543 (1-3):71-75.

Taylor NR, Vonitzstein M (1994) Molecular modeling studies on ligand-binding to sialidase from influenza-virus and the mechanism of catalysis. Journal of Medicinal Chemistry 37 (5):616-624.

Tisdale M (2000) Monitoring of viral susceptibility: new challenges with the development of influenza NA inhibitors. Reviews in Medical Virology 10 (1):45-55.

Torrance L, Ziegler A, Pittman H, Paterson M, Toth R, Eggleston I (2006) Oriented immobilisation of engineered single-chain antibodies to develop biosensors for virus detection. Journal of Virological Methods 134 (1-2):164-170.

Trifonov V, Khiabanian H, Rabadan R (2009) Geographic Dependence, Surveillance, and Origins of the 2009 Influenza A (H1N1) Virus. New England Journal of Medicine 361 (2):115-119.

Tsai CH, Lee PY, Stollar V, Li ML (2006) Antiviral therapy targeting viral polymerase. Current Pharmaceutical Design 12 (11):1339-1355.

Vaisocherova H, Mrkvova K, Piliarik M, Jinoch P, Steinbachova M, Homola J (2007) Surface plasmon resonance biosensor for direct detection of antibody against Epstein-Baff virus. Biosensors & Bioelectronics 22 (6):1020-1026.

Volkman LE, Summers MD (1977) Autographa-californica nuclear polyhedrosis-virus-comparative infectivity of occluded, alkali-liberated, and non-occluded forms. Journal of Invertebrate Pathology 30 (1):102-103.

Volkman LE, Summers MD, Hsieh CH (1976) Occluded and nonoccluded nuclear polyhedrosis-virus grown in trchoplusia ni-comparative neutralization, comparative infectivity, and invitro growth studies. Journal of Virology 19 (3):820-832.

von Itzstein M (2007) The war against influenza: discovery and development of sialidase inhibitors. Nat Rev Drug Discov 6 (12):967-974.

vonItzstein M, Dyason JC, Oliver SW, White HF, Wu WY, Kok GB, Pegg MS (1996) A study of the active site of influenza virus sialidase: An approach to the rational design of novel anti-influenza drugs. Journal of Medicinal Chemistry 39 (2):388-391.

Vonitzstein M, Wu WY, Kok GB, Pegg MS, Dyason JC, Jin B, Phan TV, Smythe ML, White HF, Oliver SW, Colman PM, Varghese JN, Ryan DM, Woods JM, Bethell RC, Hotham VJ, Cameron JM, Penn CR (1993) Rational design of potent sialidase-based inhibitors of influenza-virus replication Nature 363 (6428):418-423.

Wagner R, Matrosovich M, Klenk HD (2002) Functional balance between haemagglutinin and neuraminidase in influenza virus infections. Reviews in Medical Virology 12 (3):159-166.

Wakefield L, Brownlee GG (1989) RNA-binding properties of influenza-A virus matrix protein M1. Nucleic Acids Research 17 (21):8569-8580.

Watowich SJ, Skehel JJ, Wiley DC (1994) Crystal-structures of influenza-virus hemagglutinn in complex with high-affinity receptor analogs. Structure 2 (8):719-731.

Wetherall NT, Trivedi T, Zeller J, Hodges-Savola C, McKimm-Breschkin JL, Zambon M, Hayden FG (2003) Evaluation of neuraminidase enzyme assays using different substrates to measure susceptibility of influenza virus clinical isolates

to neuraminidase inhibitors: Report of the neuraminidase inhibitor susceptibility network. Journal of Clinical Microbiology 41 (2):742-750.

Wilson NS, Jennifer A · Baker, Michael G (2012) The 2009 influenza pandemic: a review of the strengths and weaknesses of the health sector response in New Zealand. The New Zealand medical journal (125)

Wintermeyer SM, Nahata MC (1995) Rimantadine - A clinical perspective. Annals of Pharmacotherapy 29 (3):299-310.

Woods JM, Bethell RC, Coates JAV, Healy N, Hiscox SA, Pearson BA, Ryan DM, Ticehurst J, Tilling J, Walcott SM, Penn CR (1993) 4-Guanidino-2,4-dideoxy-2,3-dehydro-N-acetylneuraminic acid is a highly effective inhibitor both of the sialidase (neuraminidase) and of growth of a wide-range of influenza-A and influenza-B viruses in-vitro. Antimicrobial Agents and Chemotherapy 37 (7):1473-1479.

Wu ZL, Ethen C, Hickey GE, Jiang W (2009) Active 1918 pandemic flu viral neuraminidase has distinct N-glycan profile and is resistant to trypsin digestion. Biochemical and Biophysical Research Communications 379 (3):749-753.

Xu X, Zhu X, Dwek RA, Stevens J, Wilson IA (2008) Structural Characterization of the 1918 Influenza Virus H1N1 Neuraminidase. Journal of Virology 82 (21):10493-10501.

Yano T, Nobusawa E, Nagy A, Nakajima S, Nakajima K (2008) Effects of single-point amino acid substitutions on the structure and function neuraminidase proteins in influenza A virus. Microbiology and Immunology 52 (4):216-223.

Yongkiettrakul S, Boonyapakron K, Jongkaewwattana A, Wanitchang A, Leartsakulpanich U, Chitnumsub P, Eurwilaichitr L, Yuthavong Y (2009) Avian influenza A/H5N1 neuraminidase expressed in yeast with a functional head domain. Journal of Virological Methods 156 (1-2):44-51.

Yuen KY WS (2005) Human infection by avian influenza A H5N1. Hong Kong Med J 11(3):189-199.

Appendix A: ExPASy - ProtParam data

NA-DNA sequence:

atgaacccgaaccagaaaattattaccattggcagcatttgcctggtggtgggcctgattagcctgattctgcagattggcaacattattagcatttggatta
gccatagcattcagaccggcagccagaaccataccggcatttgcaaccagaacattattacctataaaaacagcacctgggtgaaagataccaccagc
gtgattctgaccggcaacagcagcctgtgcccgattcgcggctgggcgatttatagcaaagataacagcattcgcattggcagcaaaggcgatgtgtttg
tgattcgcgaaccgtttattagctgcagccatctggaatgccgcacctttttctgacccagggcgcgctgctgaacgatcgccatagcaacggcaccgt
gaaagatcgcagcccgtatcgcgcgctgatgagctgcccggtgggcgaagcgccgagcccgtataacagccgctttgaaagcgtggcgtggagcgc
gagcgcgtgccatgatggcatgggctggctgccattggcattagcggcccggataacggcgcggtggcggtgctgaaatataacggcattattaccga
aaccattaaaagctggcgcaaaaaaattctgcgcacccaggaaagcgaatgcgcgtgcgtgaacggcagctgctttaccattatgaccgatggcccga
gcgatggcctggcgagctataaaatttttaaaattgaaaaaggcaaagtgaccaaaagcattgaactgaacgcgccgaacagccattatgaagaatgca
gctgctatccggataccggcaaagtgatgtgcgtgtgccgcgataactggcatggcagcaaccgcccgtgggtgagctttgatcagaacctggattatc
agattggctatatttgcagcggcgtgtttggcgataacccgcgcccgaaagatggcaccggcagctgcggcccggtgtatgtggatggcgcgaacgg
cgtgaaaggctttagctatcgctatggcaacggcgtgtggattggccgcaccaaaagccatagcagccgccatggctttgaaatgatttgggatccgaa
cggctggaccgaaaccgatagcaaatttagcgtgcgccaggatgtggtggcgatgaccgattggagcggctatagcggcagctttgtgcagcatccg
gaactgaccggcctggattgcattcgcccgtgcttttgggtggaactgattcgcggccgcccgaaagaaaaaaccatttggaccagcgcgagcagcatt
agcttttgcggcgtgaacagcgataccgtggattggagctggccggatggcgcggaactgccgtttaccattgataaa

NA- protein sequence

```
        10         20         30         40         50         60
MNPNQKIITI GSICLVVGLI SLILQIGNII SIWISHSIQT GSQNHTGICN QNIITYKNST

        70         80         90        100        110        120
WVKDTTSVIL TGNSSLCPIR GWAIYSKDNS IRIGSKGDVF VIREPFISCS HLECRTFFLT

       130        140        150        160        170        180
QGALLNDRHS NGTVKDRSPY RALMSCPVGE APSPYNSRFE SVAWSASACH DGMGWLTIGI

       190        200        210        220        230        240
SGPDNGAVAV LKYNGIITET IKSWRKKILR TQESECACVN GSCFTIMTDG PSDGLASYKI

       250        260        270        280        290        300
FKIEKGKVTK SIELNAPNSH YEECSCYPDT GKVMCVCRDN WHGSNRPWVS FDQNLDYQIG

       310        320        330        340        350        360
YICSGVFGDN PRPKDGTGSC GPVYVDGANG VKGFSYRYGN GVWIGRTKSH SSRHGFEMIW

       370        380        390        400        410        420
DPNGWTETDS KFSVRQDVVA MTDWSGYSGS FVQHPELTGL DCIRPCFWVE LIRGRPKEKT

       430        440        450
IWTSASSISF CGVNSDTVDW SWPDGAELPF TIDK
```

ProtParam data for NA

Number of amino acids: 454

Molecular weight: 50143.7

Theoretical pI: 7.45

Amino acid composition:

Ala (A)	16	3.5%
Arg (R)	20	4.4%
Asn (N)	25	5.5%
Asp (D)	25	5.5%
Cys (C)	19	4.2%
Gln (Q)	11	2.4%
Glu (E)	17	3.7%
Gly (G)	44	9.7%
His (H)	10	2.2%
Ile (I)	41	9.0%
Leu (L)	21	4.6%
Lys (K)	23	5.1%
Met (M)	7	1.5%
Phe (F)	16	3.5%
Pro (P)	21	4.6%
Ser (S)	51	11.2%
Thr (T)	29	6.4%
Trp (W)	16	3.5%
Tyr (Y)	14	3.1%
Val (V)	28	6.2%
Pyl (O)	0	0.0%

Total number of negatively charged residues (Asp + Glu): 42
Total number of positively charged residues (Arg + Lys): 43

Atomic composition:

Carbon	C	2218
Hydrogen	H	3409
Nitrogen	N	609
Oxygen	O	669
Sulfur	S	26

Formula: $C_{2218}H_{3409}N_{609}O_{669}S_{26}$
Total number of atoms: 6931

Extinction coefficients:

Extinction coefficients are in units of M^{-1} cm^{-1}, at 280 nm measured in water.

Ext. coefficient 109985
Abs 0.1% (=1 g/l) 2.193, assuming all pairs of Cys residues form cystines

Ext. coefficient 108860
Abs 0.1% (=1 g/l) 2.171, assuming all Cys residues are reduced

Estimated half-life:
The N-terminal of the sequence considered is M (Met).

The estimated half-life is: 30 hours (mammalian reticulocytes, in vitro).
>20 hours (yeast, in vivo).
>10 hours (Escherichia coli, in vivo).

Instability index:

The instability index (II) is computed to be 29.54
This classifies the protein as stable.

Aliphatic index: 74.67

Grand average of hydropathicity (GRAVY): -0.250

Appendix B: Induced fit docking results

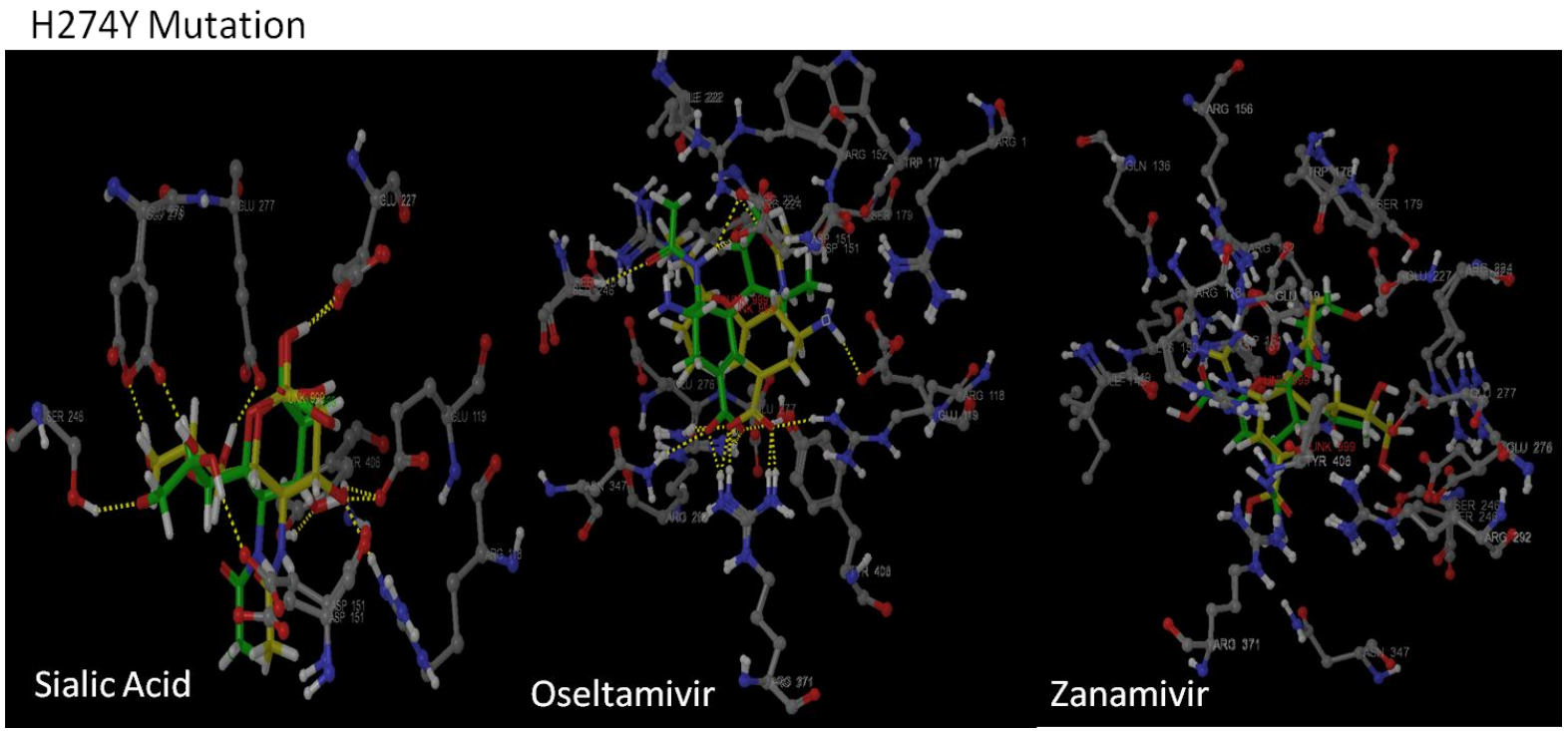

Figure B-1: Overlaid images of sialic acid, oseltamivir and zanamivir interaction with wild-type and H274Y mutant NA. The ligands are shown in green colour in wild-type interactions and are shown in yellow in H274Y mutant interactions. Oseltamivir deviates significantly in the H274Y interaction when compared to the wild-type interaction and thereby decreasing the drug's binding affinity.

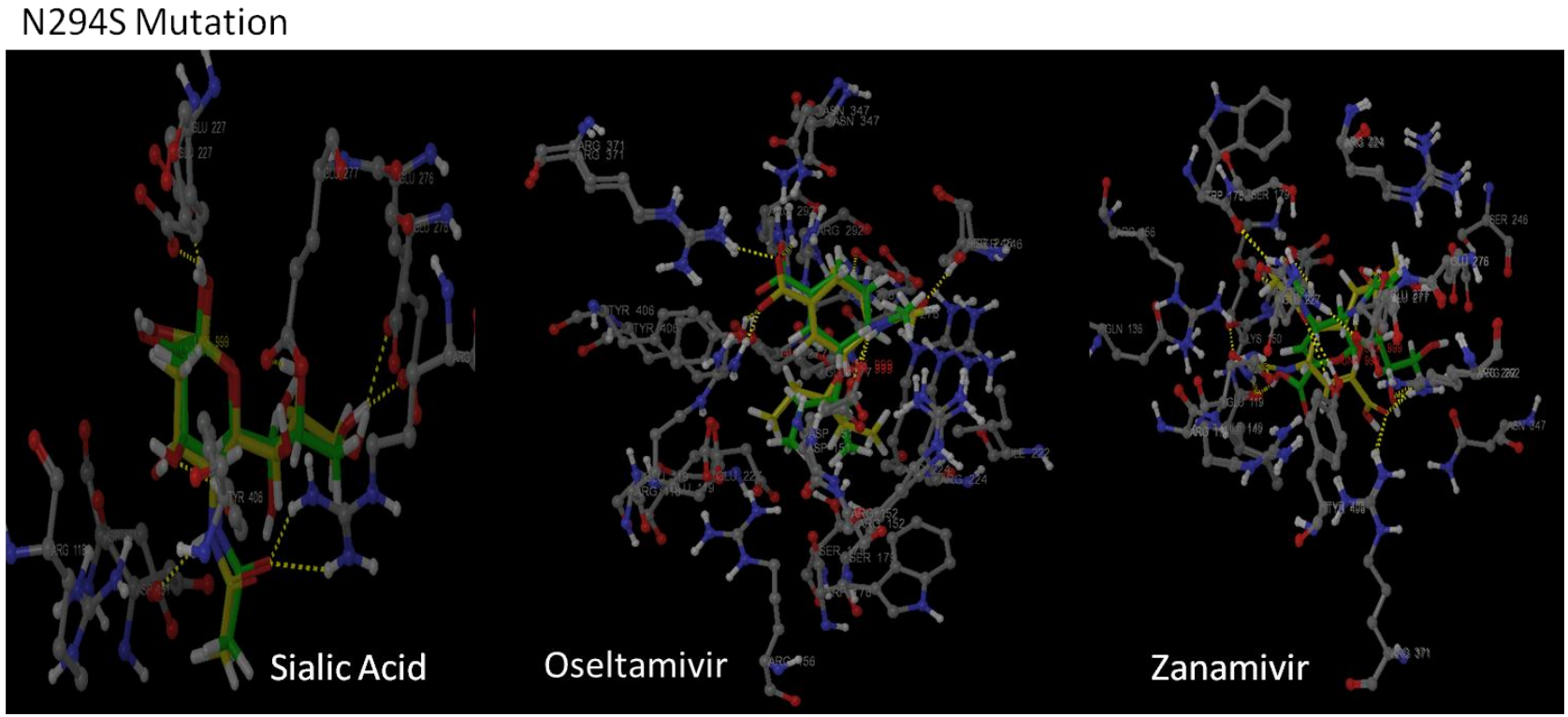

Figure B-2: Overlaid images of sialic acid, oseltamivir and zanamivir interaction with wild-type and N294S mutant NA. The ligands are shown in green colour in wild-type interactions and are shown in yellow in N294S mutant interactions. All three ligand's interaction with the mutant is identical to the wild-type protein.

H274N Mutation

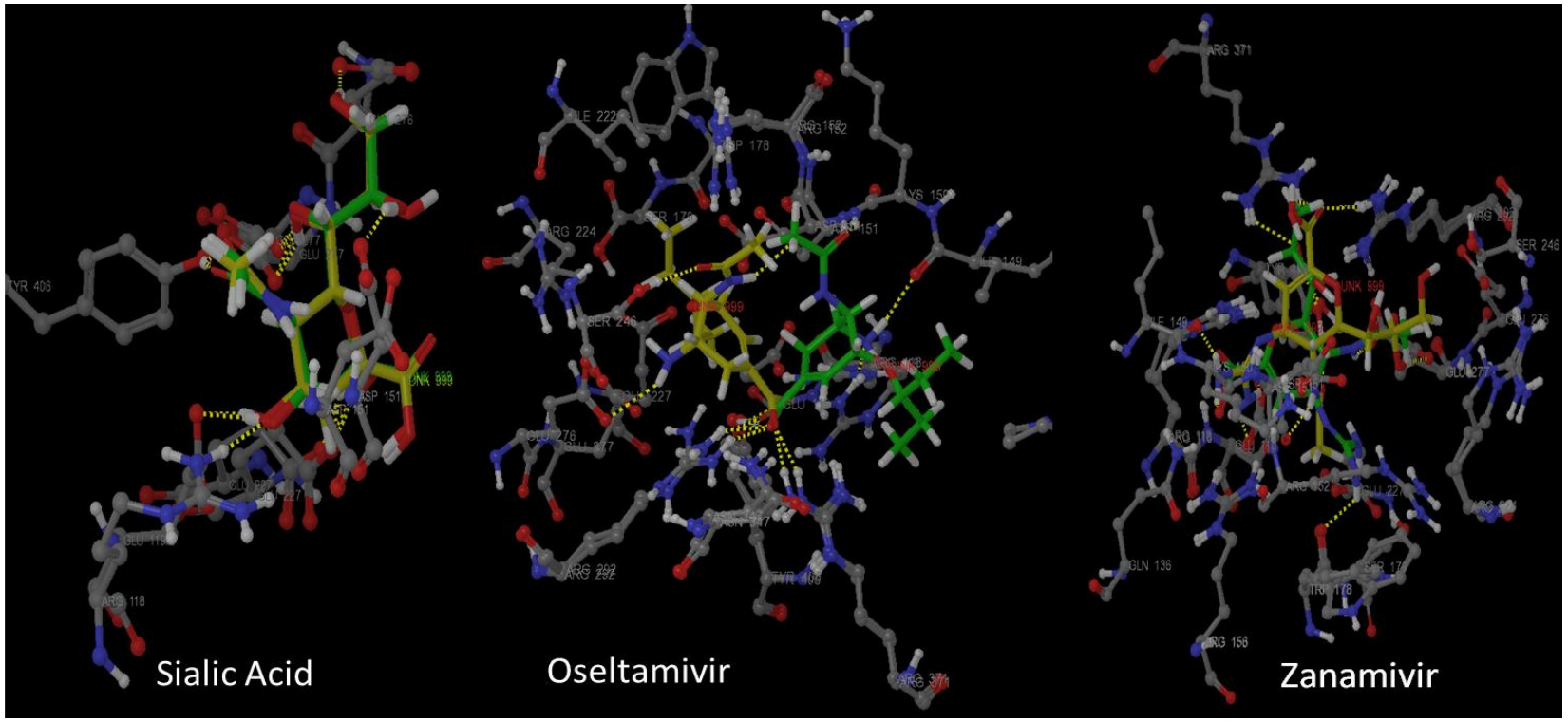

Figure B-3: Overlaid images of sialic acid, oseltamivir and zanamivir interaction with wild-type and H274N mutant NA. The ligands are shown in green colour in wild-type interactions and are shown in yellow in H274N mutant interactions. Oseltamivir deviates significantly in the H274N interaction when compared to the wild-type interaction and thereby decreasing the drug's binding affinity.

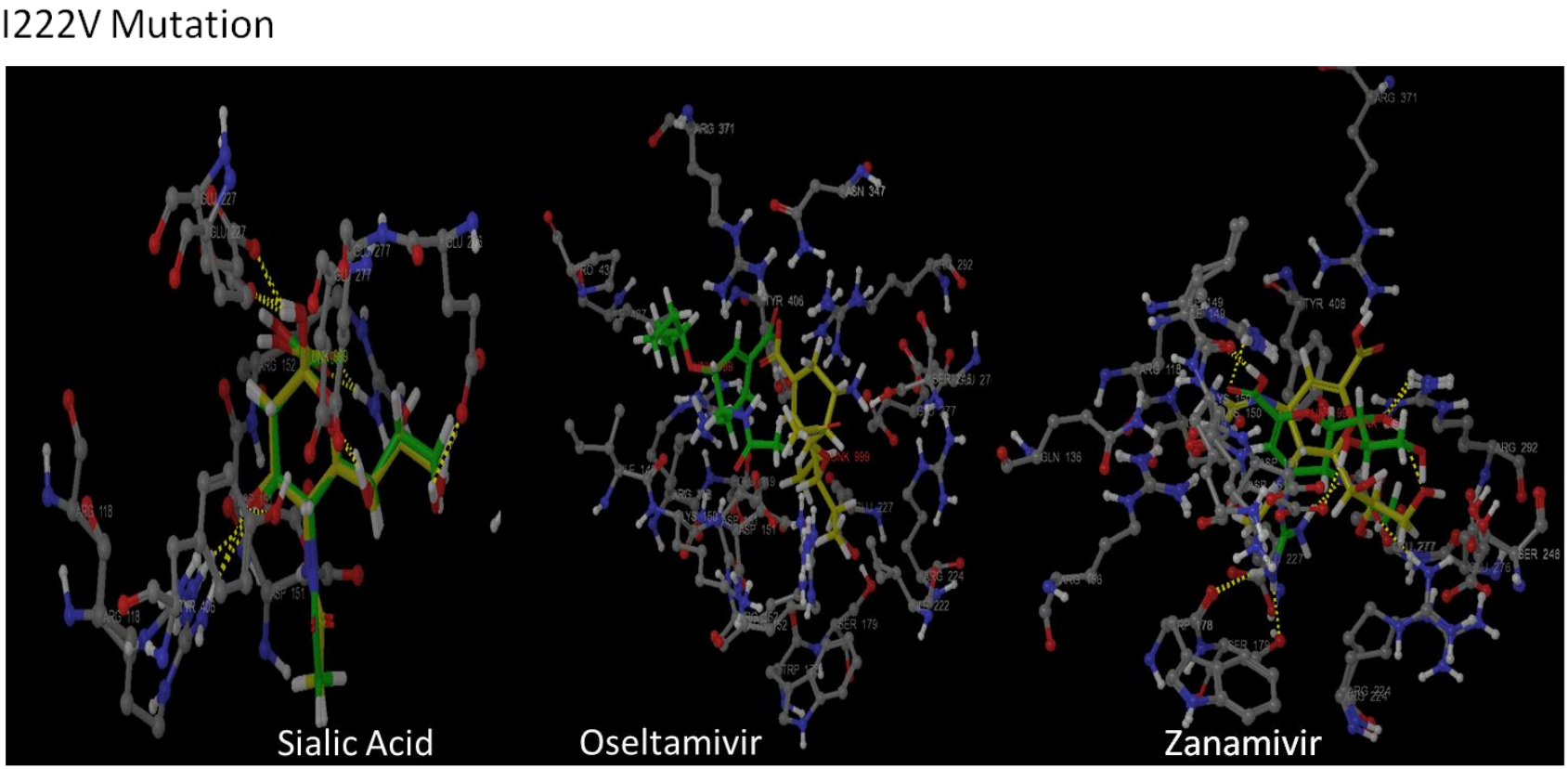

Figure B-4: Overlaid images of sialic acid, oseltamivir and zanamivir interaction with wild-type and I222V mutant NA. The ligands are shown in green colour in wild-type interactions and are shown in yellow in I222V mutant interactions. Antiviral drugs, oseltamivir and zanamivir deviate significantly in the I222V interaction when compared to the wild-type interaction. However, this change in confirmation has increased binding affinity for the antiviral drugs (detailed discussion provided in Chapter 3).

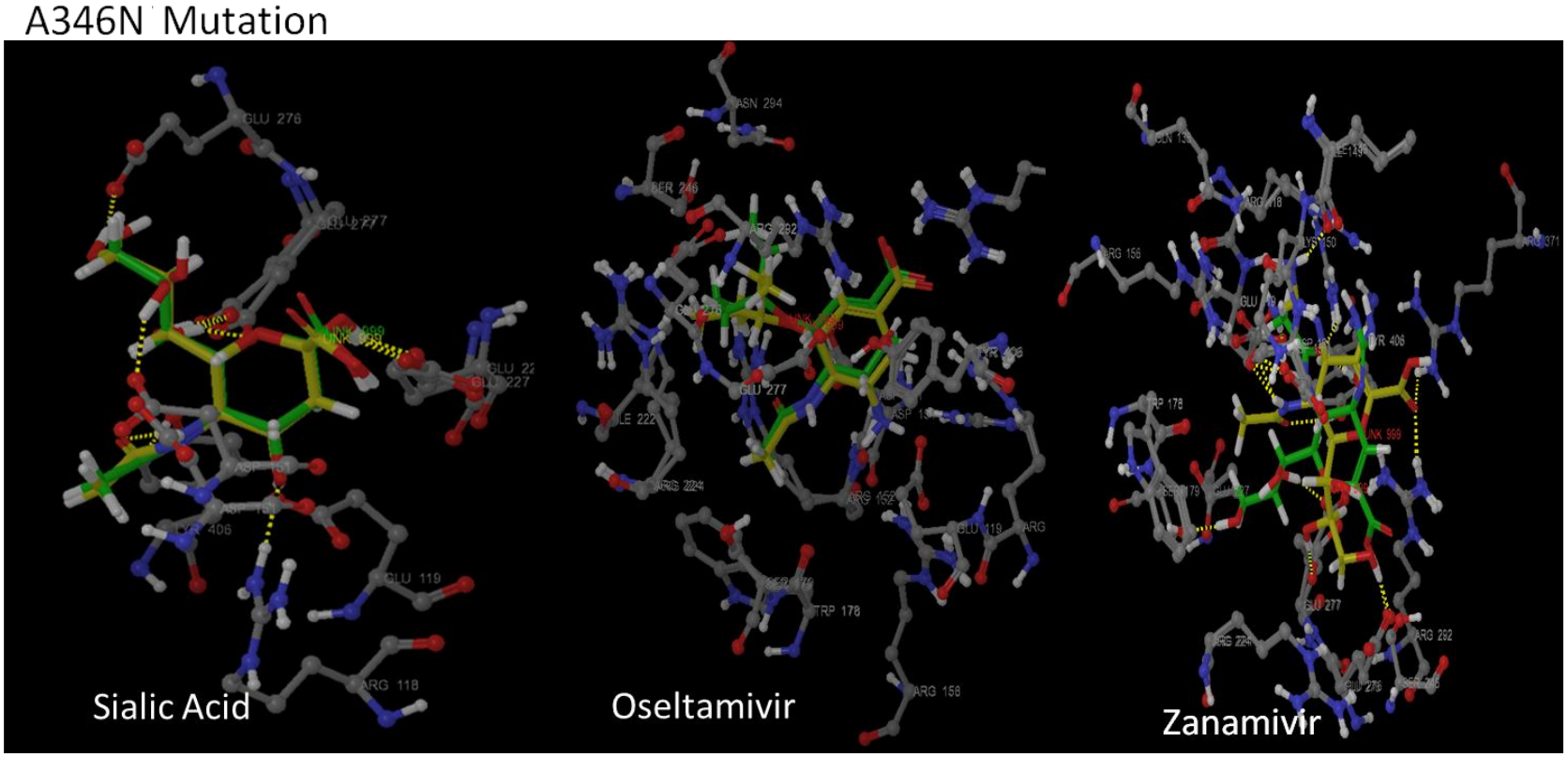

Figure B-5: Overlaid images of sialic acid, oseltamivir and zanamivir interaction with wild-type and A346N mutant NA. The ligands are shown in green colour in wild-type interactions and are shown in yellow in A346N mutant interactions. Zanamivir deviates significantly in the A346N interaction when compared to the wild-type interaction. However, this change in confirmation has increased binding affinity for zanamivir (detailed discussion provided in Chapter 3).

Appendix C: Densitometry analysis

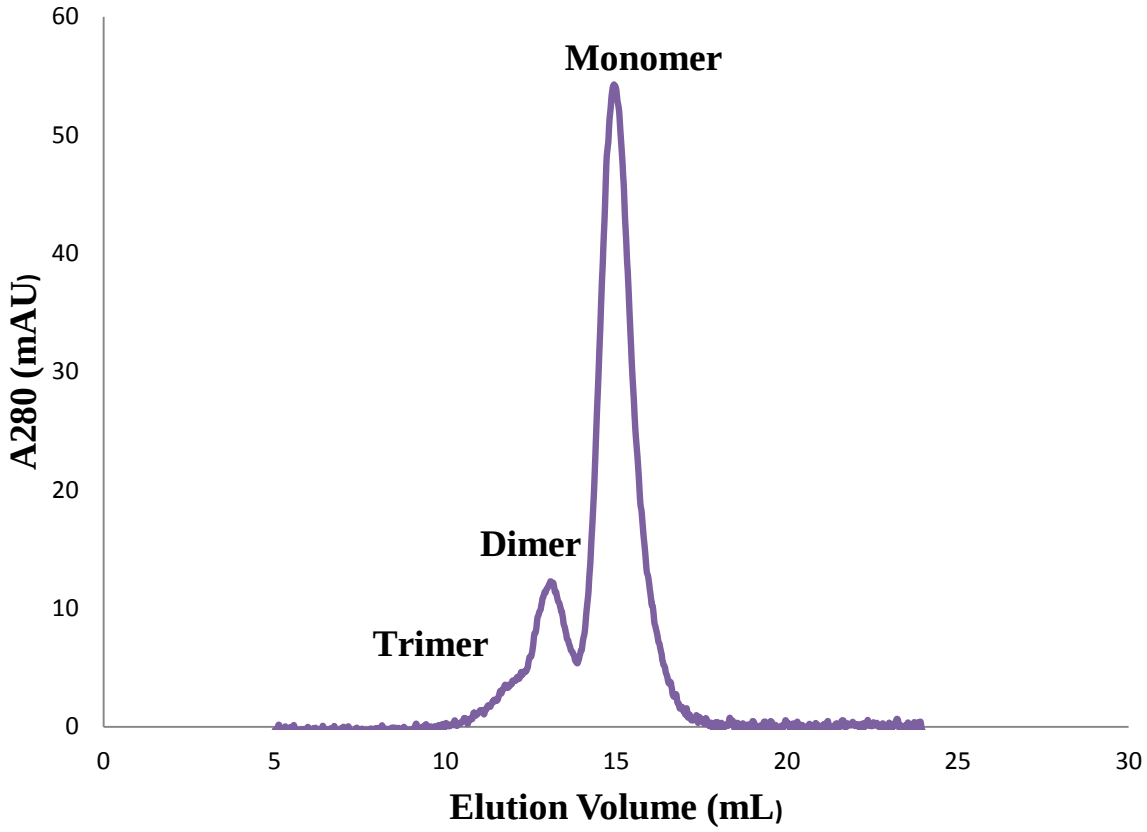

Figure C-1: Size exclusion chomatogram of BSA using 24 mL superdex 200 gel filtration column. BSA monomers was used for densitometry analysis.

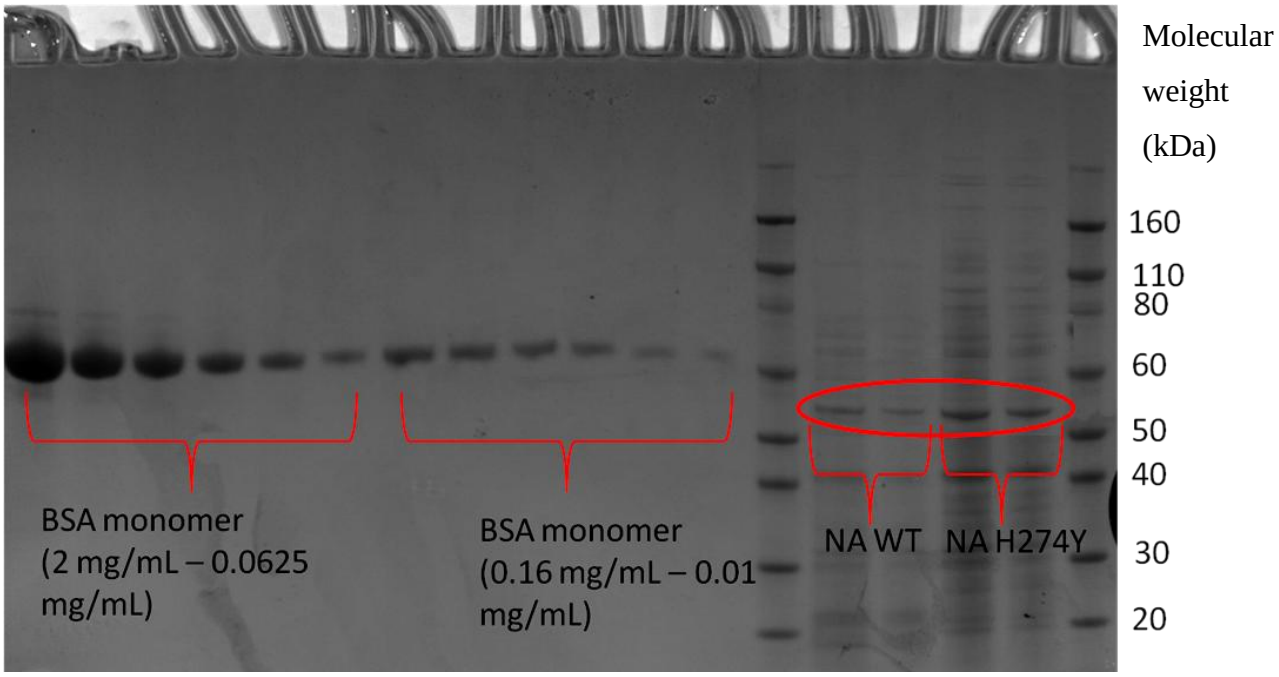

Figure C-2: SDS-page analysis of BSA monomer , IEX purified NA wild-type (neat and 2X diluted) IEX purified NA H274Y mutant (neat and 2X diluted, under reducing condition and stained with coomassie blue.

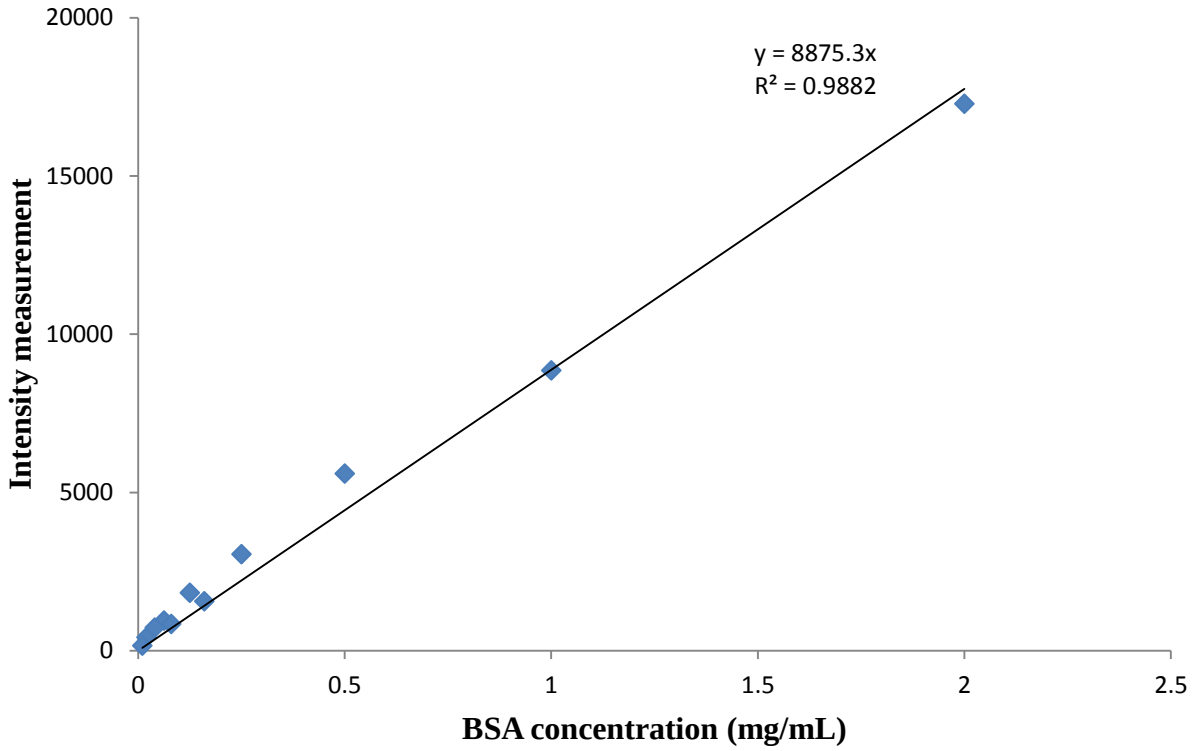

Figure C-1: BSA standard curve for correlation between band intesity and protein concentration. The intensity data shown in the graph are mean ± S.D. of duplicate measurements. The error bars are smaller than the symbol.

Appendix D: Preliminary SPR results

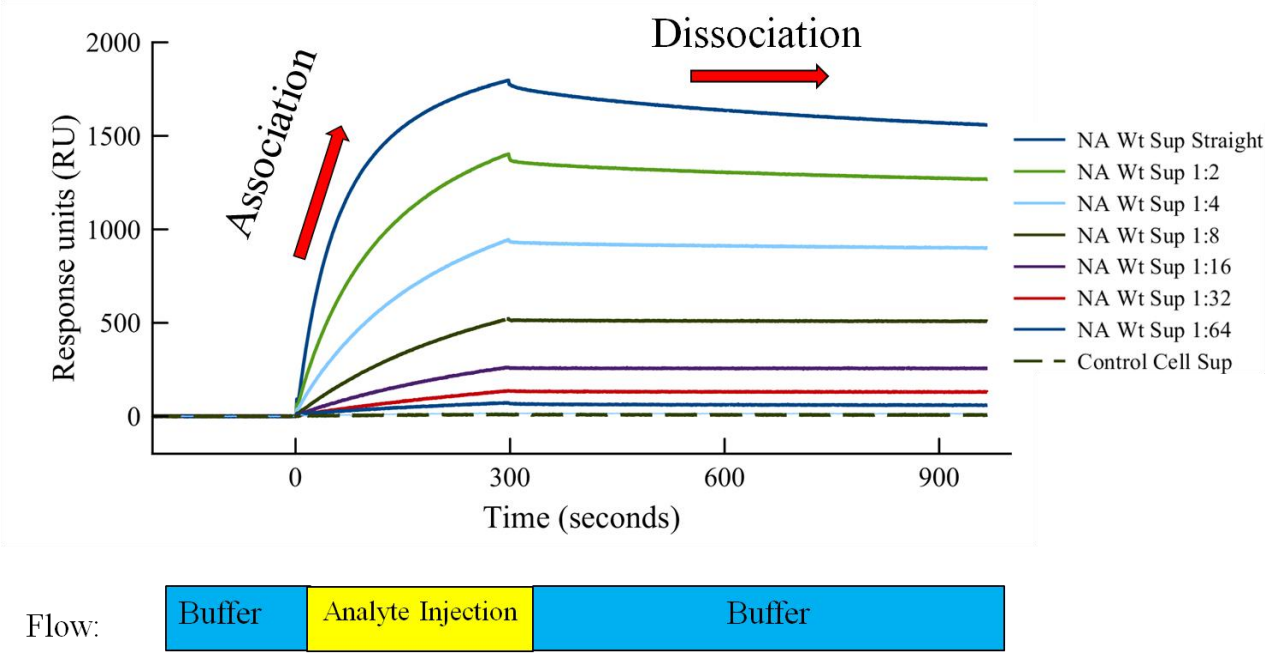

Figure D-1: Reference-subtracted duplicate SPR sensograms showing binding curves for various concentrations of NA wild-type cell culture supernatant with zanamivir-spacer conjugate immobilized on the chip surface. The control supernatant (control sup) is the supernatant obtained from cells that were not infected with recombinant baculovirus.

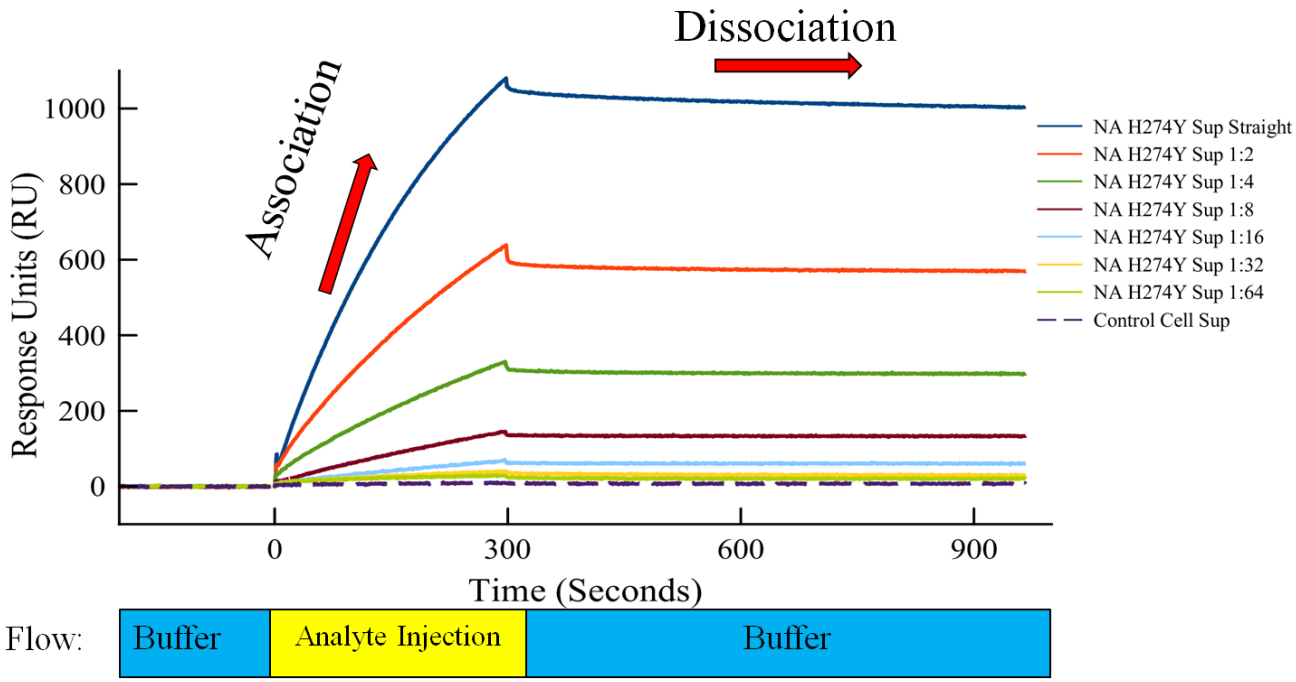

Figure D-2: Reference-subtracted duplicate SPR sensograms showing binding curves for various concentrations of NA H274Y mutant cell culture supernatant with zanamivir-spacer conjugate immobilized on the chip surface. The control supernatant (control sup) is the supernatant obtained from cells that were not infected with recombinant baculovirus.

Appendix E: Hydrogen bond interactions

Table E-1: Hydrogen bond interactions observed in zanamivir-H274Y mutant docked structure

Hydrogen bond interaction	Bond length (Å)
A:ARG118:HH11 - A:GLU119:OE1	1.47
A:GLU119:OE2 - A:ARG156:NH1	2.73
A:GLU119:OE2 - A:ARG156:NH2	2.61
A:ASP151:OD2 - A:ARG152:NH1	2.56
A:ASP151:OD2 - A:ARG152:NH2	3.14
A:ARG152:HH11 - A:ASP151:OD2	1.56
A:ARG156:HH11 - A:GLU119:OE2	1.82
A:ARG156:HH12 - A:ASP151:O	1.77
A:ARG156:HH21 - A:GLU119:OE2	1.62
A:GLU277:OE2 - A:ARG292:NH1	3.07
A:GLU277:OE2 - A:TYR406:OH	2.55
A:GLU277:OE2 - :UNK:O	3.06
A:ARG292:HH11 - A:TYR406:OH	2.07
A:ARG292:HH12 - A:GLU277:OE1	1.53
A:ARG292:HH21 - :UNK:O	2.26
A:ARG292:HH22 - A:ASN294:OD1	1.69
A:GLY348:H - A:ASN347:OD1	2.24
A:ARG371:HH21 - :UNK:O	2.35
A:ARG371:HH22 - A:GLY348:O	1.64

A:TYR406:HH - A:GLU277:OE2	1.59
:UNK:O - A:GLU277:OE2	3.06
:UNK:O - :UNK:O	2.65
:UNK:N - :UNK:N	2.34
:UNK:N - A:ILE149:O	3.21
:UNK:N - :UNK:N	2.34
:UNK:H - :UNK:O	1.95
:UNK:H - A:GLU119:OE1	1.81
:UNK:H - A:ASN347:OD1	1.98

Table E-2: Hydrogen bond interactions observed in zanamivir-H274Y mutant crystal structure

Hydrogen bond interaction	Bond length (Å)
B:TRP97:N - B:GLN395:OE1	2.98
B:ARG118:NH1 - B:ZMR1002:O1B	2.76
B:ARG118:NH1 - B:HOH73:O	2.77
B:ARG118:NH2 - B:GLU425:OE1	3.07
B:ARG152:NH1 - B:ZMR1002:O10	2.94
B:ARG152:NH1 - B:HOH681:O	3.09
B:ARG156:NH1 - B:ASP151:O	2.83
B:ARG156:NH1 - B:HOH40:O	3.03
B:ARG156:NH2 - B:GLU119:OE2	3.07
B:SER179:OG - B:GLU227:OE2	2.61
B:ARG224:NE - B:GLU276:OE2	3.08
B:ARG224:NH2 - B:GLU276:OE2	2.74

B:ARG292:NE - B:ASN294:OD1	3.00
B:ARG292:NH1 - B:GLU277:OE1	2.90
B:ARG292:NH1 - B:TYR406:OH	2.92
B:ARG292:NH1 - B:ZMR1002:O1A	3.17
B:ARG292:NH2 - B:ASN294:OD1	2.84
B:ARG292:NH2 - B:GLY348:O	3.09
B:ARG292:NH2 - B:ZMR1002:O1A	3.19
B:ASN294:ND2 - B:SER246:O	3.03
B:ASN294:ND2 - B:HOH806:O	2.92
B:LYS366:NZ - B:ASP396:OD1	2.74
B:ARG371:NH1 - B:ZMR1002:O1B	2.97
B:ARG371:NH1 - B:HOH485:O	2.97
B:ARG371:NH2 - B:GLY348:O	2.88
B:ARG371:NH2 - B:ZMR1002:O1A	2.75
B:TYR406:OH - B:GLU277:OE1	3.13
B:TYR406:OH - B:GLU277:OE2	2.49
B:TYR406:OH - B:ZMR1002:O6	3.04
B:ZMR1002:O1B - B:HOH631:O	3.18
B:ZMR1002:N5 - B:ZMR1002:O10	2.18
B:ZMR1002:N5 - B:ZMR1002:NH1	3.06
B:ZMR1002:N5 - B:HOH500:O	2.79
B:ZMR1002:O7 - B:HOH597:O	2.80
B:ZMR1002:O7 - B:HOH772:O	2.87
B:ZMR1002:O9 - B:GLU276:OE2	2.70
B:ZMR1002:O9 - B:HOH567:O	2.79

B:ZMR1002:NE - B:ASP151:OD1	2.95
B:ZMR1002:NE - B:ZMR1002:O10	3.20
B:ZMR1002:NH1 - B:TRP178:O	3.09
B:ZMR1002:NH1 - B:GLU227:OE2	3.07
B:ZMR1002:NH1 - B:HOH500:O	3.17
B:ZMR1002:NH2 - B:ASP151:O	2.97
B:ZMR1002:NH2 - B:TRP178:O	2.75
B:HOH40:O - B:GLU119:OE1	2.68
B:HOH40:O - B:ASP151:OD1	2.77
B:HOH40:O - B:HOH68:O	2.86
B:HOH485:O - B:HOH499:O	2.86
B:HOH485:O - B:HOH809:O	2.84
B:HOH500:O - B:GLU227:OE2	2.74
B:HOH500:O - B:GLU277:OE2	2.69
B:HOH500:O - B:ZMR1002:NH1	3.17
B:HOH500:O - B:HOH583:O	2.91
B:HOH546:O - B:ZMR1002:O1A	3.00
B:HOH546:O - B:HOH507:O	3.02
B:HOH546:O - B:HOH772:O	2.73
B:HOH546:O - B:HOH806:O	2.65
B:HOH567:O - B:ZMR1002:O9	2.79
B:HOH567:O - B:HOH557:O	2.97
B:HOH567:O - B:HOH597:O	2.76
B:HOH583:O - B:ZMR1002:O8	3.08
B:HOH583:O - B:HOH500:O	2.91

B:HOH583:O - B:HOH605:O	2.81
B:HOH588:O - B:HOH631:O	3.01
B:HOH597:O - B:ZMR1002:O7	2.80
B:HOH597:O - B:HOH567:O	2.76
B:HOH597:O - B:HOH654:O	2.82
B:HOH631:O - B:ASP151:OD1	2.69
B:HOH631:O - B:ZMR1002:O1B	3.18
B:HOH631:O - B:HOH73:O	2.75
B:HOH631:O - B:HOH588:O	3.01
B:HOH772:O - B:ASP151:OD2	3.21
B:HOH772:O - B:ZMR1002:O6	3.18
B:HOH772:O - B:ZMR1002:O7	2.87
B:HOH772:O - B:HOH546:O	2.73
B:HOH809:O - B:HOH485:O	2.84
B:HOH809:O - B:HOH547:O	2.70
B:TRP97:N - B:GLN395:OE1	2.98
B:ARG118:NH1 - B:ZMR1002:O1B	2.76
B:ARG118:NH1 - B:HOH73:O	2.77
B:ARG118:NH2 - B:GLU425:OE1	3.07
B:ARG152:NH1 - B:ZMR1002:O10	2.94
B:ARG152:NH1 - B:HOH681:O	3.09
B:ARG156:NH1 - B:ASP151:O	2.83
B:ARG156:NH1 - B:HOH40:O	3.03
B:ARG156:NH2 - B:GLU119:OE2	3.07
B:SER179:OG - B:GLU227:OE2	2.61

B:ARG224:NE - B:GLU276:OE2	3.08
B:ARG224:NH2 - B:GLU276:OE2	2.74
B:ARG292:NE - B:ASN294:OD1	3.00
B:ARG292:NH1 - B:GLU277:OE1	2.90
B:ARG292:NH1 - B:TYR406:OH	2.92
B:ARG292:NH1 - B:ZMR1002:O1A	3.17
B:ARG292:NH2 - B:ASN294:OD1	2.84
B:ARG292:NH2 - B:GLY348:O	3.09
B:ARG292:NH2 - B:ZMR1002:O1A	3.19
B:ASN294:ND2 - B:SER246:O	3.03
B:ASN294:ND2 - B:HOH806:O	2.92
B:LYS366:NZ - B:ASP396:OD1	2.74
B:ARG371:NH1 - B:ZMR1002:O1B	2.97
B:ARG371:NH1 - B:HOH485:O	2.97
B:ARG371:NH2 - B:GLY348:O	2.88
B:ARG371:NH2 - B:ZMR1002:O1A	2.75
B:TYR406:OH - B:GLU277:OE1	3.13
B:TYR406:OH - B:GLU277:OE2	2.49
B:TYR406:OH - B:ZMR1002:O6	3.04
B:ZMR1002:O1B - B:HOH631:O	3.18

Table E-3: Hydrogen bond interactions observed in oseltamivir-H274Y mutant docked structure

Hydrogen bond interaction	Bond length (Å)
A:ARG118:HH11 - A:GLU119:OE1	1.47
A:ASP151:OD2 - A:ARG152:NH2	3.14
A:ARG152:HH22 - A:ASP198:OD2	1.49
A:ARG156:HH11 - A:GLU119:OE2	1.82
A:ARG156:HH12 - A:ASP151:O	1.77
A:SER179:HG - A:GLU227:OE2	1.53
A:ASP198:OD2 - A:ARG152:NH2	2.54
A:ARG224:HE - A:GLU276:OE2	1.95
A:ARG224:HH21 - A:TYR274:OH	1.70
A:ARG224:HH22 - A:GLU276:OE2	1.50
A:THR225:H - A:SER179:OG	2.07
A:GLU227:OE2 - A:SER179:OG	2.51
A:SER246:HG - :UNK:O	2.10
A:GLU277:OE2 - A:ARG292:NH1	3.07
A:GLU277:OE2 - A:TYR406:OH	2.55
A:GLU277:OE2 - :UNK:N	2.71
A:ARG292:HE - A:GLU276:OE1	1.63
A:ARG292:HH11 - A:TYR406:OH	2.07
A:ARG292:HH12 - A:GLU277:OE1	1.53
A:ARG292:HH22 - A:ASN294:OD1	1.69
A:TYR406:HH - A:GLU277:OE2	1.59
:UNK:H - A:GLU277:OE2	1.70

Table E-4: Hydrogen bond interactions observed in oseltamivir-H274Y mutant crystal structure

Hydrogen bond interaction	Bond length (Å)
A:ARG118:NH1 - A:GLU425:OE1	2.84
A:ARG118:NH2 - A:G39800:O1B	2.70
A:ARG118:NH2 - A:HOH876:O	3.02
A:ARG152:NH2 - A:G39800:O10	2.79
A:ARG224:NE - A:GLU276:OE1	2.69
A:TYR274:OH - A:GLU276:OE1	2.72
A:ARG292:NE - A:ASN294:OD1	2.94
A:ARG292:NH1 - A:ASN294:OD1	2.76
A:ARG292:NH1 - A:GLY348:O	3.16
A:ARG292:NH2 - A:GLU277:OE1	2.83
A:ARG292:NH2 - A:TYR406:OH	2.95
A:ASN294:ND2 - A:SER246:O	2.90
A:TYR347:OH - A:G39800:O1A	2.92
A:TYR347:OH - A:HOH953:O	2.66
A:ARG371:NH1 - A:TYR347:OH	2.99
A:ARG371:NH1 - A:GLY348:O	3.04
A:ARG371:NH1 - A:G39800:O1A	2.68
A:ARG371:NH2 - A:G39800:O1B	2.77
A:ARG371:NH2 - A:HOH890:O	2.87
A:TYR406:OH - A:GLU277:OE1	3.05
A:TYR406:OH - A:GLU277:OE2	2.55
A:G39800:N5 - A:HOH861:O	2.89

A:G39800:N4 - A:GLU119:OE2	2.91
A:G39800:N4 - A:HOH885:O	2.63
A:HOH861:O - A:GLU227:OE2	2.70
A:HOH861:O - A:GLU277:OE2	2.66
A:HOH885:O - A:TRP178:O	2.64
A:HOH885:O - A:GLU227:OE2	3.11
A:HOH885:O - A:G39800:N4	2.63
A:HOH907:O - A:GLU119:OE2	2.87
A:HOH907:O - A:ASP151:OD1	2.91
A:HOH907:O - A:HOH891:O	2.63
A:HOH949:O - A:SER246:OG	2.66